ELECTROSPINNING OF COMPOSITE SILICA/PVA NANOFIBRES AND TESTING OF THEIR EFFECTS ON THE IMPEDANCE OF AN AIR GAP

By

Yeshiv Singh 208504125

Supervisor: Dr I Davidson

Co. Supervisors: Prof D Ramjugernath, Dr L Chetty

Submitted in partial fulfilment of the requirements for the degree of Master of Science in Engineering

Electrical Engineering Programme

School of Engineering

University of KwaZulu Natal

Durban

November 2014

ACKNOWLEDGEMENTS

The work done to produce this thesis was multidisciplinary by nature. Multiple laboratories were used and many people contributed knowledge toward work done. The following people/UKZN bodies are acknowledged for being a part of the research presented in this thesis.

- Dr L Chetty (Ethekwini Municipality) for proposing the initial topic and providing guidance throughout the research
- Prof D Ramjugernath (Chemical Engineering UKZN) for use of the thermodynamics laboratory (Chemical Engineering Building on UKZN Howard College Campus) and guidance on the chemistry related sections of the research
- Dr I Davidson (Electrical Engineering UKZN) for the use of the high voltage DC laboratory (Behind printing and services building on UKZN Westville Campus) and guidance throughout the research
- Prof ThavendranGovender for use of the peptide laboratory (Chemistry building on UKZN Westville Campus)
- Microscopy and microanalysis unit for use of the ZEISS scanning electron microscope (Room 50, level 4, E Block – E1, UKZN Westville Campus)
- Chemistry – Westville Campus for use of an infrared spectrometer

ABSTRACT

Electrospinning is a quick method of producing long continuous fibres with diameters in the nanometre range. At first, only polymers wereelectrospun. In recent practices, inorganic materials have also been electrospun by combining them with polymers in the electrospinning solution. A number of experiments dealing with electrospinning and applications of silica nanofibres have been presented by different authors. None of these experiments dealt with any electrical properties of silica nanofibres. The experimentation presented herein deals with the effects of composite silica/PVA nanofibres on the electrical impedance of an air gap.

Literature covering electrospinning in general and electrospinning of silica is discussed in detail. For the electrospinning process, parameters affecting the morphology of nanofibres are presented by referring to experiments done by other researchers. For silica, the theory behind formation of a silica sol is discussed.

All apparatus used in the experimentation is listed. In particular, the electrospinning setup had to be designed, built and optimized. The design of the setup is presented. Included in the design is the construction of a high voltage DC supply to be used to apply high voltage to the spinneret of the setup. The optimization of the setup and the solution used to electrospin fibres is covered in the discussion of the experimental procedure.

The fibres were successfully fabricated with reasonable uniformity and nano-sized diameters. These parameters were checked using a scanning electron microscope. Some images taken of the fibres by the microscope are presented with the calculated average fibre diameters. The rest are in the appendix. The chemical composition of the fibres was confirmed using Fourier transform infra-red, the results of which are discussed. The impedance of an air gap with and without fibres was calculated using values measured by an oscilloscope. Measurements were taken over a range of frequencies to observe the change in the reactive component of the impedance. Based on results obtained, it was concluded that composite silica/PVA nanofibres reduce the impedance of an air gap and are therefore ineffective as an insulating material.

TABLE OF CONTENTS

FIGURES

TABLES

VARIABLES

F_e	Force of the Electric Field
V	Applied Voltage
L	Length of Capillary
R	Radius of Capillary
H	Distance between High Voltage Electrodes
F_γ	Force of Surface Tension
γ	Surface Tension
φ	Angle of Attachment
V_C	Critical voltage of electrospinning
m	mass of droplet in kg
g	gravitational acceleration (9.8 m.s-2)
d	inner diameter of cylinder in mm
γ	surface tension in N/mm
$\overline{R}$	Normalised Radius
$\overline{Z}$	Normalised Position on the Vertical Axis through a Vertical Electrospinning Jet
m	Flow Index
Z_T	Test cell impedance
R_m	10MΩ measurement resistor
V	Function generator applied voltage (Taken as 0^0 phase angle reference)
V_m	Amplitude of measured voltage
θ	Angle of measured voltage
I	Current from function generator
I_T	Current from test cell

ACRONYMS

AC	Alternating Current
DC	Direct Current
PVA	Poly(Vinyl Alcohol)
TEOS	Tetraethoxysilane
PVP	Poly(Vinyl Pyrrolidone)
CNMR	Carbon Nuclear Magnetic Resonance
XRD	X-Ray Diffraction
FTIR	Fourier Transform Infra-Red
SEM	Scanning Electron Microscope
AFM	Atomic Force Microscope
FEG-SEM	Firing Electron Gun Scanning Electron Microscope

1. INTRODUCTION

The properties of materials change when their dimensions are reduced to nano-scale. This is due to the high surface area to volume ratio of nano-size particles [1]. Nano-materials are often synthesised and sometimes combined with another material as a composite to create a material with desirable properties for a particular application [1]. Nano-materials can be synthesised by various means. One method which is of particular interest is electrospinning due to its simplicityand ability to produce long continuous nanofibres[1]. Electrospinning is a novel way of producing polymer fibres with nano-sized diameters in the range of hundreds of nanometres. Nanofibres synthesised using electrospinning have many real world applications. Depending on the polymer precursors used in the electrospinning process, application of the fibres are currently being investigated in the following fields[2]: (a.) Cosmetics, (b.) Protective clothing, (c.) Nano-sensors, (d.) Life sciences, (e.) Tissue engineering and (f.) Filtering media.

Although electrospinning makes wide use of polymer precursors to synthesise polymer nanofibres, other types of nanofibres can also be produced using this technique. Composite nanofibres have been synthesised by introducing inorganic nano-particles into the polymer precursor [3]. The introduction of the inorganic material gives the polymer nanofibres new properties. For example, titanium dioxide can be added to a polymer precursor to produce a nano-fibrous catalyst with enhanced photo-catalytic properties[3]. In another experiment, addition of carbon nanotubes to the polymer precursor has yielded semiconductor-like properties from the electrospun fibres[4]. Other applications include [3]: (a.) Other types of catalysts, (b.) Filters, (c.) Laminates, (d.) Sensors and (e.) Biotechnological applications. In some experiments conducted by other researchers, the composite nanofibres are heated in an oven to remove the polymer. This process creates inorganic nanofibres. Inorganic materials such as carbon, copper and silica have been successfully fabricated as nanofibres [5], [6], [7].

There have been many experiments involving the fabrication of silica nanofibres for use in various applications. Electrospun silica nanofibres were first introduced in an article by Shao [7]. Thereafter in other experiments, silica nanofibres were electrospun using different precursors to induce variations in the silica nanofibres produced. Some of these variations include mesoporous silica (for use in sensors, catalysts, optical devices

and magnetic devices)[8], coated silica nanofibres [9] (for use on spacecraft) and silica nanotubes (for use in single molecule detection)[10]. A possible application which has not yet been investigated is in electrical insulation. The good dielectric and thermal properties of silica make it a potentially suitable material for use as an electrical insulator. Nanofibres fabricated for this purpose would need to be hydrophobic. This means that the electrospinning process should not leave traces of hydrophilic substances in the fibres[11].

This research investigation seeks to determine the possible effects of composite silica/PVA nanofibreson the impedance of an air gap. The fundamental theory of electrospinning and electrospinning of silica is discussed. Design and construction of the electrospinning apparatus used is also presented. The major apparatus which were designed and constructed included the solution delivery system, the plate used to collect the nanofibres and the high voltage DC supply. The methods used for characterizing the electrospun fibres are defined in detail. Conclusions on which electrospinning parameters are most suitable for producing the most uniform fibres with the smallest possible diameters are made based on the results of characterizing the electrospun fibres.

The possible application of the fibres to electrical insulation was of interest. A good electrical insulator is defined by many different properties depending on the application (voltage level, power rating, pollution level etc.). Some general properties a good insulator should possess include: (a.) High breakdown strength (voltage at which failure of insulation occurs)[12], [13], [14]&[15], (b.) High dielectric strength (sometimes expressed as permittivity or dielectric constant) [16], [17], [14]&[18]and (c.)Resistance per meter (sometimes expressed as conductance which is the inverse of resistance) [19].

Once PVA/silica nanofibres were electrospun, the electrical properties of the fibres were tested using a technique called impedance spectroscopy. Impedance is important due to its links to dielectric strength and resistance. The permittivity is calculated using the capacitance of a sample [20]. The capacitance of a sample is usually obtained by first measuring its reactance (calculated from impedance) and then applying a known equivalent circuit model for the material [21]. Typically if the reactance of a sample is higher than that of another sample at a particular frequency it can be said that the capacitance is higher and as a result, the permittivity (dielectric strength) is lower. The

groundwork for developing a model for the behaviour of a material is measuring its response over a range of frequencies. Investigating impedance over a range of frequencies has been called impedance spectroscopy [21].

Impedance spectroscopy was performed on electrospun composite PVA/silica nanofibres. The data obtained includes the absolute impedance, the reactance, the resistance and the phase angle of the voltage across the sample with respect to the input waveform.The results of impedance testing on the fibres wereanalysed so that conclusions could be drawn on the effects of different fibre morphologies on the impedance of an air gap.

2. LITERATURE REVIEW

This literature review shall cover some background information on electrospinning and existing research on electrospinning parameters. Existing research into simulation of electrospinning is also presented and explored as a possible means of predicting the outcomes of any electrospinning experiment. Since composite silica/PVA nanofibres were of interest in this dissertation, information on the preparation of a polymer solution containing silica was also researched and noted. Methods of characterizing nanofibres produced by electrospinning are discussed as well.

2.1. The Electrospinning Process

The electrospinning process was first developed as an alternative to spinning yarn [2]. The rate of production of yarn from electrospinning, however, was too slow to be used commercially [2]. More recently electrospinning has been used as a simple method of fabricating nanofibres [2]. The process can create nano sized fibres due to the Taylor effect, where an electric field elongates and accelerates a pendant of solution [22].

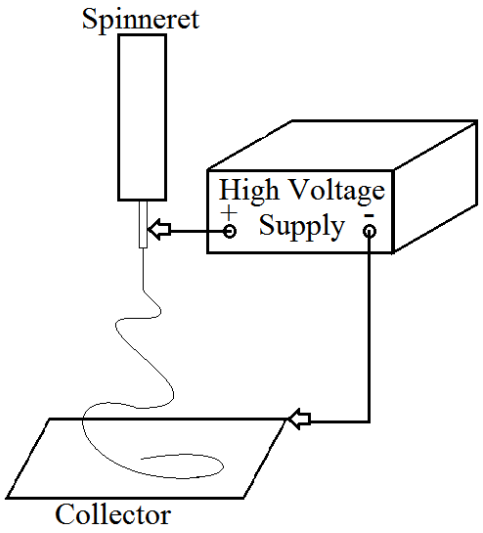

Figure 2.1: Basic electrospinning setup with the major components labelled

The basic electrospinning setup shown in Figure 2.1 consists of a spinneret used to dispense solution, a high voltage electrode placed in the solution and a collector plate which is electrically grounded. When the high voltage electrode is energised, a strong electric field is formed between the spinneret and the collector plate [22]. This field creates repulsive forces within the now charged solution. When the repulsive forces are greater than the surface tension of the droplet at the end of the spinneret, a stream of solution will be formed from the droplet. The droplet takes on a shape widely known as

the Taylor cone [22]. The stream is stretched to a nano sized diameter by the electric field. The solvent from the solution evaporates due to the electric field. The resulting nanofibres are deposited on the collector plate [22].

There are many factors affecting the process which can alter the produced nanofibres. They can be grouped into three main controlling factors which are [2]: (a.) Processing parameters, (b.) Solution parameters and (c.) Ambient parameters.

2.2. Electrospinning Processing Parameters

Processing parameters deal with changes in the electrospinning setup which comprises of the spinneret, the voltage source and the collector [22]. Processing parameters can be classed as [22]: (a.) Field control, (b.) Delivery system, (c.) Collection system, (d.) Applied voltage, (e.) Feed/Flow rate and (f.) Tip to collector distance.

2.2.1. Field Control

In simple electrospinning setups the electrospun fibres are collected in a non-woven mesh due to the instability at the end of the electrospinning jet. The movement of the jet is controlled by the electric field created by the applied voltage [22]. Changing the shape of the electric field can therefore introduce a measure of control over the area of deposition of the electrospun fibres. Field control is implemented by modifying the ground electrode whilst adding a non-conductive collector and/or adding auxiliary electrodes of a particular shape [22]. Various field control methods have been attempted, each method with its own merits and disadvantages.

A simple method of field control is converting the ground electrode to a point electrode and placing it below a rotating, non-conductive collector. This setup was tested by Carnell *et al* [23]. The setup yielded highly aligned fibres on the collector. It was also found that by moving the ground electrode along the length of the collector, the electrospun fibres could be wound around the rotating collector in a helical fashion [23]. The use of a non-conductive collector does however limit the size of the collector [22]. This is because the electrode distance away from the point of collection is dependent on the size of the collector and the electric field at that point is weaker the further away the ground electrode is [23].

Parallel plate electrodes have been used in an experiment documented by Arras *et al* to collect aligned electrospun nanofibres [24]. The parallel plate configuration involves

two auxiliary flat electrodes placed on either side of the electrospinning jet. Arras *et al* showed that changing the orientation of these electrodes (varying the angle from vertical) could change the direction of the electrospinning jet [24]. Some whipping and instability in the electrospinning jet still occurs but in a direction parallel to the auxiliary plate electrodes [24].

Auxiliary ring electrodes can concentrate the electric field at their centre. This makes the electrospinning jet travel in almost a straight line. In an experiment involving electrospinning of polyethylene oxide, Deitzel *et al* showed that ring electrodes reduce the area of deposition of electrospun nanofibres on a flat grounded collector significantly [25]. The same experiment also showed that fibres collected on a rotating grounded collector after passing through the ring electrodes were highly aligned [25]. Disadvantages of the ring electrode setup have been cited as difficulty of installation by Teo*et al*[22].

2.2.2. Delivery System

The delivery system of an electrospinning setup has classically been a syringe or pipette used as a spinneret [22]. There have however been attempts at different delivery systems for use in commercial production of nanofibres. This is due to a single spinneret having a production rate too low for commercial use [22].

Angammana *et al* demonstrated that using two spinnerets negatively affected the electrospinning process due to field cancellation [26]. The porous drum delivery system was found to be effective in mass producing nanofibres. The precursor solution is placed in a porous drum which spins allowing fibres to be electrospun onto a cylindrical collector encircling the drum. Field control for the porous drum delivery system becomes difficult and electrospun fibres are deposited in a random manner on the collector [22].

Other methods of delivery include [22]: (a.) Coaxial spinnerets and orthogonal spinnerets to produce hollow nanofibres, (b.) Gas Jacket electrospinning for creation of smooth fibres and (c.) Bicomponent spinnerets for electrospinning of fibres containing two different materials.

2.2.3. Collection System

A typical collector in an electrospinning setup is a flat plate which doubles as the ground electrode. Variations of this typical setup have been tried in various experiments in a bid to collect more aligned fibres [22].

For collection of aligned fibres the rotating drum collector is commonly used. It consists of a cylinder which has its rotation controlled by a DC motor [23], [24]. The drum may double as a ground electrode or may be non-conductive with the ground electrode below or inside it. The electrospinning jet is pulled by the rotation of the drum as well as the force of the electric field to create aligned fibres [24]. Arras *et al* showed that increasing drum speed increased the alignment of the electrospun nanofibres [24]. Although the fibres are aligned by use of the rotating drum there is still a significant amount of random deposition [24]. More aligned fibres may be collected by substituting the cylinder like drum with a wire drum made of many parallel wires connected to a disc at each end [27]. This is done at the cost of the volume of electrospun fibres which may be collected at one go [27].

For highly aligned fibres the knife edge rotating disc collector is used [22]. The knife edge rotating disc collector is a thin disc with a sharp edge all along its circumference. The disc doubles as the grounded electrode leading to concentration of the electric field at the sharp edge of the disc [22]. The highly concentrated field makes the electrospun fibres land on the sharp edge of the disc. In this way highly aligned fibres are collected [22]. The number of fibres which may be collected using this method, however, is very low. This is because the area available for deposition of fibres is low due to the thin edge of the collector [22].

A water bath collector allows for collection of fibres of longer length. The water bath collector is simply a water filled container with the ground electrode inside the water [28]. Electrospun fibres are forced to pass into the water. Seo *et al* demonstrated that a water bath collector is also conducive to the fabrication of highly porous nanofibres. It was also demonstratedby Seo *et al* that factors such as pH level and ionic concentration of the water bath affect the morphology of electrospun fibres.

Other types of collectors consist of various arrangements of the collecting ground electrodes with the aim of controlling area of deposition of the nanofibres during electrospinning. These electrodes are sometimes not grounded but held at a negative

potential [22], [27]. Teo *et al* (2005) performed some experimentation on parallel knife edge collecting electrodes held at -3kV potential [29]. It was found that highly aligned fibres could be collected and twisted into micron sized nanofibre bundles [29].

2.2.4. Applied Voltage

Electrospinning is dependent upon the electric field the electrospinning solution is exposed to [30]. The applied voltage therefore has an effect on electrospun fibres. A certain minimum (critical) voltage is required to initiate formation of a Taylor cone and hence the electrospinning process [30].

Gu *et al*, Rodoplu *et al* and Chowdhury *et al* each conducted experimentation which showed that increasing the applied voltage decreases the diameter of the electrospun fibres[30], [31], [32]. It is theorised that higher repulsive forces within the electrospinning stream lead to more stretching since the same flow rate from the spinneret was used as for the lower voltages [31].

Rodoplu *et al* and Chowdhury *et al* took their experimentation one step further to show that at a particular voltage above the critical voltage bead formation in the electrospun fibres became visible[31], [32]. It can therefore be concluded that the applied voltage needs to be optimised between the smallest diameter of electrospun fibres and negligible bead formation.

2.2.5. Feed/Flow Rate

The flow rate is the rate at which solution is fed to the spinneret tip. A syringe pump or infusion pump can be used to accurately control the flow rate [33]. The effects of flow rate on the electrospinning process was investigated in depth by Zargham *et al*. Zargham *et al* found that at low flow rates, the electric field accelerated the solution towards the collector faster than the solution could be dispensed[33]. This caused the Taylor cone to recede into the spinneret and reappear after a while. This instability in the Taylor cone resulted in electrospun fibres with large variations in diameter [33].

At high flow rates Zargham *et al* found that solution was being ejected from the spinneret faster than the electric field could carry it away resulting in some solution dripping away from the stream and spraying onto the collector [33]. The spraying of solution caused the area of deposition of nanofibres to increase as well [33].

For a fixed voltage level a particular flow rate is optimal [33]. The voltage level, however, also needs optimisation. The two factors should therefore be varied together until the optimum voltage and flow rate is found.

2.2.6. Tip to Collector Distance

The tip to collector distance is the distance from the dispensing end of the spinneret to the collector. Decreasing this distance has the same effect on the electric field as increasing the applied voltage [2]. This means that a stronger electric field will be present which should lead to bead formation on the electrospun fibres.

Mazoochi *et al* performed experimentation on the effects of varying the tip to collector distance and confirmed that bead formation occurred at low tip to collector distances [34]. Mazoochi *et al* also showed that increasing the tip to collector distance decreased the electrospun fibres diameter up to a point. The electrospinning stream had more exposure to the electric field and was thus stretched further resulting in a smaller diameter of fibre [34]. Further increase in the tip to collector distance in the experiment by Mazoochi *et al* yielded fibres with increased diameters. It is theorised that electric field was too weak at larger tip to collector distances [34].

2.3. Electrospinning Solution Parameters

Solution parameters deal with variations in the properties of electrospinning solution which can be used to control the morphology of electrospun fibres [2]. These parameters are [2]: 1) Solute concentration, 2) Molecular weight of solute, 3) Solution viscosity, 4) Surface tension and 5) Conductivity of solution. The molecular weight of the solute is fixed based on the type of nanofibres being electrospun [35]. The concentration, viscosity, surface tension and conductivity can all be controlled by modifying the solvent. The solution parameters are interdependent. The important parameters which change the morphology of electrospun fibres are the surface tension and the conductivity [36].

The surface tension may be controlled by varying the viscosity of the solution [36]. The results of at least three experiments point to surface tension being in inverse proportion to the solution viscosity [36], [37], [38]. The viscosity is in turn controlled by varying the solute concentration in the solvent [36], [37], [38]. Molecular weight also affects viscosity but this is constant for a particular solute. At least three independent experiments have shown that when the surface tension is high, a mixture of fibres and

droplets are electrospun. The high surface tension causes molecules on the outside of the electrospinning jet to move together breaking up the stream into droplets [36], [37], [38]. The experiment by Deitzel *et al* demonstrated that at low surface tension, the electrospun fibres had significantly non uniform diameters [36]. It was theorised that the surface tension was too low to hold the electrospinning jet in one stream so that secondary streams branched off from the main stream creating a number of fibres of smaller diameter [36].

High conductivity in the electrospinning solution was shown to increase the diameter of electrospun fibres by Mit-uppatham *et al* [39]. The conductivity is affected by the molecular weight of the solute and the number of ions present in the solution. The molecular weight is fixed but the number of ions in the solution can be altered by adding a salt/acid into the solution which will dissociate into ions (Example table salt with formula NaCl) [39], [40].

2.4. Ambient Parameters

Ambient parameters affecting the electrospinning process are the room temperature and the humidity level at which electrospinning takes place. There is very little experimental work done on the effects of temperature and humidity on electrospinning. One paper by De Vriez*et al* showed that humidity and temperature affected the evaporation rate of solvent from the electrospinning jet [41]. The experimentation documented therein demonstrated that some electrospinning solutions which have solutes which can absorb water produce nanofibres of smaller average diameters when electrospun under relatively high humidity levels [41]. The theory was that extra water meant that the jet would take longer to solidify due to the evaporation of solvent taking longer [41]. This longer flight time of the jet allows the electric field to stretch the jet further thereby creating fibres of a smaller diameter. If the humidity is too high however, the solvent will not completely evaporate before the jet reaches the collector and a web like film instead of fibres will be electrospun [41].

De Vrieze *et al* also revealed that both high and low temperatures have a similar effect on the electrospun fibres average diameter but achieved the effect by different mechanisms [41]. At a low temperature evaporation of the solvent from the electrospinning jet is slower therefore the electric field has more time to stretch the jet

to a smaller diameter. At high temperatures the viscosity of the solution is decreased allowing the electric field to have more influence on the electrospinningjet [41].

A study by Casper *et al* showed that electrospinning solutions which did not absorb water developed pores when the humidity level increased [42]. This was due to water droplets forming on the surface of the jet and then evaporating after the jet had hardened. The average diameter of the pores was shown to increase with the relative humidity by Casper *et al* [42].

2.5. Solutions Used in Electrospinning of Silica

The first attempt at using electrospinning to synthesise silica nanofibres was presented in 2002 in a paper by Shao *et al* [7]. Since then there have been a few variations of the methodology presented by Shao *et al*. The different variations produce silica nanofibres for with different morphology. Most of the existing methodologies for electrospinning silica nanofibres involve adding silica to a polymer solution and removing the polymer by calcinations after electrospinning. The silica can be introduced by preparation and addition of various chemicals to the polymer to be electrospun.These chemicals include tetraethoxysilane (TEOS) which needs to be hydrolysed before use, Silatrane which needs to be prepared as a powder before use and spin on glass (SOG). No other means of introducing silica into an electrospinning solution have been attempted at the time of writing of this review.

2.5.1. Spin on glass (SOG)

Spin on glass was first used to create silica nanofibres in 2004 by Kameoka *et al* [43]. The resulting silica nanofibres were tested as mechanical oscillators. The preparation of the electrospinning solution was simply adding Poly(Vinyl Pyrrolidone) (PVP) to SOG intermediate coating solution [43]. The resulting nanofibres were calcinated above 200^0C to vaporise the PVP [43]. A second experiment by Wang *et al* used a similar set up and the same electrospinning solution but used a second syringe to insert oil into the centre of the electrospinning jet, creating silica nanotubes [10]. X ray diffraction in both experiments showed that the polymer was not completely removed by calcination [10], [43].

2.5.2. Silatrane

Silatrane is a white powder which has to be produced in a lab [44]. It is produced by mixing pure amorphous silica into a solution with ethylene glycol and triethanolamine

[44]. The solution must be heated and the excess ethylene glycol must be removed leaving the white silatrane powder as a precipitate [44]. Silatrane has only been used in an electrospinning solution in one experiment by Krissanasaeranee *et al*. The silatrane powder was put in solution with water and PVA to create the electrospinning solution. The results of the experiment by Krissanasaeranee *et al* revealed that the use of silatrane as a source of silica favoured the formation of silicon carbon bonds and even some silica crystals above a certain calcination temperature.

2.5.3. Tetraethoxysilane (TEOS)

The chemical used most commonly to introduce silica particles to an electrospinning solution is TEOS. In order to prepare TEOS for electrospinning it has to be hydrolysed by adding an acid such as phosphoric acid or hydrochloric acid [7], [8]. TEOS has been electrospun in conjunction with polyvinyl alcohol (PVA), polyvinyl pyrrolidone (PVP) and even in a sol gel state without a polymer.

In an experiment by Zhao *et al*, TEOS was electrospun with the polymer PVP [8]. Hydrochloric acid was used to hydrolyse the TEOS in this case [8]. In addition to the existing solution a triblock copolymer was included. The triblock copolymer was found to give the electrospun silica nanofibres a mesoporous structure after calcination [8].

Choi *et al* presented results of an experiment where a silica sol was used as the electrospinning process [45]. This was the only experiment where an inorganic compound was electrospun without the presence of a polymer. The silica sol was prepared from TEOS, ethanol, hydrochloric acid and water [45]. The electrospun silica nanofibres did not require calcinations since no polymer was used in the solution. The experimental procedure used by Choi *et al* has the fastest execution time from start to finish. The disadvantage of using this method is that silanol containing hydroxyl groups will be prevalent in the electrospun fibres [45]. The hydroxyl groups give the silica nanofibres a hydrophilic property which is not suitable for use in high voltage dielectrics since it decreases the breakdown strength.

When TEOS is electrospun with PVA, the solvent used is water. Phosphoric acid is added in order to hydrolyse the TEOS [7]. TEOS electrospun in solution with Poly(Vinyl Alcohol) (PVA) shows the most promise for application as a dielectric. An experiment by Shao *et al* showed that when calcination was performed on the electrospun silica/PVA composite fibres at a sufficiently high temperature (550^0C), all

traces of the polymer were removed [7]. This method is also attractive due to no hydroxyl groups in the form of silanol being formed in the electrospun fibres. This means that the fibres will have a hydrophobic nature (will not absorb water). This is important for high voltage electrical applications since the presence of water in a dielectric weakens its breakdown voltage. The downside to this method is the same as for most of the other methods: A long calcination time is needed [7]. One of the early aims of the experimentation presented in this dissertation was to replicate the work of Shao. The relevant reactions involving TEOS were therefore investigated. These included the hydrolysis reaction and the catalysing of the hydrolysis reaction.

TEOS has a chemical formula of $Si\ (OC_2H_5)_4$[46]. TEOS belongs to a group of chemicals called alkoxides which consist of oxygen and an ethyl group (denoted by *Eth* in Equations (1) through (3)) [47]. An alkoxide containing silicon (such as TEOS) is called an alkoxysilane. Alkoxysilanes react with water to produce polymeric species containing oxygen and silicon atoms. Three main half reactions are responsible for the production of these polymeric species [47], [48], [49]: 1) Hydrolysis (forward half in equation (1)), 2) Alcohol Condensation (forward half in Equation (2)) and 3) Water condensation (forward half in Equation (3)).

$$\equiv Si - OEth + H_2O \rightleftharpoons \equiv Si - OH + EthOH \quad (1)$$

$$\equiv Si - OEth + HO - Si \equiv \rightleftharpoons \equiv Si - O - Si + EthOH \quad (2)$$

$$\equiv Si - OH + HO - Si \equiv \rightleftharpoons \equiv Si - O - Si \equiv + H_2O \quad (3)$$

The *Si-O-Si* bonds formed join together in chains over time resulting in solid SiO_2 [50]. The end result of making a silica sol should be a colloidal solution of silica nanoparticles (10-100nm diameter) suspended in water. Water and TEOS are rarely mixed without other chemicals being added. This is because the reaction rate is very slow and water does not mix with TEOS [51]. The reactions can therefore only occur at the interface between water and TEOS. A catalyst is needed [51].

The presence of H^+ ions (from the addition of an acid) catalyses the hydrolysis reaction [51]. Addition of an acid also decreases the pH of a solution. It has been shown that bat low pH levels the rate of the reverse half reaction in Equation (3) becomes negligible [50]. This promotes the formation of silica nanoparticles in the sol [50]. Strong acids (e.g. Phosphoric Acid, Hydrochloric Acid and Sulphuric Acid) are generally used to

catalyse the reaction between TEOS and water since experimentation has shown that weaker acids such as acetic acid have a lesser effect [50].

Water combined with the acid catalyst being used in this study (Phosphoric Acid) is not miscible in TEOS. The reaction could therefore only take place at the boundaries between the two clear liquids [52]. Absolute ethanol is miscible in all 3 chemicals therefore its addition allows the aqueous phosphoric acid and water to form a homogenous solution with TEOS upon mixing for a short period [52], [11]. It is possible for the reaction to occur without ethanol but this takes 5 hours of continuous mixing [7], [51].

2.6. Simulation of the Electrospinning Process

Modelling of the electrospinning process is challenging due to the large number of factors affecting the process of electrospinning. Not all of these factors can be accounted for accurately. There have nevertheless been a few attempts at modelling parts of the electrospinning process individually and the entire process. The electrospinning process may be split into three sections, each of which can be modelled separately. These sections are: 1) Initiation of the jet, 2) The stable portion of the jet, 3) The instability portion of the jet.

2.6.1. Initiation of the jet

There is one important output in any jet initiation experiment or simulation. This output is the critical voltage above which the electrospinning process will begin (jet initiation occurs). If it is assumed that the spinneret is facing vertically downwards, there are three forces which act on a drop of solution at the tip of the spinneret[53]: 1) Gravity, 2) The force of the electric field and 3) The force of surface tension. For spinnerets with very small diameters, as is the nature of spinnerets in electrospinning, the force of gravity becomes negligible. The force of surface tension opposes the force of the applied electric field. In order to initiate the electrospinning jet the force of the electric field must exceed the surface tension of the droplet.

There is limited literature available on the force exerted by an electric field on a fluid in a spinneret. Sir Geoffrey Taylor Published a paper on this particular force in 1966. In his paper he developed Equation (4) [54].

$$F_e = \frac{V^2 L^2}{4H^2 \ln(\frac{2L}{R}) - \frac{3}{2}} \quad (4)$$

Where,

F_e= Force of the Electric Field

V = Applied Voltage

L = Length of Capillary

R = Radius of Capillary

H = Distance between High Voltage Electrodes

Equation (4), however, only applies to parallel plate electrodes with the capillary (spinneret) inserted through the middle of one of the electrodes. The equation was however proven to be fairly accurate by comparison to experimental results [53]. In a later paper in 1969, Sir Geoffrey Taylor went on to calculate the critical voltage at which jet initiation occurs. This was done by first calculating the force of surface tension using Equation (5) [53].

$$F_\gamma = 2\pi R\gamma \cos\alpha \quad (5)$$

Where,

F_γ = Force of Surface Tension

α = Surface Tension

φ = Angle of Attachment

The unit used for surface tension was dyn/cm (1 dyn = 10^{-5} N). The angle of attachment is the angle at which a curved surface of a droplet makes with the end of the spinneret. It was found that as the critical voltage was reached, the angle of attachment became equal to 49.3^0[53]. Substituting for the angle of attachment and equating F_γ from (5) and F_e from (4), Taylor derived an expression for the critical voltage of electrospinning. The expression is shown in Equation (6) [53].

$$V_C = \sqrt{\frac{4H^2}{L^2}\left(\ln\frac{2L}{R} - \frac{3}{2}\right)(1.3\pi R\gamma)(0.09)} \qquad (6)$$

The factor of 0.09 was added so that the calculated voltage would be in kilovolts. Taylor explains that (6) is not an exact solution but can provide a guideline to the voltage range which should be tried in experimentation [53].

Equation (6) allows calculation of the critical voltage of electrospinning based on 4 parameters. A MATLAB code was written to vary each of these parameters while holding the other three parameters constant to see the effect on the critical voltage. The first parameter to be varied was the radius of the capillary from 0 cm to 0.1 cm. The surface tension was held at 29 dyn/cm. The distance between electrodes was held at 10 cm. The length of the capillary was held at 1.66 cm. The radius is a parabolic function of the critical voltage (see Figure 2.2).

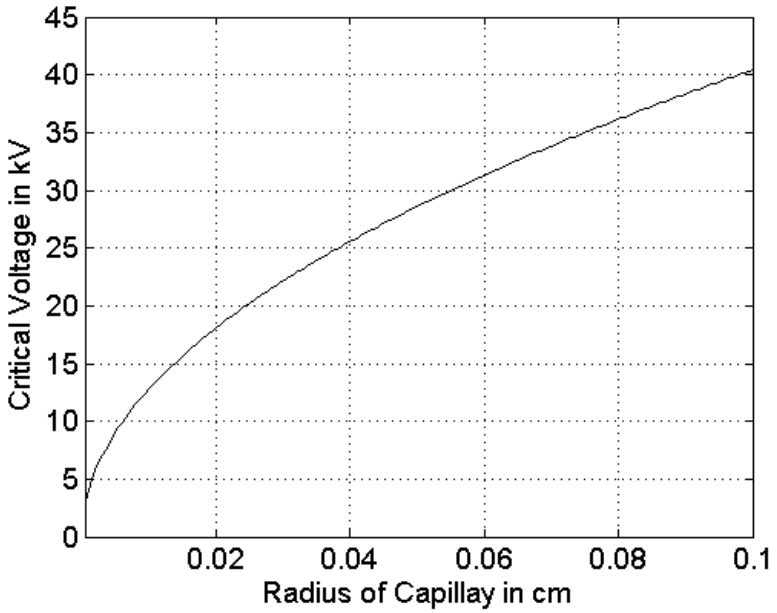

Figure 2.2: Critical Voltage as a Function of Radius of Capillary

For the variation of capillary length from 0 cm to 3 cm its radius was held at 0.05 cm. The surface tension and distance between electrodes were held at 29 dyn/cm and 10 cm respectively. It was found that the critical voltage decreases as the length of the capillary increases but for impractically low capillary lengths the critical voltage also decreases (Figure 2.3).

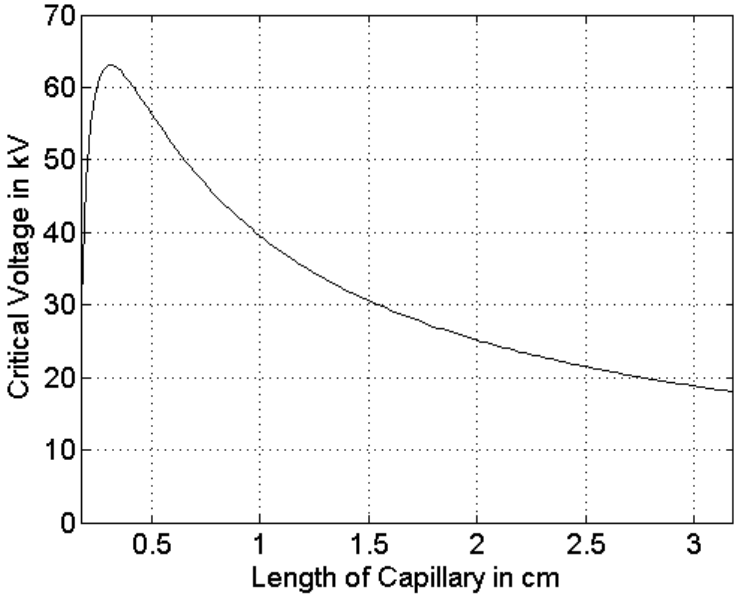

Figure 2.3: Critical Voltage as a Function of Length of Capillary

The distance between the electrodes was varied from 0 cm to 20 cm which would be impractical since the length of the capillary was held at 1.66 cm which was greater than 0 cm. The surface tension and radius of capillary were held at 29 dyn/cm and 0.05 cm respectively. The distance between electrodes was found to be directly proportional to the critical voltage (Figure 2.4).

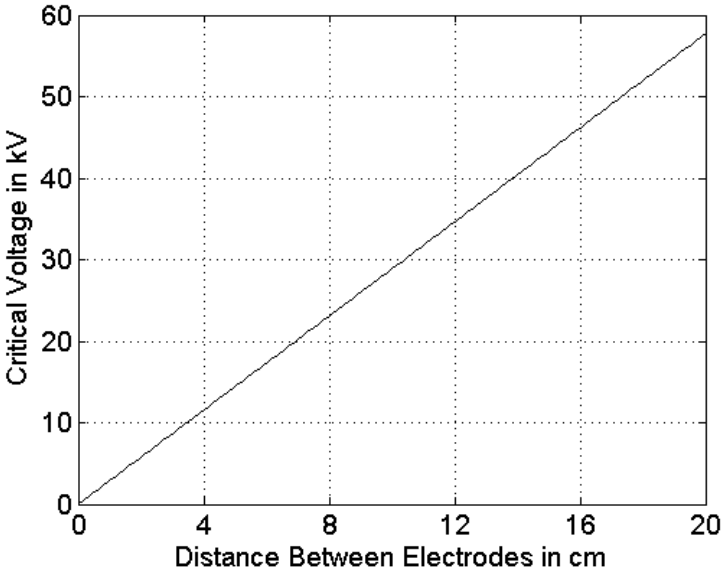

Figure 2.4: Critical Voltage as a Function of Distance between Electrodes

The surface tension was varied from 0 dyn/cm to 400 dyn/cm. The capillary length, capillary radius and distance between electrodes were held at 1.66 cm, 0.05 cm and 10

cm respectively. The critical voltage was a power function of the surface tension (Figure 2.5).

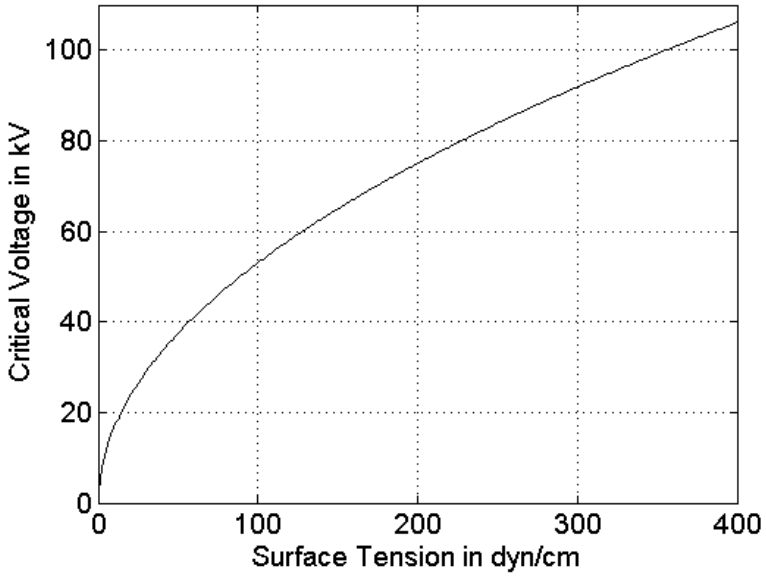

Figure 2.5: Critical Voltage as a Function of Surface Tension

Surface tension can be calculated using the pendant drop test (Figure 2.6) [55].

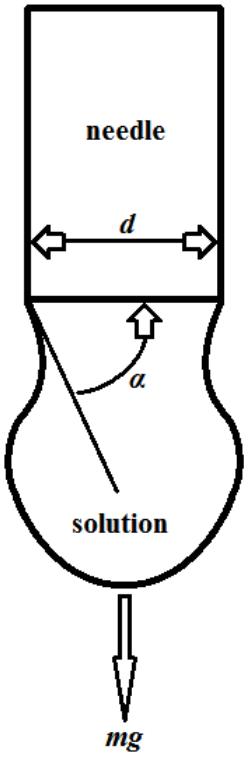

Figure 2.6: Zoomed in blunt needle tip with droplet showing dimensions and forces relevant to the pendant drop test

In the pendant drop test the mass of a droplet at the tip of a cylinder is related to the surface tension of the liquid being tested by Equation (7) [55]. The equations left hand side represents the force of gravity on the droplet while the right hand side represents the force of surface tension. When a droplet falls from a needle the force of gravity must have become greater than the force of surface tension. At the point when the droplet starts to fall the two forces can be equated so that the surface tension can be calculated.

$$mg = \pi d\gamma sin\alpha \tag{7}$$

Where,

m = mass of droplet in kg

g = gravitational acceleration (9.8 m.s^{-2})

d = inner diameter of cylinder in mm

γ = surface tension in N/mm

α = angle of attachment

2.6.2. Stable section of jet

Research into the stable section of the electrospinning jet was done by Spivak *et al* [56]. The important output variable which was considered was the radius of the electrospinning jet as a function of distance from the spinneret. The forces considered in the experiment were [56]: 1) Inertial, 2) Surface tension, 3) Electrostatic and 4) Viscous. The gravitational forces were neglected due to gravity having a negligible effect when the jet has small initial diameter (45μm in the case of the model and experiment presented by Spivak *et al*) [56]. The main variable inputs to the model were [56]: 1) Current density, 2) Average electric field and 3) Initial radius. Equation (8) is the differential equation used by Spivak *et al* to calculate jet radius for a particular point on the jet [56].

$$\frac{d}{d\overline{Z}}\left\{\overline{R}^{-4} + \left(N_W \overline{R}\right)^{-1} - N_E^{-1}\overline{R}^2 - N_R^{-1}\left(\frac{d\overline{R}}{d\overline{Z}}\right)^m\right\} = 1 \tag{8}$$

Where,

$\overline{R}$ = Normalised Radius

$\overline{Z}$ = Normalised Position on the Vertical Axis through a Vertical Electrospinning Jet

m= Flow Index

N_E, $N_W$and $N_R$are dimensionless inertial ratios to electrostatic forces, surface tension forces and viscous forces respectively [56]. Each ratio is defined by its own equation dependant on both volumetric flow rate (calculated from current density and initial radius) and current density [56]. The experimental results obtained by Spivak *et al* compared well to their simulated results. The disadvantage of this simulation was that the final diameter of the electrospun fibres could not be determined. The model only works up to the point when whipping instability occurs.

2.6.3. Complete jet modelling

When modelling of instability in electrospinning was considered, the entire jet was modelled rather than the unstable section only. This is because the point at which the instability became significant is important. The existing models for complete jet modelling can be categorised into those which model the jet path so that the simulated path resembles a practical electrospinning jet and those which model possible causes of disturbances leading to jet instability.

2.6.4. Jet path modelling

Among the first to attempt modelling of the entire electrospinning jet was Reneker *et al* in 2000. Reneker *et al* developed a model which showed that when Coulombic forces exceeded the surface tension in the horizontal direction (assuming vertical electrospinning) whipping instability occurred [57]. Coulombic forces in the model could only increase when a disturbance (a section of the jet moved a small distance so that a bend exists in the jet) was present in the electrospinning jet [57]. This was due to the fact that coulombic forces in the horizontal direction can only occur when the jet is not perfectly vertical. The disturbance was inserted at the point of delivery of solution [57]. The model by Reneker *et al* gave an insight into the possible mechanics of jet instability and focused on reproducing the jet path of electrospinning. The origin of the disturbance however could only be theorised. The model also produced a jet path in which the whipping instabilities were much closer together than in practical electrospinning [57].

In 2001 Yarin*et al* added evaporation of solvent and solidification of the jet to the Renekker*et al* model [58]. This increased the spacing between instabilities making the modelled jet path closer to practical electrospinning results. These added quantities realistically could not be measured [58]. The simulation inputs were therefore guessed.

2.6.5. Possible causes of disturbance to the jet

The model by Hohman*et al* in 2001 concentrated on the effects of surface charge density on the electrospinning jet [59], [60]. It was found that interaction between the electric field and surface charge created instabilities. High surface charge in the model resulted in whipping instability while low surface charge density resulted in axisymmetric instability (formation of areas of increased/decreased jet diameter)[59], [60]. A measure of the effect of surface charge density on jet instability could not be practically quantified [59], [60]. Further work on the effects of the electric field on instability was done on a model by Feng in 2002. The model by Feng also highlighted upstream effects in the spinneret as possible causes of disturbances [61].

2.7. Methods of Nanofibre Characterization

Various methods of characterizing nano materials exist. The methods commonly used can be divided into chemical characterization, morphological characterization and mechanical characterization.

2.7.1. Chemical characterization

Chemical characterization involves determining the chemical composition of a sample. Some techniques used include carbon nuclear magnetic resonance spectroscopy (C-NMR), X-ray diffraction (XRD), X-ray photoelectron spectroscopy, Fourier transform infra-red (FTIR), and elementary analysis [62]. From various journal publications cited in this thesis, it is clear that the most commonly used methods of chemical characterization for nanofibres are XRD and FTIR. These techniques are useful since they do not destroy sample materials so that the same sample may be used in other tests afterwards [62].

FTIR makes use of the infra-red spectrum to determine the composition of samples [63]. A beam of infra-red light is directed at a sample. The sample absorbs certain frequencies in the infra-red spectrum [63]. The remaining frequencies are detected by a sensor. Different materials absorb different parts of the spectrum therefore, based on

which frequencies are absorbed, the compounds present in the sample can be determined [63].

XRD uses X-ray radiation to determine the composition of samples [64]. A sample is bombarded with X-rays to get it to emit secondary radiation [65]. The secondary radiation is measured in terms of angle and intensity [65]. The materials present in a sample are determined based on which angles of radiation are measured [65]. The intensity is an indication of how much of a particular material is present [65].

2.7.2. Morphological characterization

Morphological characterization deals with the physical appearance of a sample [66]. Due to the small size of nano materials, only an electron microscope is suitable for analysing appearance. Most experiments dealing with nanofibres make use of a scanning electron microscope (SEM) to analyse the morphology of fibres. A scanning electron microscope bombards samples with electrons which bounce off the sample onto a detector [67]. In this way an image of the sample is formed by the microscope. Typically nanofibres are morphologically characterized by the average diameter of a number of fibres in a sample.

2.7.3. Mechanical characterization

Mechanical characterization deals with the mechanical properties of samples. According to the review published by Tan *et al* [68], three types of mechanical testing have been done on nanofibres. These include: 1) Nano-tensile testing, 2) Bend testing and 3) Nano indentation.

Nano tensile testing allows a stress vs. strain curve to be developed for a nanofibre[68]. It involves pulling a fibre from one end while the other end is fixed until the fibre fails [68]. Testing can be performed inside an electron microscope (in situ) or outside [68]. In situ testing was performed by Haque*et al* by developing a micro cantilever system operated by the piezoelectric effect [69]. After this in 2005, Tan *et al* performed a nano tensile test externally by using a cantilever setup as the collector plate in an electrospinning experiment [70]. The fibres deposited on the cantilever were cut until only one remained.

In order to obtain the Young's modulus of a nanofibre, a three point bend test may be conducted [68]. To perform a three point bend test a nanofibre has both its ends fixed

while a force is applied to its centre. Such an experiment was performed by Lee *et al* by using an atomic force microscope (AFM) [71]. The atomic force microscope has a pyramidal tip which can apply a force to the centre of a fixed fibre [71].

The elastic modulus of a fibre can be obtained from nano indentation [68]. A nano sized point (usually inside an AFM) is used to indent a fibre by a certain distance [72]. The depth of the indent after the point is removed can be used to calculate hardness and elastic modulus [72]. Nano indentation inside an AFM was performed by Chen *et al* [72].

2.8. Impedance Spectroscopy

Impedance spectroscopy is the measurement of the impedance of a material over a range of applied voltage frequencies. The technique was first used on electrospun nanofibres by Myat in 2013 [73]. Myat utilized a frequency analyser to measure various electrical quantities over a range of frequencies.

3. EXPERIMENTAL SETUP

The apparatus used in the research presented in this thesiswere designed, procured or available in an accessible laboratory. Four main groups of apparatus were used in four tasks. These were: 1) Mixing the electrospinning solution, 2) Electrospinning of the solution to create nanofibres, 3) Characterizing the composition and morphology of the nanofibres and 4) Performing impedance spectroscopy on the nanofibres.

3.1. Apparatus Used to Mix Electrospinning Solution

Muchequipmentwas utilized in producing the electrospinning solution. An important apparatus was the fume hood. A fume hood had to be used since some of the chemicals being used such as TEOS and Phosphoric acid are dangerous when inhaled (according to their MSD sheets). A hot plate stirrer was used to agitate all the solutions involved while simultaneously heating them. Every step in the process of making the electrospinning solution required heat and agitation for a period of time. To measure the mass of each chemical being used, a mass balance and syringes were used. The syringes were necessary since some of the chemicals needed to be added drop wise to a solution. Beakers of various sizes contained the different solutions while they were being agitated by the hotplate stirrer. When the solution was ready for electrospinning it was placed into 50ml plastic vials with caps and stored in a fridge.

3.2. Electrospinning Apparatus

The initial apparatus consisted of a syringe driven by a syringe pump, a square 10cmx10cm solid copper collector plate which was connected to ground and a high voltage DC generator (flyback converter) which would provide high voltage to the syringe. Various parts of the setup had to be modified for optimisation purposes or due to circumstance.

3.2.1. Design of copper collector plates

The copper collector plates were designed so that no corona would occur on them. For this purpose all the edges were rounded with 0.5cm radius as shown in Figure 3.1. These plates were created using CNC milling. An upper plate was made initially with a hole in the centre for the needle so that the calculation of critical voltage of electrospinning could be tested. This was removed since some of those voltages were unattainable with the DC power supply built.

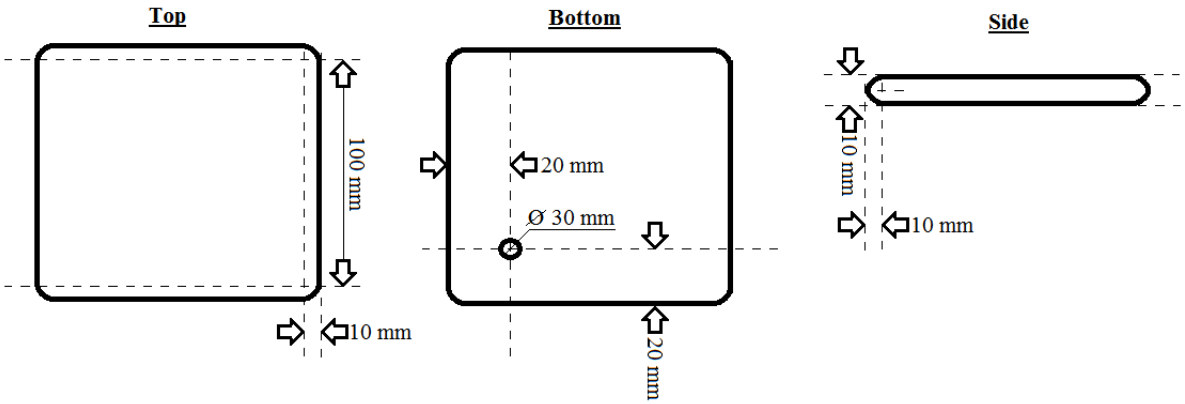

Figure 3.1 : Different views of a copper plate used as a collector in the electrospinning setup

The 30mm hole on the bottom of the plate was threaded so that a lug may be screwed in for connection of ground.

3.2.2. Design of perspex housing

The perspex housing consists of two pieces, a stand and a cover. Three stands were made with different heights (10, 15 and 20cm) for variable tip to collector distance. The stands were square on the top with each side measuring 10cm so that the edges of the copper plates would sit in line with the edges of the stand. Each stand had a hole for the ground cable to pass through to the threaded hole on the copper collector. The cover was built so that its inner dimensions were 10cm x 10cm. The purpose of the cover is to mitigate interference to the jet path (air flow from the lab air conditioning, dust particles in the lab etc.).

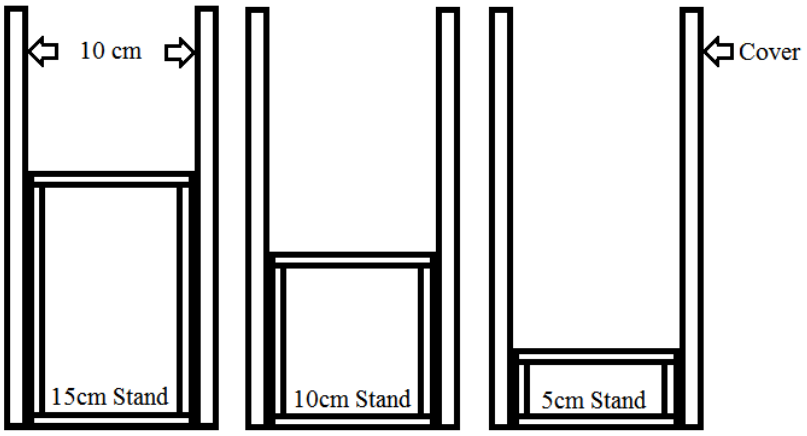

Figure 3.2: Line drawing of the perspex housing used to keep dust and significant air flow from interfering with the electrospinning process

3.2.3. Optimisation of solution delivery system

Solution was delivered to the spinneret using a syringe pump. Initially significant corona appeared on the syringe pump servo motor. In order to determine parameters which could be adjusted to mitigate corona, an equivalent circuit of the electrospinning setup was drawn (Figure 3.3).

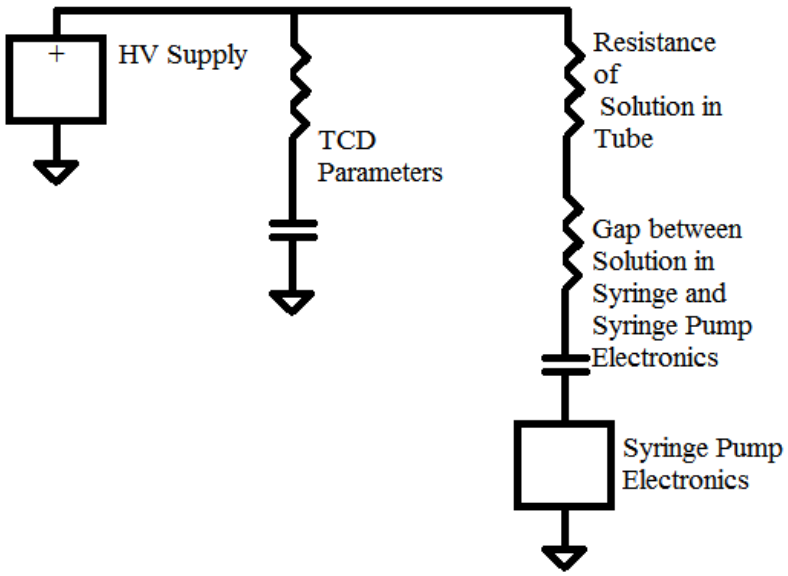

Figure 3.3: Equivalent circuit of the electrospinning setup showing different parts modelled as resistors or capacitors connected in series or parallel

The distance between spinneret and the copper collector also known as the tip to collector distance (TCD) and solution-syringe pump gap were modelled as capacitances and resistances while the solution was modelled as a resistance. In order to reduce the potential appearing on the syringe pump electronics the resistance of the solution in the syringe was increased by adding a length of tubing between the syringe and the needle. This allowed the solution to take the majority of voltage potential so that corona inception could not occur on the syringe pump electronics.

3.2.4. Design of high voltage supply

The requirements for a high voltage DC supply to be used in electrospinning experiments in this study are as follows: 1) The voltage output should be controllable, 2) The voltage output should remain constant at the any selected value, 3) The voltage ripple should be minimal, 4) Selected voltage values should be reproducible in multiple experiments and 5) The maximum voltage output should not be lower than 12kV

A voltage supply with these characteristics could not be made available in a suitable time frame therefore a supply was designed and constructed using equipment and parts

readily available in the high voltage laboratory. The various types of high voltage DC supplies which were considered for construction are: 1) Switch mode DC power supply, 2) Walton Cockcroft voltage multiplier and 3) Flyback converter. All supplies use 220V single phase power or 400V phase to phase 3 phase power because those are the only sources available in the HVDC lab.

The Switch mode power supply operates in stages. The first stage rectifies AC into DC [74]. The DC is then inverted to high frequency AC in the next stage [74]. The final stage rectifies the high frequency AC to DC [74]. A switch mode power supply works in this manner because rectifying high frequency AC as opposed to 50Hz AC mitigates ripple voltage [74]. The output voltage is controlled by varying the firing angle of the semiconductor devices in the final rectifier [74]. A switchmode supply was not available for use in the lab at the time of the experimentation and would have been costly and time consuming to construct or buy.

The Walton Cockcroft voltage multiplier uses a number of voltage doubler circuits to convert AC input into the circuit to high voltage DC [75]. This supply requires a variac to control the output voltage by controlling the AC input voltage [75]. The available Walton Cockcroft high voltage multiplier did not have sufficient accuracy in terms of setting a voltage level.

A flyback converter works on the principle of a buck-boost chopper. It uses a diode on the output of a transformer to achieve inductor like behaviour. A transformer which has this setup is known as a flyback transformer and can be easily obtained from any old cathode ray tube device. The first stage of a flyback converter outputs pulsed DC using a semiconductor switch to switch in a DC source at high frequency [76]. The second stage consists of the flyback transformer. It needs an input of high frequency pulsed DC to output high voltage steady DC [76]. The flyback converter was viable to construct because of the availability of parts and the fact that some of the complicated circuitry for triggering the semiconductor switch could be replaced by a function generator which was available for use in the lab. The flyback converter had more exact control over its voltage output than the Walton Cockroft high voltage multiplier.

The basic circuit for a flyback converter is very similar to that of a buck boost chopper (Figure 3.4).

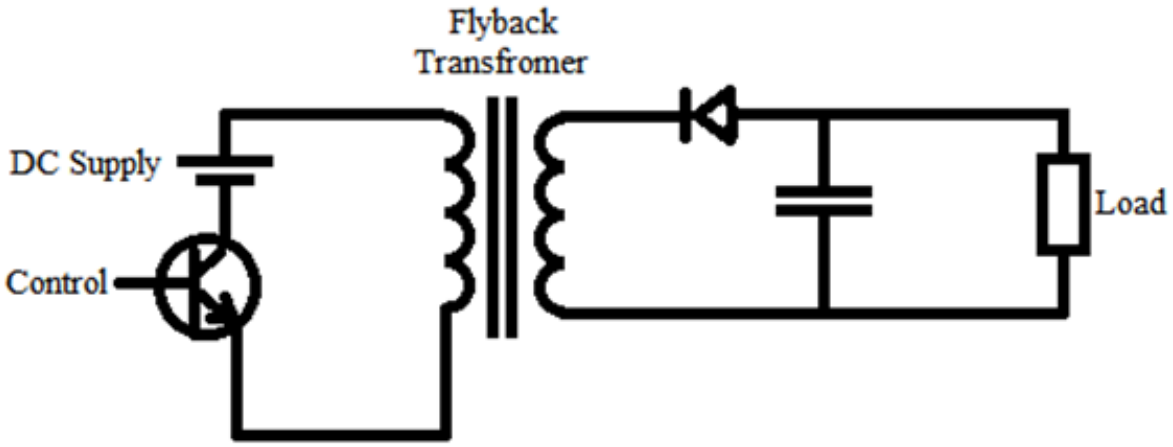

Figure 3.4: Flyback converter high voltage DC supply basic circuit

The control signal applied is usually high frequency pulsed DC set to an on state voltage specific to the semiconductor switch being used. Only continuous conduction mode allows for a relatively steady DC output from the flyback converter so only it will be discussed [76]. In continuous conduction mode there are two states of interest from the control signal, the on and off states [76].

In the on state the semiconductor switch will be forward biased allowing the DC supply to give current to the primary coil of the flyback transformer [76]. The diode on the output of the secondary coil becomes reverse biased and prevents the flow of current [76]. The secondary coil simply stores the energy from the DC supply. For the on state the basic flyback converter circuit can be simplified so that a short circuit appears in place of the semiconductor switch and an open circuit appears in place of the diode (Figure 3.5). In this state the capacitor discharges any stored charge to the load [76].

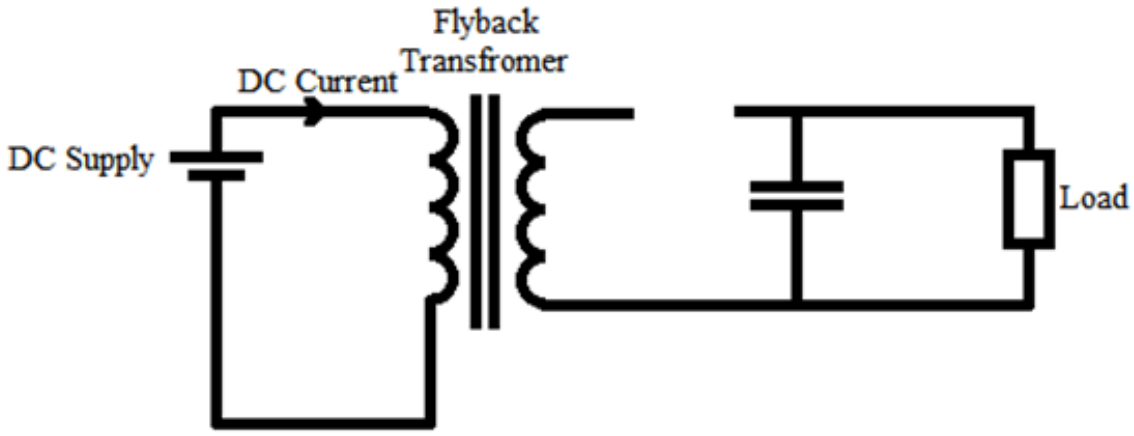

Figure 3.5: Flyback converter on state

In the off state the semiconductor switch will be reverse biased, open circuiting the DC supply as shown in figure 3.6 [76]. The energy in the secondary coil of the flyback transformer now discharges with reversed polarity. This causes the diode to be forward biased allowing the load to receive current [76]. The capacitor charges during the off state. The duty cycle of the pulsed DC has to be high enough to prevent the secondary coil from completely discharging before the next on state [76].

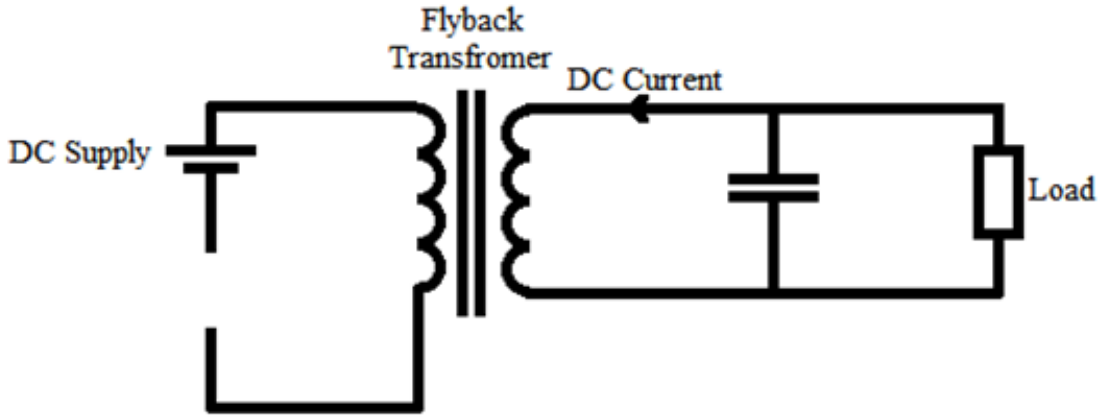

Figure 3.6: Flyback converter off state

In the first stage of the flyback converter a semiconductor device is needed to switch a DC supply at high frequency. A high voltage BJT was used as the semiconductor switch. Its control signal was produced from a function generator. The design considerations were to: 1)Ensure the base-emitter voltage of the BJT was within the ratings of the BJT, 2) Manage the voltage spike caused by leakage inductance in the primary of the flyback transformer, 3) Find a frequency and duty cycle at which the maximum steady DC output voltage could be obtained from the output of the flyback transformer and 4) Minimize the percentage ripple voltage in the output.

The base-emitter junction in the BJT had to be saturated in order for the BJT to switch on. The saturation voltage for the base-emitter junction for the BU508D BJT being used is 1.5V and the absolute maximum voltage is 5V. The output of the function generator was set to a peak voltage of 3V. A 10Ω resistor was placed in series with the base terminal in order to limit current draw from the function generator (maximum current 1A) since the BJT could draw up to 2.5A from its base.

The BJT being used has a reverse blocking voltage of 1500V. This is more than sufficient to deal with the 700V voltage spike on turn off. The voltage spike creates a

small oscillation due to resonance with stray capacitances. The design can possibly be further optimised by introducing a voltage clamp on the collector of the BJT.

The optimal frequency and duty cycle of the flyback converter were determined by varying them through the function generator and monitoring the output on an oscilloscope. It was found that the duty cycle had a significant effect on the voltage ripple. Ripple up to 8kV could be obtained at low duty cycle percentages (below 20% duty). Duty cycles higher than 80% duty resulted in a drop in output voltage. The best trade-off between ripple voltage and output voltage magnitude was 50% duty. The frequency was increased in steps of 5 kHz in order to determine which frequency yielded the highest output voltage.

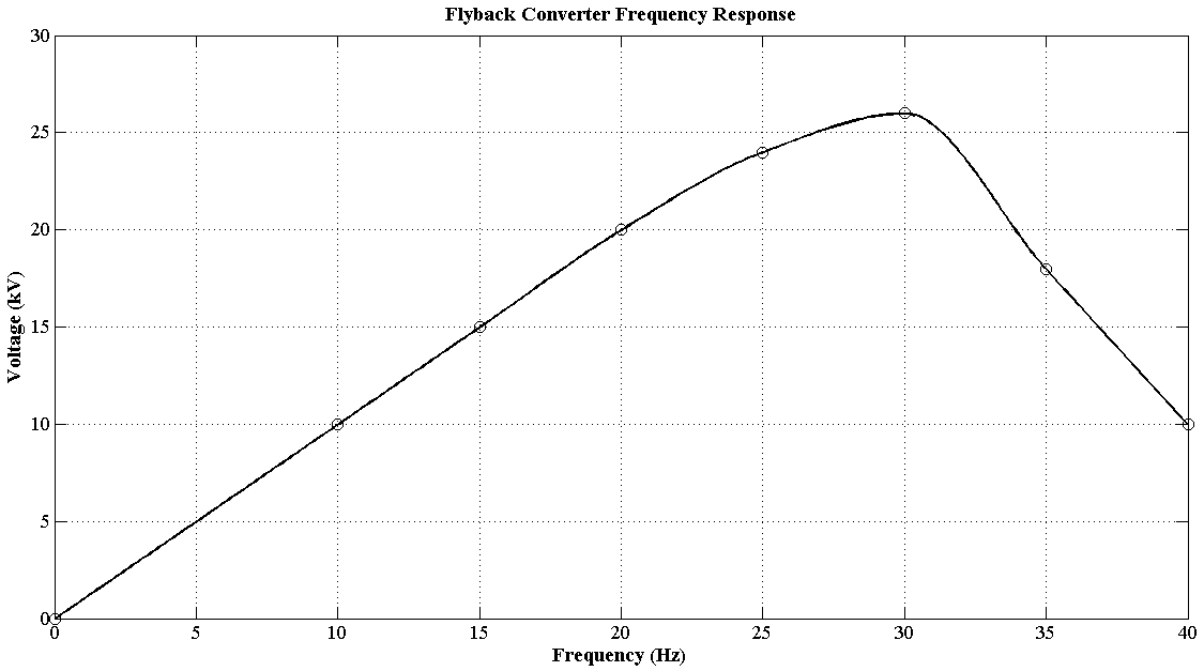

Figure 3.7: Frequency response of flyback converter for input frequency from a function generator showing peak output at 30 kHz

A frequency of 30 kHz was found to be optimal from Figure 3.7. Ripple voltage measurements were taken at the maximum possible voltage. The ripple voltage with no output capacitance was measured to be almost 2.75kV peak to peak (Figure 3.8). This was unacceptably high. Output capacitance (in parallel with the load) was added in order to smooth the output voltage.

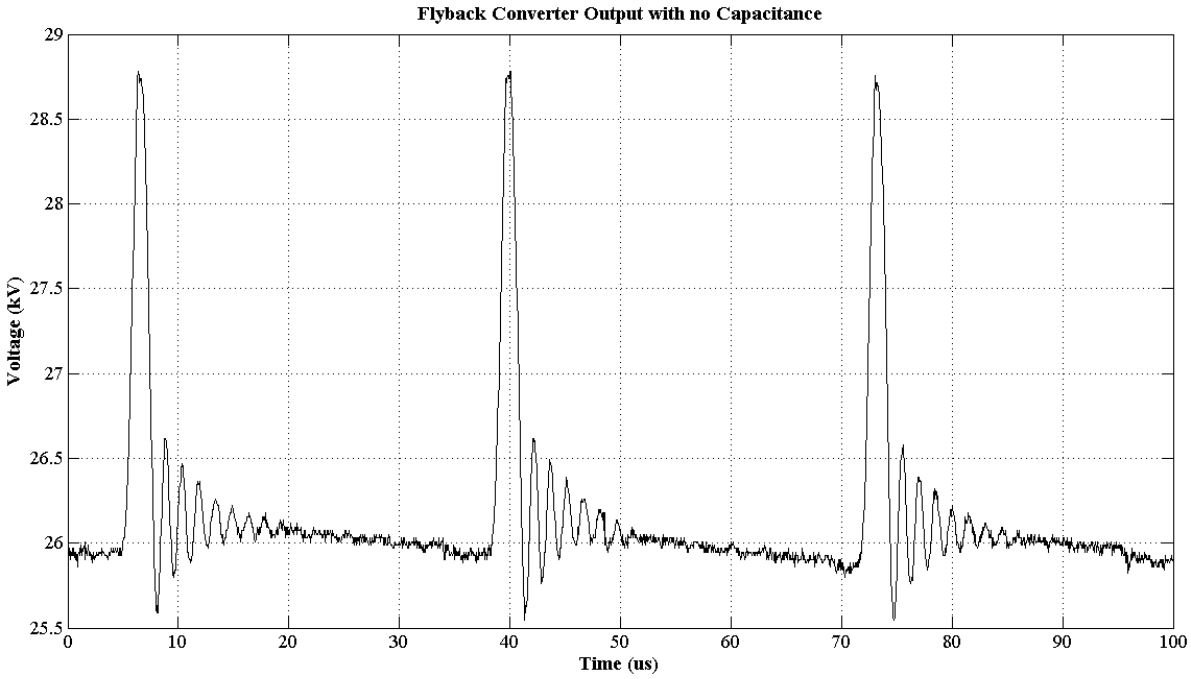

Figure 3.8: Flyback converter output with no parallel capacitors

Initially a capacitor bank of 1.5μF was added. This capacitance was too high since it slowed down the converter rise time to such an extent that it never ramped up. The capacitor bank was tested using a capacitance meter to confirm its capacitance and to confirm the capacitors were in working condition. High voltage capacitors with significant capacitance were unavailable. Low capacitances of 2nF (Figure 3.9) and 4nF (Figure 3.10) were tested. These yielded good results with the 4nF capacitor cutting the voltage ripple to about 700V.

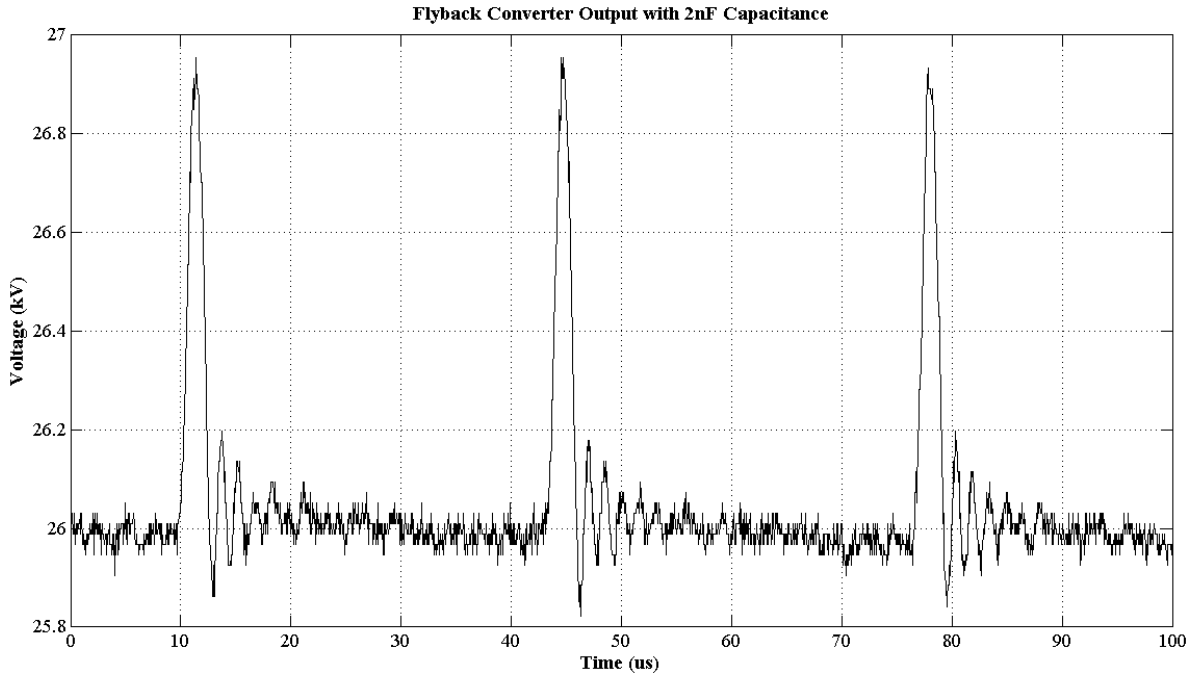

Figure 3.9: Flyback converter output with 2nF capacitor in parallel

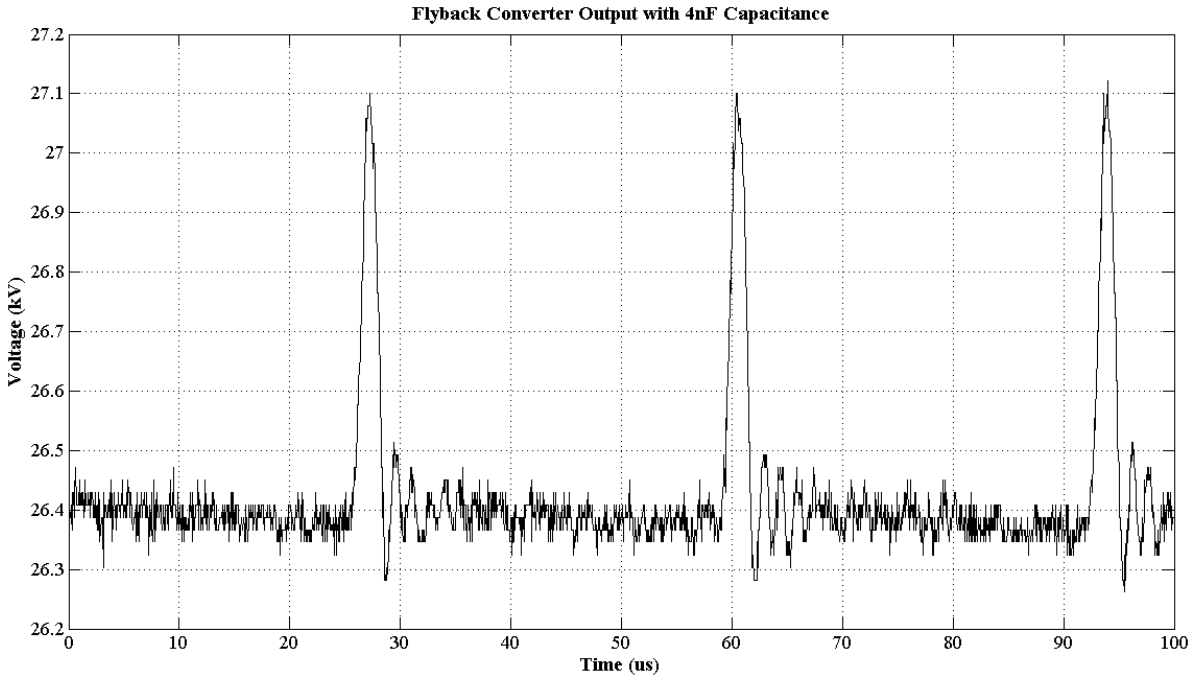

Figure 3.10: Flyback converter output with 4nF capacitor in parallel

Eventually a 100nF high voltage capacitor became available and it was able to bring the ripple voltage down to 340V which equates to approximately 1.3% ripple (Figure 3.11).

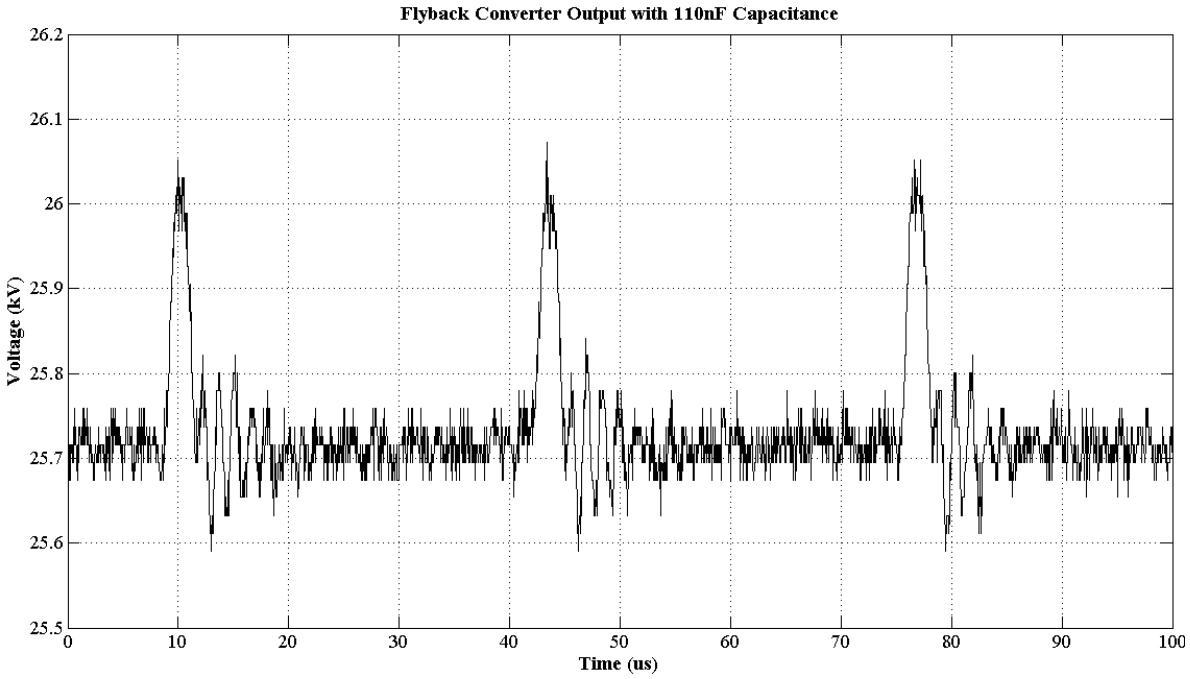

Figure 3.11: Flyback converter output with 100nF capacitor in parallel

3.3. Apparatus Used for Nanofibre Characterization

For morphological characterization, a Zeiss scanning electron microscope was used. A Perkin Elmer Spectrum RX I FT-IR infra-red spectrometer was used to perform FTIR so that the composition of electrospun nanofibres could be determined.

To perform impedance spectroscopy, a test setup was designed. A function generator was used to apply a sin wave of varying frequency to nanofibre samples. The current output from the samples were measured using a Yokogawa signal explorer oscilloscope.

4. EXPERIMENTAL PROCEDURE

The experimental procedure for producing nanofibres and performing impedance spectroscopy on them includes: 1) Producing the solution to be electrospun, 2) Electrospinning the solution, 3) Ensuring the fibres are of acceptable diameter and composition and 4) Performing impedance spectroscopy. Each of these sections are discussed in detail. The discussion explains the procedure used and any optimizations performed on the procedure and/or test setup.

4.1. Mixing the Solution (Precursor) to be Electrospun

The chosen method of fabricating the precursor using Poly (Vinyl Alcohol), TEOS, phosphoric acid and water had to be modified since the original method proposed by *Shao et al* was too long (required one day for one batch). The reagents used were: (a.) Tetraethoxysilane (TEOS) 98% Reagent Grade, (b.) 98% pure phosphoric acid crystals, (c.) 99.9% pure lab grade absolute ethanol, (d.) 99% hydrolysed Poly(vinyl alcohol) crystals M_w 31000-50000 and (e.) deionised water.

4.1.1. Producing silica sol

Initially the method presented in [7] was used to produce the silica sol since it was the method which produced silica nanofibres with no hydroxyl groups present. It required water, TEOS and phosphoric acid to be mixed continuously for 5 hours. This did not work as after 5 hours the solution was still bi-phase. Based on the results of experimentation reported in [52]and [11] it was decided that absolute ethanol should be introduced into the solution. The molar ratios of reagents used to form silica sol as reported in [77] were used as a reference point. TEOS (6.11g, 0.0293mol), water (17.5g, 0.9714mol), 85% wt aqueous phosphoric acid (4.2125g prepared by simultaneously heating and mixing the crystals and water) and 99.9% pure absolute ethanol (2.367g, 0.0537mol) were mixed at 80^0C. After just half an hour of continuous mixing a clear homogenous solution was obtained.

4.1.2. Producing aqueous poly (vinyl alcohol)

Two methods were considered for the preparation of aqueous poly (vinyl alcohol) for the purpose of electrospinning. The first method was documented by *Shen et al* during research into PVA/silica hybrid materials. It involved mixing solid PVA crystals into water at 60^0C [78]. When this method was tried in the lab, the crystals never fully dissolved into the water. There were always sticky masses of PVA in the solution. The second method was used by *Pirzada et al* to form precursors for an electrospinning

experiment [79]. This method is the same as the first except the crystals were mixed at 80-90^{0}C instead of 60^{0}C. When the second method was tried, it was found that the PVA crystals became sticky and agglomerated into a large sticky mass which prohibited the movement of the magnetic stirring bar and did not dissolve. Upon further experimentation it was found that mixing the crystals at 60^{0}C for one hour and then increasing the temperature to 80-90^{0}C for another hour of mixing dissolved the crystals completely so that a clear viscous homogenous solution was obtained. It was found that the best equipment to mix 30ml of aqueous PVA is a 100ml beaker and a stirrer bar large enough to almost span the diameter of the beaker. This setup leaves the solution level not much higher than the stirrer bar ensuring that all the PVA crystals are sufficiently agitated and evenly heated. Sufficient agitation is required to prevent the crystals sticking to the sides of the beaker.

4.1.3. Introduction of PVA to the silica sol

The method presented in [7] was used at first to combine the silica sol and the aqueous PVA. The two components were mixed together briefly then placed into a water bath (held at 60^{0}C) for 12 hours. This process seems to have accelerated the aging of the sol. At the end of 12 hours the solution had completely aged into a gel which was not suitable for electrospinning. A method used by Prizada et al was considered next [79]. The silica sol (30g) and the aqueous PVA (30g) were mixed continuously for one hour at 80^{0}C. A clear homogenous solution which was highly viscous was obtained.

4.1.4. Optimisation of the solution viscosity and surface tension measurement

For the optimisation, various gap distances and voltages were used. Most often only one set of parameters produced a deposition large enough foranalysing in the electron microscope. The standard test procedure was to ramp up the voltage until the most stable electrospinning jet was observed at the tip of the spinneret. If it was found that no fibres were produced the gap distance was decreased in decrements of 5cm from a starting point of 20cm. All tests were conducted using a 15 gauge needle as the spinneret. The object of optimisation of the solution was to obtain good quality fibres (few beads and acceptable differences in diameter) and to find a solution that would be easy to work with. If the electrospinning jet is stable then the fibres produced will have relatively uniform diameter and bead formation will be low [55]. A video camera with 52x optical zoom was used to check the stability of the electrospinning jet.

Initially the 10% aqueous PVA solution was used. It was found that this solution solidified into a gel within 15 minutes of production. This prevented proper electrospinning from occurring. For a gap distance of 15cm, the gel would be drawn out in a thick stream. The thick stream (2mm calculated relative to the inner diameter of the spinneret which was 2mm) would flashover to the collector when the gel was close enough to the collector (Figure 4.1).

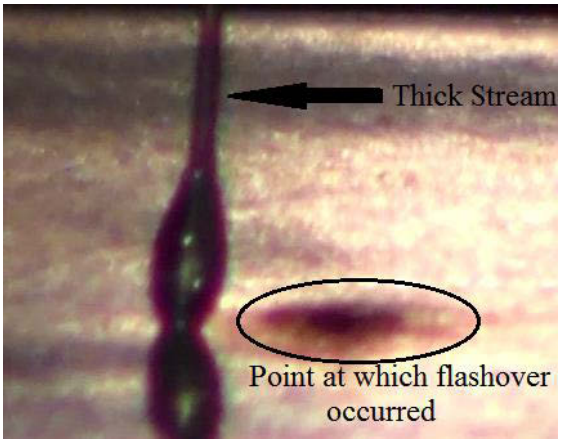

Figure 4.1: Thick stream formed during attempted electrospinning of 10% aqueous PVA combined with silica solin 1:1 ratio

Since it took longer than 15 minutes to move the solution from the chemistry lab where it was synthesized to the high voltage lab where the HV supply was, using 10% aqueous PVA was not feasible. The PVA concentration had to be changed. Leach *et al* presented a concept called the critical entanglement concentration of a solution [80]. The critical entanglement concentration is the concentration at and above which a stable electrospinning jet could be obtained [80]. The method used by Leach *et al* to find this concentration was to start at a low concentration and go up until a stable jet is achieved [80]. It was stated that typically a solution which was at the critical entanglement concentration is visibly viscous but not gel like [80].

PVA concentrationwas controlled by varying the percentage mass of PVA used in solution. A mass of 1g PVA was tried to start. Increments of 0.5g were made until electrospinning produced proper fibres instead of micro beads or a film. Both the 1g and 1.5g PVA solutions resulted in discontinuous jets which sprayed a thin film of liquid onto the collector instead of depositing fibres. A 2g PVA solution (6.66% Aqueous) electrospun at 9kV across a 5cm gap resulted in a discontinuous jet but yielded some nanofibres. Other larger gap distances and voltages either sprayed solution onto the collector or did not draw solution from the needle tip.

It was later found that refrigeration of the solution allowed it to maintain the viscosity it possessed when it was synthesized for long periods of time in excess of 2 weeks. The 3g PVA solution was used once more at a voltage of 19kV and a gap distance of 15cm.It was found that this solution had a greater yield of nanofibres than the 2g solution.Lower gap distances resulted in a wet deposit. The area of deposition of fibres for this sample was found to have increased significantly. There was also a noted increase in bead formation (Figure 4.2 illustrates what bead formation looks like).

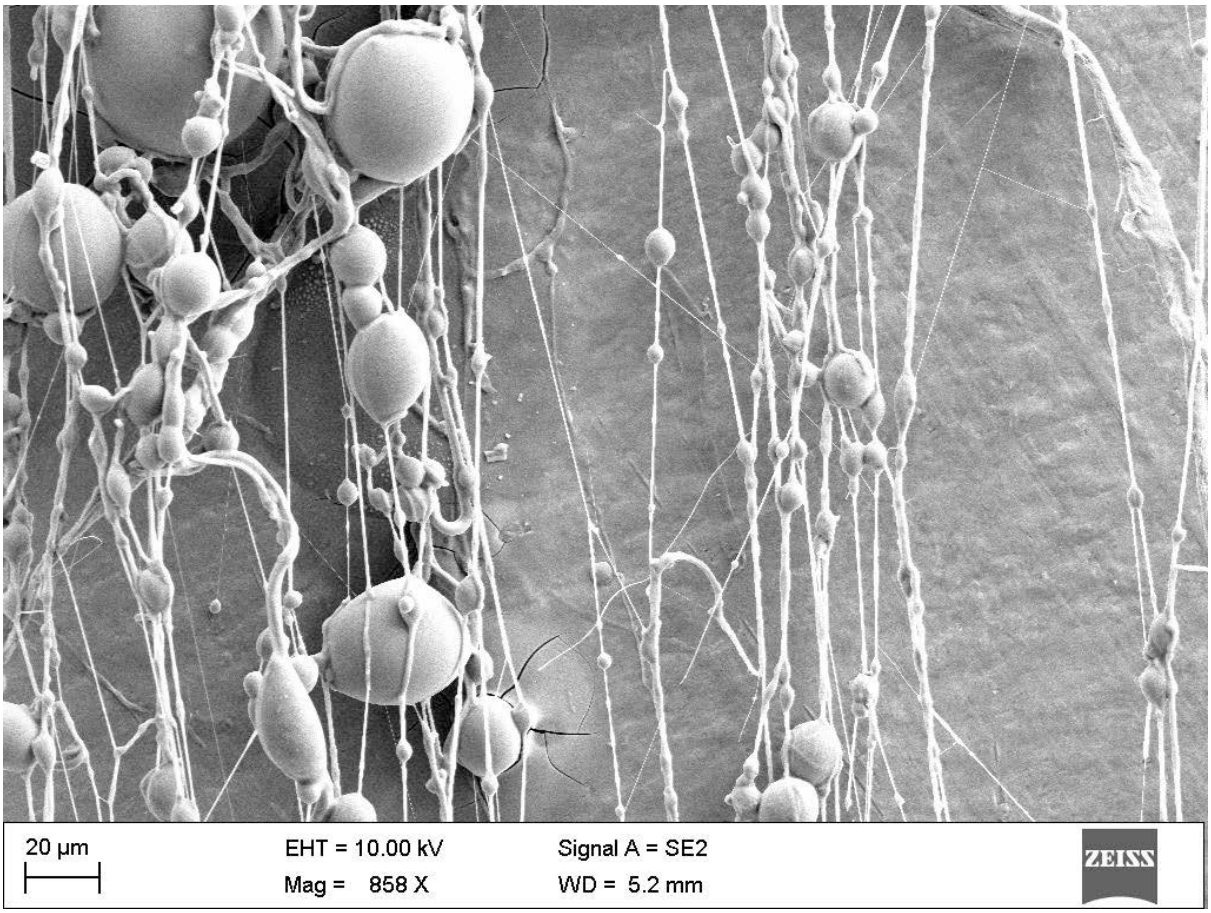

Figure 4.2: SEM image of electrospun nanofibres which experienced bead formation

The electrospinning jet was still discontinuous which meant the fibre diameter would have a high variance. The discontinuity can be attributed to insufficient polymer chains per unit volume present in the solution. The solution can therefore not hold itself together for a continuous jet. The ratio of polymer to silica sol was raised from 1:1 to 2:1 in order to give the jet more stability. A voltage of 19kV and a gap distance of 15cmproduced viable fibres but the jet still had some discontinuity. Due to time constraints, the fibres obtained through electrospinning using the 3g PVA solution in a ratio of 2:1 were deemed acceptable for testing.This iteration of the solution produced a

wet deposit at lower gap distances while electrospinning could not occur at a gap distance of 20cm. A higher voltage than 25kV may have initiated electrospinning at a 20cm gap distance but corona onset on the syringe pump occurs past 25kV therefore it was decided not to try it. Variations in other parameters in the setup while using this solution are presented in results and discussion.

4.2. Electrospinning of Solution

Once the precursor solution was deemed acceptable and a known operating point for fibre formation was identified, experimentation on varying various processing parameters was carried out. The operating point at which fibre formation was known to occur was found during optimization of the electrospinning precursor solution. The operating point included: (a.) An applied voltage of 19kV, (b.) A tip to collector distance of 15cm, (c.) A 15 gauge needle as the spinneret and (d.) A flow rate of 4ml/h.

The experimental procedure consists of:

- Loading precursor solution into the delivery system
- Preparing the collector
- Arranging the desired processing parameters
- Preparing the electrospinning area for video capture
- Ramping up the voltage.

4.2.1. Loading up the precursor

Before the experiment can begin a vial of precursor solution is taken out of refrigeration and loaded into the delivery system. A 1ml syringe has to be used in the syringe pump since its small diameter allows the syringe pump to easily pump continuously at the low flow rates required. The PVC tubing connecting the syringe to the spinneret requires 10ml of solution to fill it completely. The precursor solution is therefore first loaded into a 10ml syringe (Figure4.3).

Figure 4.3: 10ml syringe used to fill PVC tubing with solution to be electrospun

The 10ml syringe is used to inject the solution into the tubing until it half fills the spinneret connected at the end of the tubing (Figure4.4).

Figure 4.4: 1ml gastight syringe with 15 gauge stainless steel blunt needle used as spinneret in electrospinning setup

The opening of the spinneret is then blocked while the 10ml syringe is removed so that the solution does not flow out. The 1ml syringe loaded with 1ml of solution is then inserted where the 10ml syringe was and injected until 0.5 ml remains. Once this is done the precursor solution fills the spinneret completely to the end of the needle. The 1ml syringe is then loaded into the syringe pump (Figure4.5).

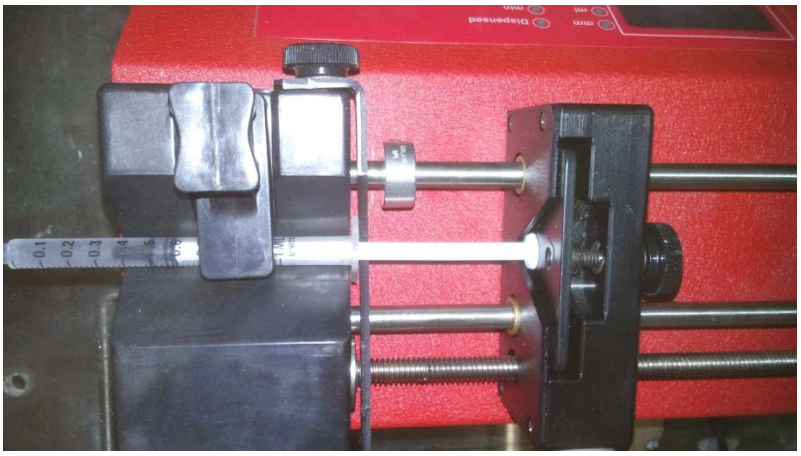

Figure 4.5: 1ml disposable syringe loaded into syringe pump allowing control of solution flow from the spinneret

4.2.2. Prepping the collector for electrospinning

The collector consisted of a 1cm thick square copper plate (Figure4.6). Once electrospinning takes place it is difficult to remove the fibres from the collector without destroying the fibre distribution. The fibres have to be removed since the entire copper plate could not fit inside the electron microscope for fibre characterization. The collector is therefore wrapped in heavy aluminium foil (Some iron content present). The foil can be removed and cut to size once electrospinning is done.

Figure 4.6: Bare copper plate which was used as a grounded collector in the electrospinning setup

Insulation tape was used to hold the foil in place (Figure4.7).

Figure 4.7:Copper plate wrapped in heavy foil which nanofibres can deposit on

4.2.3. Arranging processing parameters and preparing area for video capture

The spinneret is taped onto a box so that its dispensing end faced the collector plate. The collector is moved toward the spinneret until the gap distance is 15cm. This is measured using a measuring tape. The inner diameter of the syringe has to be input to the syringe pump and the desired flow rate is set. A black box is placed on one side of the spinneret and collector so that the clear electrospinning jet can be clearly seen.

4.2.4. Ramping up the voltage

Before application of voltage the flyback converter is switched on. This is done by first turning on a variable DC power supply. A 30 kHz square wave (3Vp-p) is applied from the function generator to the triggering circuit which chops the DC power supplies voltage so that high frequency pulsed DC is fed to the flyback transformer. The voltage output is then increased slowly by increasing the voltage on the DC power supply. Pumping of solution from the syringe pump is only triggered after the desired voltage is achieved. This is to mitigate variance in fibre diameter caused by changing voltage. When 0.5ml of solution has been used, the syringe pump is switched off before the voltage is brought down.

4.3. Nanofibre Characterization

Physical, chemical and electrical properties of electrospun nanofibres were of interest. FTIR, scanning electron microscopy and impedance spectroscopy were used to determine some of these properties. FTIR was performed on electrospun fibres to determine their chemical composition. This method was chosen over XRD since the XRD apparatus was non-functional at the time of the experiment. Scanning electron microscopy was used to determine the physical properties (diameter and area of

deposition) of electrospun nanofibres. Impedance spectroscopy was used to determine the reactance and resistance of electrospun fibres over a range of applied voltage frequencies.

4.3.1. FTIR

The output of performing FTIR is a graph of intensity versus wavelength. One can tell what material a sample is made of by checking which wavelengths have dips in intensity. A range of wavelengths over which significant dip in intensity occurs is commonly known as an absorption band. Every material has its own unique absorption band. The materials of interest in this study are PVA and silica. FTIR results for the electrospun fibres were compared to results presented in three publications. These publications analysed the FTIR spectra of composite PVA/silica nanofibres[81], [82], [83].They found that PVA had a smooth absorption peak between wave numbers 3500 $cm^{-1}$and 3000 cm^{-1}followed by a sharp peak between wave numbers 3000 $cm^{-1}$and 2500cm^{-1}[81], [82], [83]. It was also found that the addition of silica introduced a sharp absorption peak between wavenumbers 1000 $cm^{-1}$and 1100cm^{-1}[81], [82], [83]. If absorption peaks similar to these are obtained from infra-red spectroscopy performed on electrospun nanofibresthen the fibres can be confirmed as composite PVA/silica fibres.

4.3.2. SEM analysis

Magnified images of the electrospun fibres were taken using a Zeiss FEG-SEM. On each sample, five images of random areas were taken at 5000x magnification. Two types of analysis were performed on the pictures. These were to obtain the average fibre diameter and finding the average area of deposition of fibres.

The average fibre diameter was first calculated for each individual picture. The average of averages for all pictures from the same sample determined the average fibre diameter for that particular sample. For a single picture the fibre diameter was measured for each 1μm of fibre. The measurements were performed using open source software called ImageJ [84]. All the diameter measurements were summed and divided by the total length of fibre visible in the picture.

The average area of deposition shall be defined as the average area of foil (fibres were deposited on this foil during electrospinning) not visible due to deposited fibres. Calculation of this quantity was performed with the help of the software ImageJ [84]. First each image was transformed to a two bit image (black and white). At this point the

fibres appear as black and the foil appears as white. The software ImageJ detects all boundaries between white areas and black areas then finds the total area of all the white areas. The area of deposition was then calculated by subtracting the total area of all white areas from the total area depicted in the image and dividing by the total area of 1971.2962 $\mu m^2$to give a percentage. Average area of deposition for a particular sample was calculated by averaging the areas of deposition of all the images taken from that sample.

4.3.3. Impedance Spectroscopy

The effects of adding nanofibres to an air gap were investigated. Fibres of varying average diameter and areas of deposition were used in different experiments. Conductivity of lanthanum manganitenanofibres was investigated by Myat[73] in which an LCR analyser was used to take measurements. Since an LCR analyser was not available for use in the experiments involving composite silica/PVA nanofibres, an oscilloscope was used successfully. The voltage waveforms displayed on the oscilloscope were used to determine impedance of the test samples. The test setup electrical connections are depicted in figure 4.8.

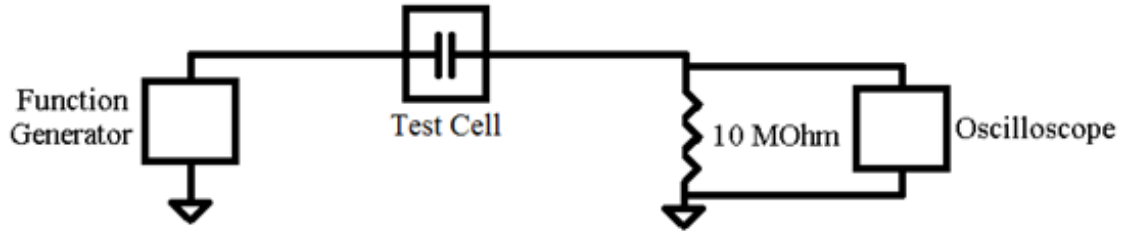

Figure 4.8:Impedance test apparatus showing major components

A 20V_{p-p} sin wave of variable frequency was applied by the function generator. Since the air gap was 1cm in length, large impedance measurements were expected. In order to measure the resulting small currents a 10MΩ resistor was employed. With the 10MΩresistor, small currents of the order of μA could be measured as volts by the oscilloscope. Measurements were taken over a range of frequencies so that the frequency response of the test cell could be graphed. The test cell comprises of two plane copper electrodes (discs) held 1cm apart by a piece of Perspex tubing (Figure 4.9). Nanofibres were introduced into the 1cm gap and subjected to testing. In an attempt to reduce noise signals in the measurement system, a smooth aluminium ring was placed around the test cell and grounded. Measurements could not be performed below 1000 Hz since the amplitude of measured signals became lower than the

amplitude of noise signals. Accurate measurement was also impossible above 10 kHz due to the bandwidth of the measurement probe being used.

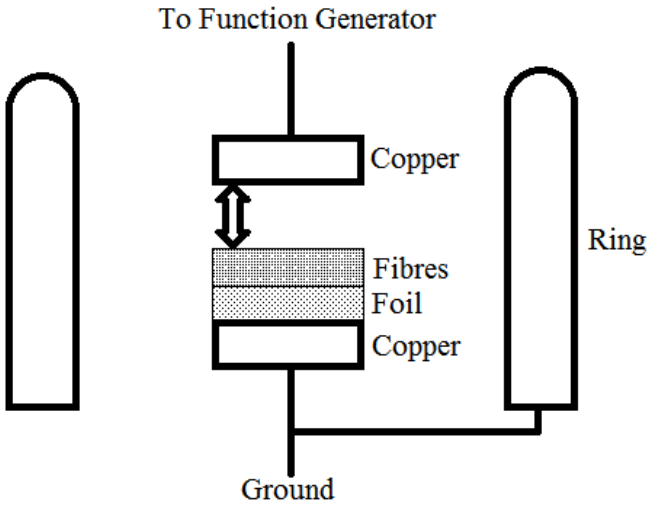

Figure 4.9: Test cell used in the impedance test apparatus shown in exaggerated detail

Voltage was measured across the 10 MΩresistor from 1000 Hz to 10 kHz in steps of 1000 Hz. The phase difference between the output voltage waveform and the input from the function generator was also measured at each step. These two values were used in Equation 9 (derivation in Appendix A1) to calculate the impedance of the test cell.

$$Z_T = R_m\left(\frac{V}{V_m \angle \theta} - 1\right) \quad (9)$$

Where,

Z_T = Test cell impedance

R_m = 10MΩ measurement resistor

V = Function generator applied voltage (Taken as 0^0 phase angle reference)

V_m = Amplitude of measured voltage

θ = Angle of measured voltage

5. RESULTS AND DISCUSSIONS

Various sets of results were obtained from the characterization of the nanofibres. These include:

a) Results from chemical characterization of silica/PVA fibres
b) Results from morphological characterization of silica/PVA fibres, and
c) Results from measuring impedance of an air gap containing the fibres.

5.1. Results of analysing SEM images

SEM images were taken of six samples of nanofibreselectrospun under different conditions. Deviations in voltage, flow rate and spinneret type were effected for the different conditions.All flow rates discussed in this section occurred over 15 minutes. The first sample was electrospun using a flow rate of 4ml/h, an applied voltage of 19kV and a 15 gauge needle as a spinneret. The parameters used to produce sample one were considered as the base case. Each individual parameter was altered to produce the remaining samples so that a relationship between varying one parameter and the resulting fibre morphology could be determined. Figure5.1is an SEM image of a random area from sample one. The remaining four images are in Appendix A2.

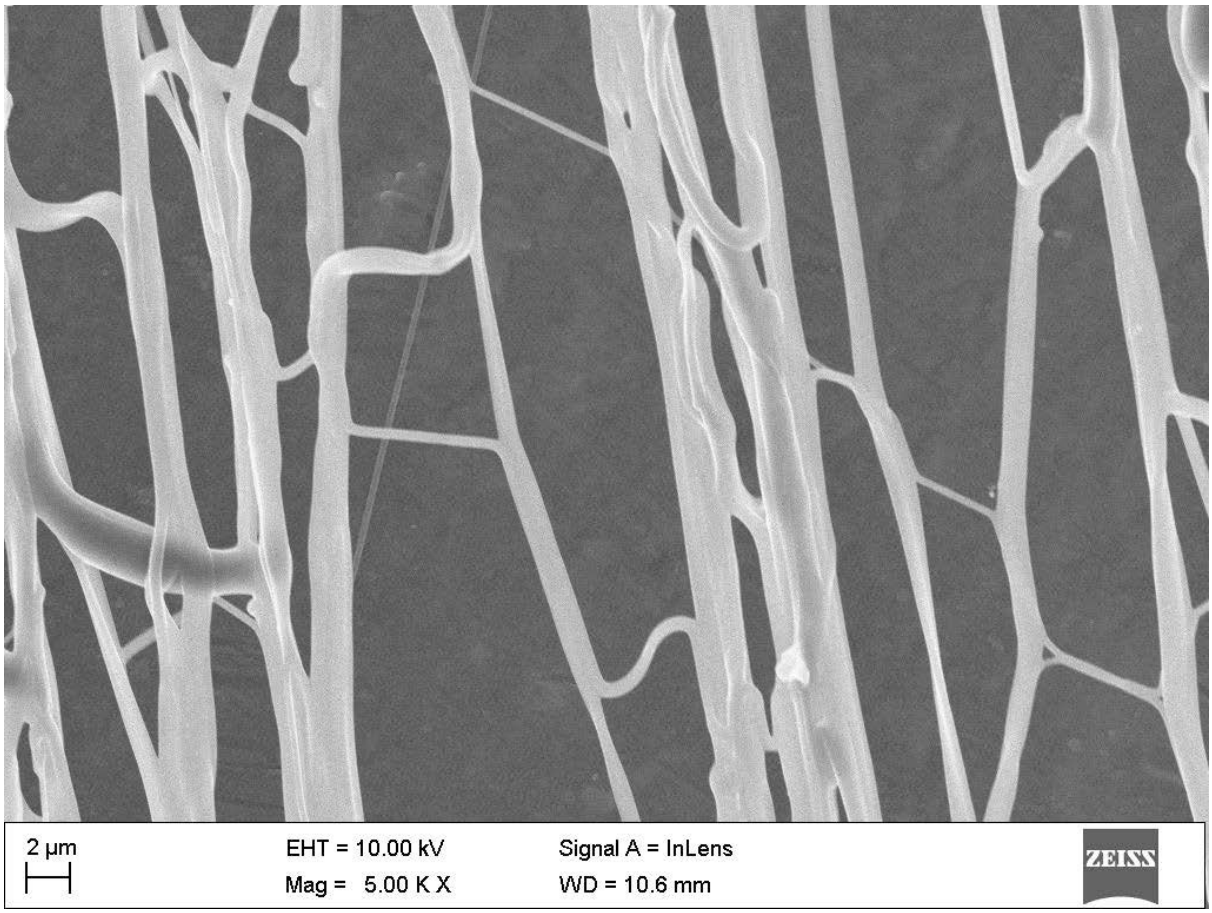

Figure 5.1: Sample 1 random area 1electrospun at 19kV, 4ml/h using a 15 gauge needle

The average diameter of fibres in this random areaapproximated to 767nm. The area not covered by fibres was calculated to be 1256.332 μm^2. The minimum fibre diameter is 220nm and the maximum fibre diameter is 1600nm. Table 1 shows all the data obtained for sample 1 (from all the five random areas) and the calculated average area of deposition.

Table 1: Results of analysis of SEM images from sample 1

Random Area	Maximum Diameter (nm)	Minimum Diameter (nm)	Average Diameter (nm)	Area Not Covered (μm^2)	Area of Deposition (%)
1	1600	220	767	1256.332	36.27
2	1733	236	884	1086.953	44.86
3	2036	259	898	1635.503	17.03
4	2700	320	934	1507.665	23.32
5	2546	302	1030	1728.504	12.32
Sample 1 Average	2700	220	903	-	26.80

There are significant deviations in both fibre diameter and area of deposition between all the random areas imaged from sample one. There are also large differences between minimum and maximum fibre diameter in each random area. This infers that the parameters used resulted in an unstable electrospinning jet. The second sample was electrospun using a flow rate of 4ml/h, an applied voltage of 13kV and a 15 gauge needle as a spinneret. Figure5.2 is an SEM image of a random area from sample two. The remaining SEM images can be found in Appendix A2.

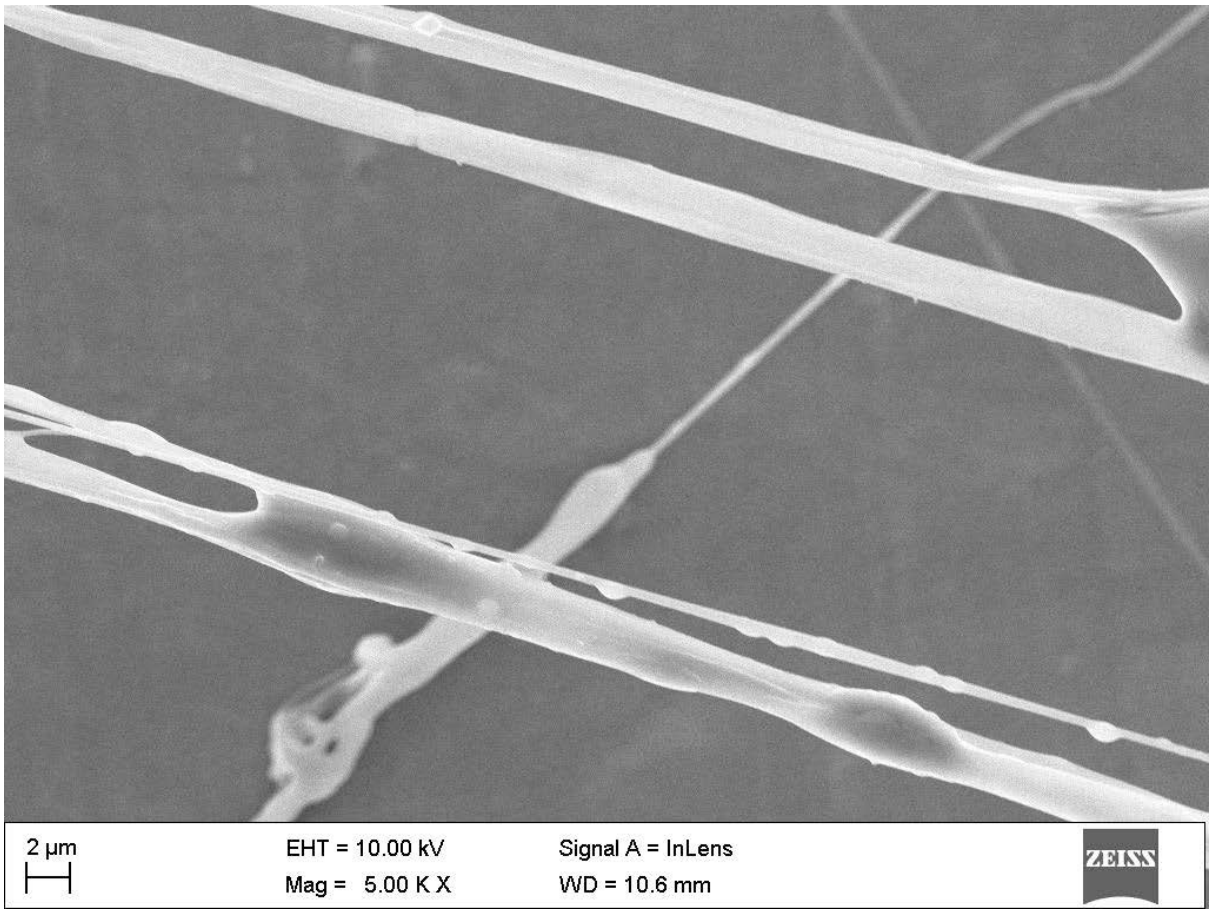

Figure 5.2: Sample 2 random area 1electrospun at 13kV, 4ml/h using a 15 gauge needle

The average diameter of fibres depicted in Figure 5.2approximated to 1276 nm. The area not covered by fibres was calculated to be 1615.085 μm^2. The minimum fibre diameter is 411 nm and the maximum fibre diameter is 2022 nm. Table 2 shows all the data obtained for sample 2 and the calculated average area of deposition.

Table 2: Results of analysis of SEM images of sample 2

Random Area	Maximum Diameter (nm)	Minimum Diameter (nm)	Average Diameter (nm)	Area Not Covered (μm^2)	Area of Deposition (%)
1	2022	411	1276	1615.085	18.07
2	1018	259	578	1883.937	4.432
3	1508	382	930	1504.768	23.67
4	1265	417	759	1793.305	9.029
5	1365	356	1110	871.916	55.77
Sample 2 Average	2022	259	930	-	22.19

Sample two introduces a decrease in applied voltage to the base case. The results in table two shows that the average diameter and area of deposition vary to a larger degree between random areas compared to sample 1. The maximum and minimum diameters in each random area of sample 2 share large differences. It can be concluded that reducing the applied voltage increases jet instability. In terms of overall average diameter, the decrease of applied voltage yielded an increase in diameter from 903 nm to 930 nm. The area of deposition decreased slightly. This means that the same volume of solution was deposited less densely. The total area over which electrospinning took place therefore increased. The third sample was electrospun using a flow rate of 4ml/h, an applied voltage of 25kV and a 15 gauge needle as a spinneret. Figure5.3 is an SEM image of a random area from sample three.

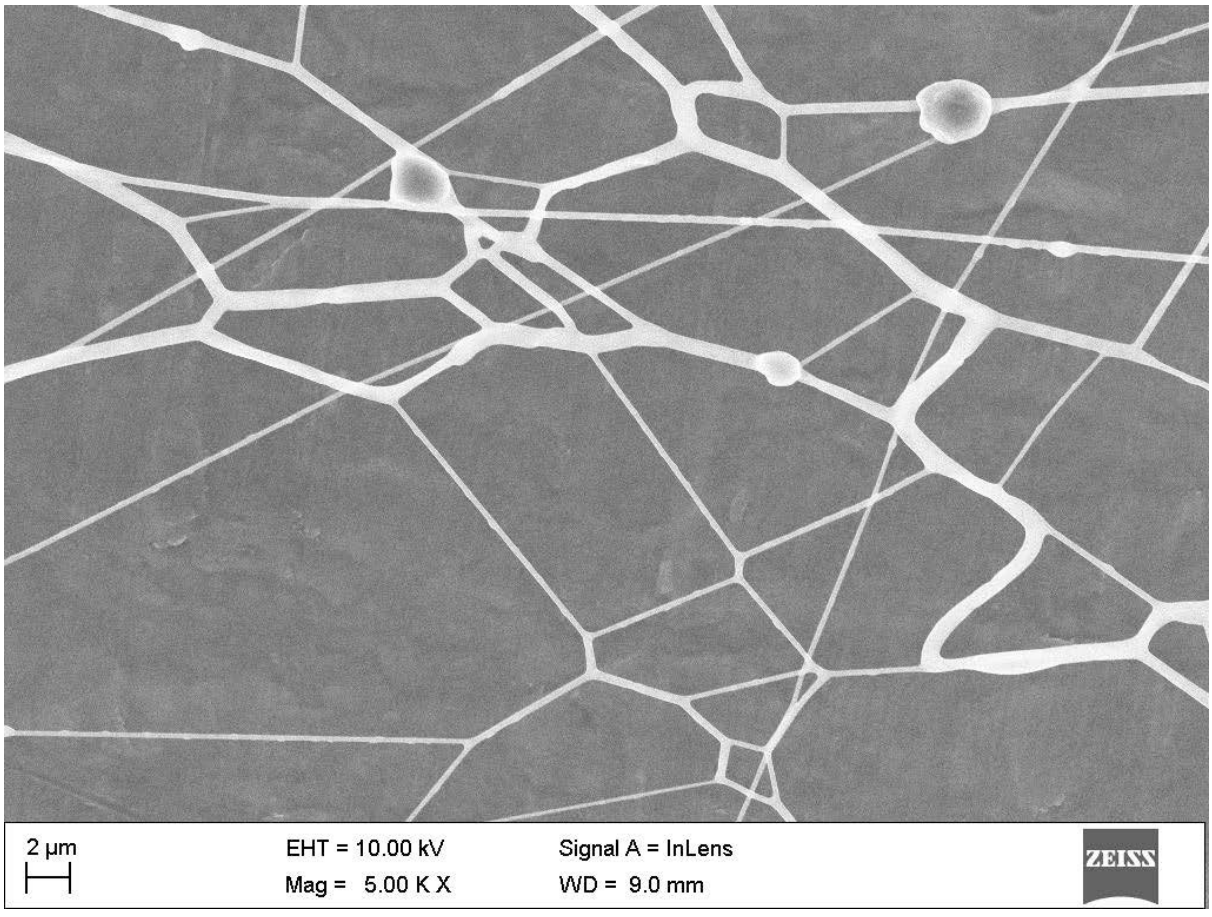

Figure 5.3: Sample 3 random area 1electrospun at 25kV, 4ml/h using a 15 gauge needle

The average diameter of fibres depicted in Figure 5.3approximated to420 nm. The area not covered by fibres was calculated to be 1724.975µm^2. The minimum fibre diameter

is 112 nm and the maximum fibre diameter is 1400 nm.Table 3 shows all the data obtained for sample 3 and the calculated average area of deposition.

Table 3: Results of analysis of SEM images of sample 3

Random Area	Maximum Diameter (nm)	Minimum Diameter (nm)	Average Diameter (nm)	Area Not Covered (μm^2)	Area of Deposition (%)
1	1400	112	420	1724.975	12.50
2	1020	150	558	1628.891	17.37
3	1309	140	457	1586.622	19.51
4	1206	175	466	1844.216	6.446
5	1583	200	620	1631.591	17.23
Sample 3 Average	1583	112	504	-	14.61

Sample three was electrospun with an increase in the applied voltage from 19 kV to 25 kV. The area of deposition and average diameters are relatively constant over the five random areas. It can therefore be said that increasing the applied voltage of electrospinning produced a more uniform distribution of fibres. The average diameter for the sample is lower than that of the base case by a large margin. Overall area of deposition for sample three is significantly lower. Increasing the applied voltage therefore decreases both the average diameter and area of deposition (area over which electrospinning took place increased). The fourth sample was electrospun using a flow rate of 3ml/h, an applied voltage of 19kV and a 15 gauge needle as a spinneret. Figure5.4 is an SEM image of a random area from sample four.

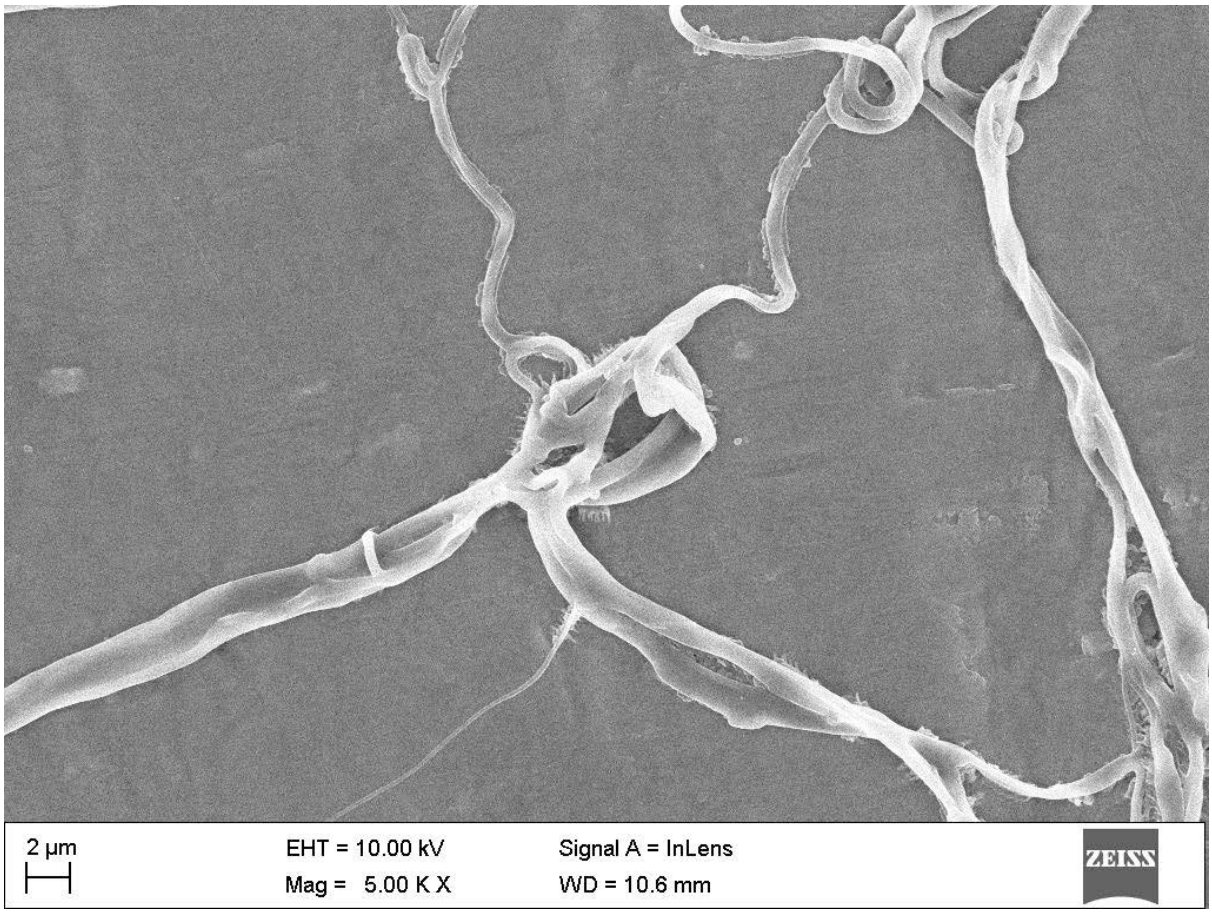

Figure 5.4: Sample 4 random area 1electrospun at 19kV, 3ml/h using a 15 gauge needle

The average diameter of fibres in the random area of sample 4 shown in Figure 5.4 approximated to 816 nm. The area not covered by fibres was calculated to be 1689.614 μm^2. The minimum fibre diameter is 527 nm and the maximum fibre diameter is 1045 nm. Table 4 shows all the data obtained for sample 4 and the calculated average area of deposition.

Table 4: Results of analysis of SEM images of sample 4

Random Area	Maximum Diameter (nm)	Minimum Diameter (nm)	Average Diameter (nm)	Area Not Covered (μm^2)	Area of Deposition (%)
1	1045	527	816	1689.614	14.29
2	1350	351	690	1842.207	6.548
3	1674	140	880	1732.542	12.11
4	837	274	497	1766.137	10.41
5	900	281	563	1722.720	12.61
Sample 4 Average	1674	140	689	-	11.19

Sample 4 was electrospun with a reduction in flow rate. The lower flow rate yielded fibres with a lower area of deposition and lower average fibre diameter compared to the base case. The area of deposition and average fibre diameters had a higher degree of uniformity over the five samples than the base case. It can be concluded that a reduction in flow rate yields more uniform fibres with smaller average diameters. The fifth sample was electrospun using a flow rate of 5ml/h, an applied voltage of 19kV and a 15 gauge needle as a spinneret. Figure5.5 is an SEM image of a random area from sample five.

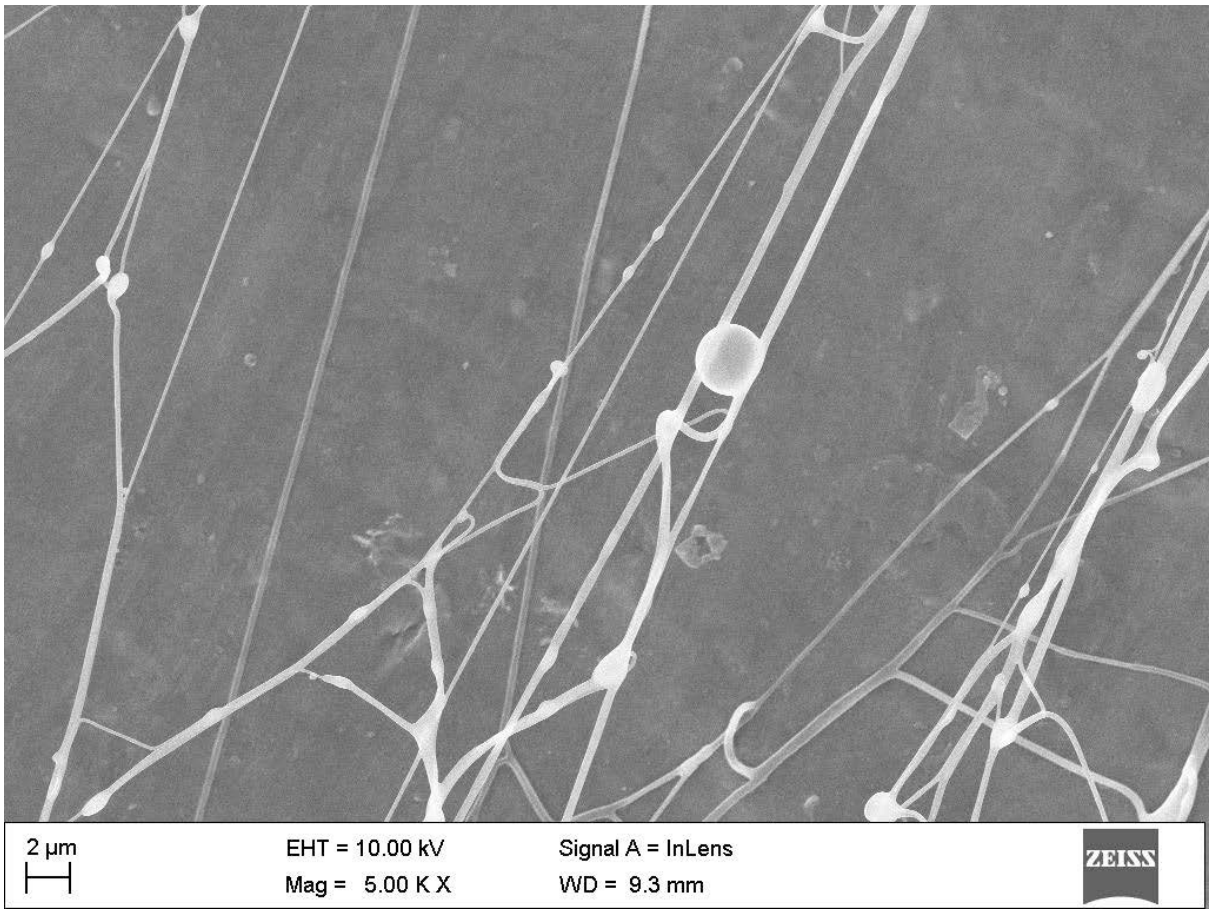

Figure 5.5: Sample 5 random area 1electrospun at 19kV, 5ml/h using a 15 gauge needle

The average diameter of fibres in random area 1 of sample 5 approximated to 339 nm. The area not covered by fibres was calculated to be 1782.176 μm^2. The minimum fibre diameter is 189 nm and the maximum fibre diameter is 472 nm.Table 5 shows all the data obtained for sample 5 and the calculated average area of deposition.

Table 5: Results of analysis of SEM images of sample 5

Random Area	Maximum Diameter (nm)	Minimum Diameter (nm)	Average Diameter (nm)	Area Not Covered (μm^2)	Area of Deposition (%)
1	472	189	339	1782.176	9.594
2	1437	169	520	1645.214	16.54
3	1210	171	471	1855.240	5.887
4	751	224	427	1810.118	8.176
5	932	208	290	1796.465	8.869
Sample 5 Average	1437	169	418	-	9.813

To produce sample 5, the flow rate was increased to 5 ml/h. Although the area of deposition over the five random areas is more uniform than in the base case, it is much smaller. The average fibre diameter also had a notable decrease and was more uniform than the base case. Interestingly the results in tables six and five show that both increasing and decreasing the flow rate from the base case decrease the average diameter of fibres produced decrease the area of deposition and result in a higher degree of uniformity. The sixth sample was electrospun using a flow rate of 4ml/h, an applied voltage of 19kV and a plastic pipette as a spinneret. Figure5.6 is an SEM imageof a random area from sample six.

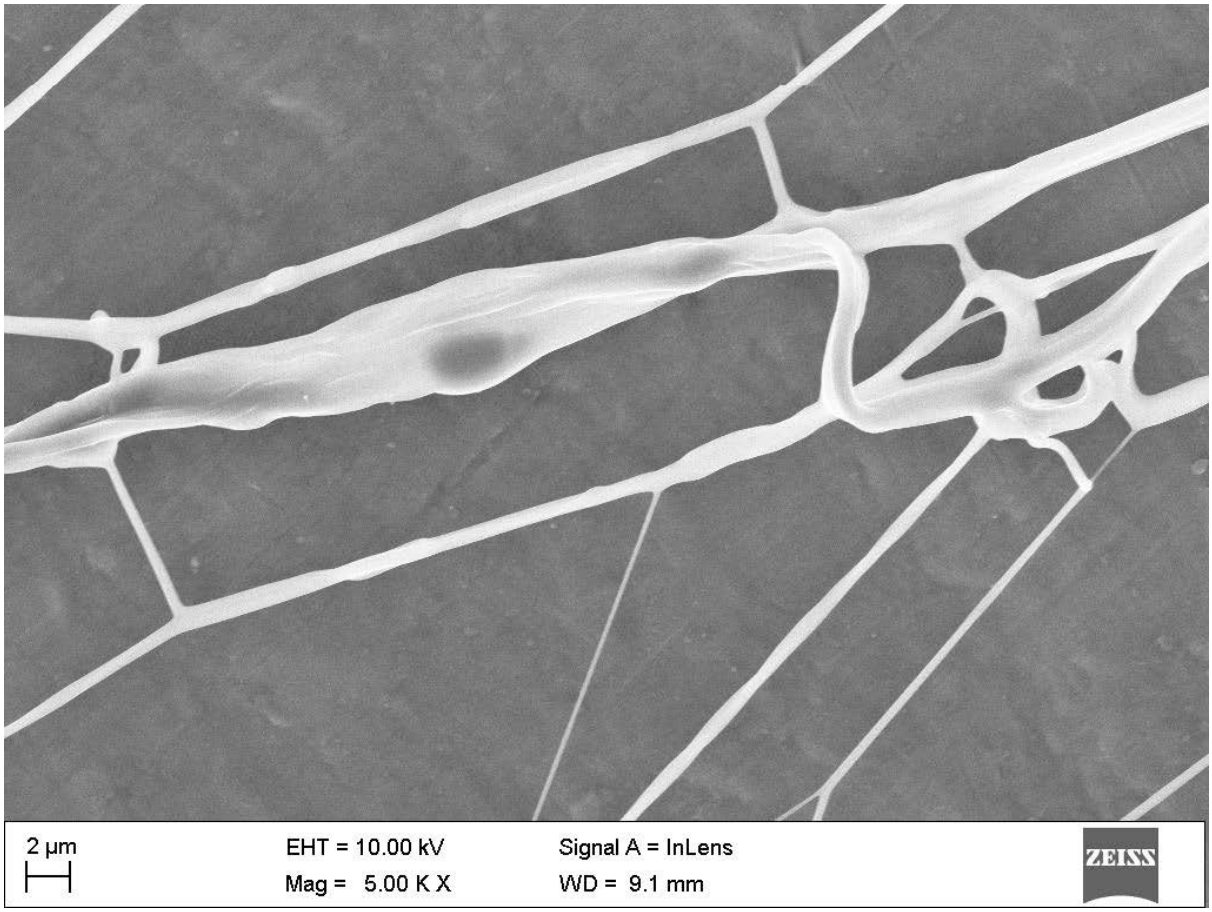

Figure 5.6: Sample 6 random area 1electrospun at 19kV, 4ml/h using a plastic pipette

The average diameter of fibres from figure 5.6approximated to 666 nm. The area not covered by fibres was calculated to be 1623.454µm^2. The minimum fibre diameter is 255 nm and the maximum fibre diameter is 1368 nm. Table 6 shows all the data obtained for sample 6 and the calculated average area of deposition.

Table 6: Results of analysis of SEM images of sample 6

Random Area	Maximum Diameter (nm)	Minimum Diameter (nm)	Average Diameter (nm)	Area Not Covered (μm^2)	Area of Deposition (%)
1	1368	255	666	1623.454	17.65
2	1000	361	658	1591.360	19.27
3	1005	595	846	1542.471	21.75
4	3387	253	1247	217.5180	88.97
5	2829	211	1091	925.6310	53.04
Sample 6 Average	3387	211	902	-	40.14

The spinneret tip was changed to a plastic pipette to produce sample 6. The plastic tip produced fibres which had a larger area of deposition which is less uniform across the five random samples than in the base case. Average diameter was almost unchanged by the plastic tip although the diameter was less uniform across the five random samples. Table 7 summarises the results of varying only the voltage applied during electrospinning.

Table 7: Effects of varying applied voltage on fibre morphology

Voltage (kV)	Maximum Diameter (nm)	Minimum Diameter (nm)	Average Diameter (nm)	Area of Deposition (%)
13	2022	259	930	22.19
19	2700	220	903	26.80
25	1583	112	504	14.61

From table 7 it can be seen that increasing the applied voltage decreases average fibre diameter while decreasing the applied voltage decreases fibre diameter. This stands to reason since voltage related directly to the electric field strength. A strong electric field (high voltage) would stretch out the electrospinning jet further, creating thinner fibres while a weak electric field (low voltage) would have less of an effect on the electrospinning jet, causing larger fibres to be formed. The significantly lower area of deposition obtained at a voltage of 25 kV can be attributed to the stronger electric field creating greater instability in the electrospinning jet. The greater instability will cause

the jet to whip further and hence deposit sparsely in a wider area. At a voltage of 13 kV the area of deposition drops slightly. This is due to the electric field being too weak to draw all the solution ejected from the spinneret towards the collector. A lower amount of solution reaching the collector would result in a lower area of deposition. Table 8 summarises the results of varying only the flow rate.

Table 8: Effects of varying solution flow rate on fibre morphology

Flow Rate (ml/h)	Maximum Diameter (nm)	Minimum Diameter (nm)	Average Diameter (nm)	Area of Deposition (%)
3	1674	140	689	11.19
4	2700	220	903	26.80
5	1437	169	418	9.813

The results of varying flow rate show that any change in flow rate (decrease or increase) decreases both average diameter and area of deposition. When the flow rate is lowered, less solution is allowed out of the spinneret. This means that the electric field exerts the same amount of force on a smaller amount of solution. The electrospinning jet is therefore stretched further and subjected to more whipping. The resulting deposition will as a result have smaller diameter and have a smaller area of deposition. For an increase in flow rate more solution exits the spinneret than the electric field is able to move. As a result, most of the solution drips out of the electrospinning jet leaving a smaller amount of solution in the electric field. The lower volume of solution is stretched thinner and subjected to more whipping. This yields fibres of smaller diameter and a smaller area of deposition. It should be noted that while changing the flow rate seems to better the resulting fibre deposition in terms of average diameter and uniformity, neither of the two flow rates resulted in efficient use of solution. For the increase in flow rate, most of the solution dripped out of the electrospinning jet. For the decrease in flow rate, whipping of the jet sometimes took the jet past the perpendicular plane to the line from the spinneret tip to the centre of the collector. This results in some of the deposition landing on the Perspex covering before the solvent can evaporate. When the solvent does not evaporate, a liquid film instead of nanofibres is formed. In this way solution is wasted. Table 9 summarises the results of varying the type of spinneret.

Table 9: Effects of varying the type of spinneret on fibre morphology

Spinneret	Maximum Diameter (nm)	Minimum Diameter (nm)	Average Diameter (nm)	Area of Deposition (%)
15 gauge needle	2700	220	903	26.80
Plastic pipette	2829	211	902	40.14

Changing the spinneret to a plastic tip resulted in fibres with negligibly different average diameter. The maximum and minimum diameters of electrospun fibres also did not change by much. Only the area of deposition changed. This result could be the due to a difference in the electric field combined with a difference in the force of surface tension between spinneret and solution. The electric field intensity changes slightly due to the voltage no longer being able to pass to the edge of the spinneret (its plastic now). High voltage is still however connected to the solution which appears at the spinneret tip. It can be said that the electric field became more concentrated due to the same level of voltage being applied to a smaller volume. The force of surface tension between solution and spinneret is possibly lower for the plastic tip. This means that less force is required from the electric field to move solution away from the spinneret. The two afore mentioned factors combined would result in solution being pulled away from the spinneret at a higher rate. This could explain the formation of multiple jets as observed during electrospinning using the plastic spinneret. The multiple jets wrap around each other creating braids as the solvent evaporates. Areas on the collector where the braids deposit will have very high areas of deposition while other areas will have a low area of deposition. This can be seen in the SEM images of random areas of sample 6 in Appendix A2. When these are averaged to get an average area of deposition for the plastic spinneret, the area of deposition is pushed up by those random areas which had high areas of deposition.

5.2. Results of impedance testing

Impedance testing was carried out on an air gap. Each nanofibre sample in Table 8 (Samples 1, 2 and 3 electrospun at 19, 13 and 25 kV respectively) was introduced into

the air gap individually to test the effects of each one on the air gap. Each sample was left on the foil it was electrospun onto. The foil was cut into a circle using a template which fit into the test devices Perspex tube. The mass of each sample was measured by first measuring the mass of a foil disc with no nanofibres and subtracting this value from the mass of a foil disc with nanofibres. Sample 3 weighed 00.256g, sample 2 weighed 0.314g and sample 1 weighed 0.303g. All measurements of mass were taken at 4 decimal places on an electronic mass balance. The raw data obtained is the peak to peak voltage measured across the 10MΩresistor and the phase difference of this voltage from the function generator output voltage. This data is presented in Appendix A3. The calculated results ofabsoluteimpedance of the air gap with different nanofibre morphologies present are displayed in Figure 5.7.

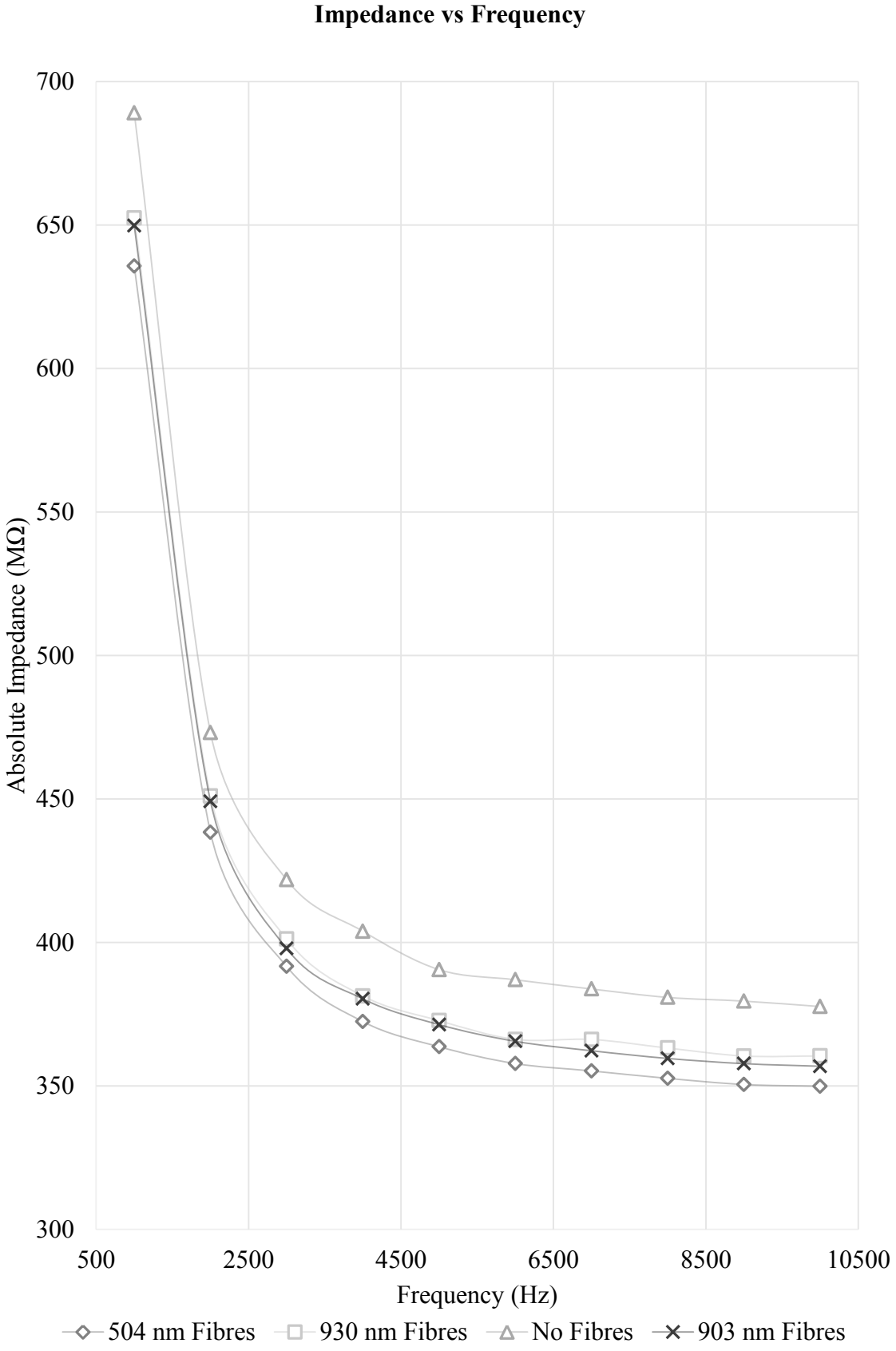

Figure 5.7: Impedance characteristics of air gaps containing different types of nanofibres

The impedance of the gap containing no fibres had the highest impedance. As average diameter of fibres introduced into the air gap is decreased, so too does the impedance. This occurs over the entire frequency range. This infers that composite PVA/silica nanofibres are more conductive than air. To better understand this result, the resistance and reactance for each sample were extracted from the impedance using the phase angle of current through the sample relative to the input voltage. The phase angle of current flowing through a sample under test was measured over a frequency range. It is displayed in Figure 5.8.

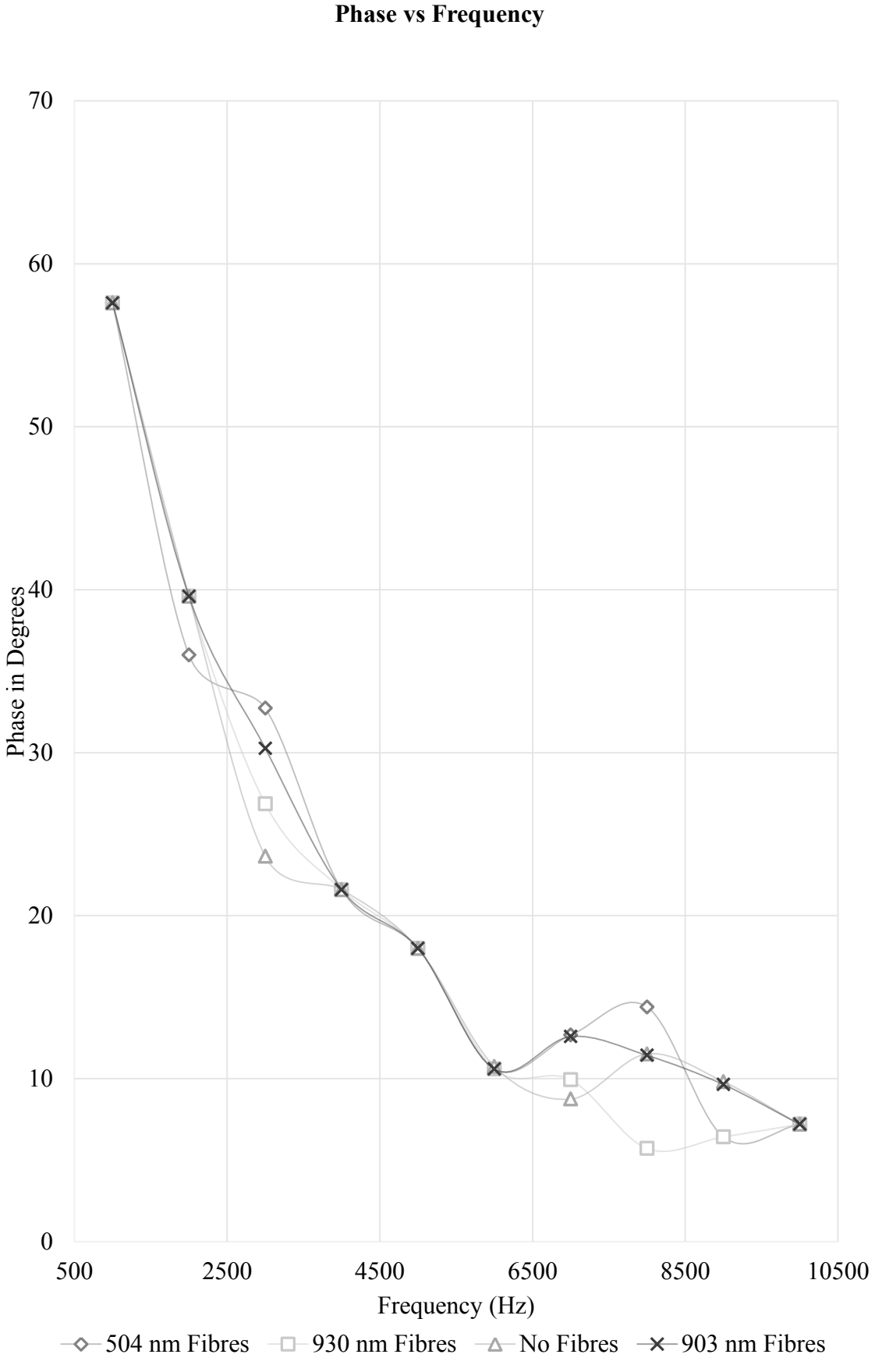

Figure 5.8: Phase angle response of air gaps containing different types of nanofibres

The phase angle for all the cases undergoes large oscillations which occur in approximately the same frequency ranges. The first set of oscillations occurs between two and four thousand Hertz while the second larger set of oscillations occurs between six and ten thousand Hertz. Interestingly, outside these frequency ranges the phase angles for all samples seem to follow each other to a high degree of approximation. It is unclear why this behaviour occurs. A possibility is that each sample has a complex equivalent circuit. Thesehighly nonlinear phase angle responses should result in nonlinear reactance and resistance as well. This is seen in the plots of reactance vs frequency (Figure 5.9) and resistance vs frequency (Figure 5.10). The negative reactance of the samples indicates their capacitive nature. The data points for reactance seem to follow a power distribution with the gap containing the 930 nm average diameter fibres producing the response with the smallest amplitude. With the plot of reactance vs frequency, it is difficult to see which sample has the highest reactance on average. The resistance response reveals clearly which samples had the larger values. The resistance of the gap containing no fibres is significantly larger than the other samples. Its lowest value (at 2000 Hz) is almost the same as the highest value from all the other samples. These findings correlate with the response of the absolute impedance. It can be concluded that differences in resistance are responsible for any differences in impedance when nanofibres are introduced into an air gap.

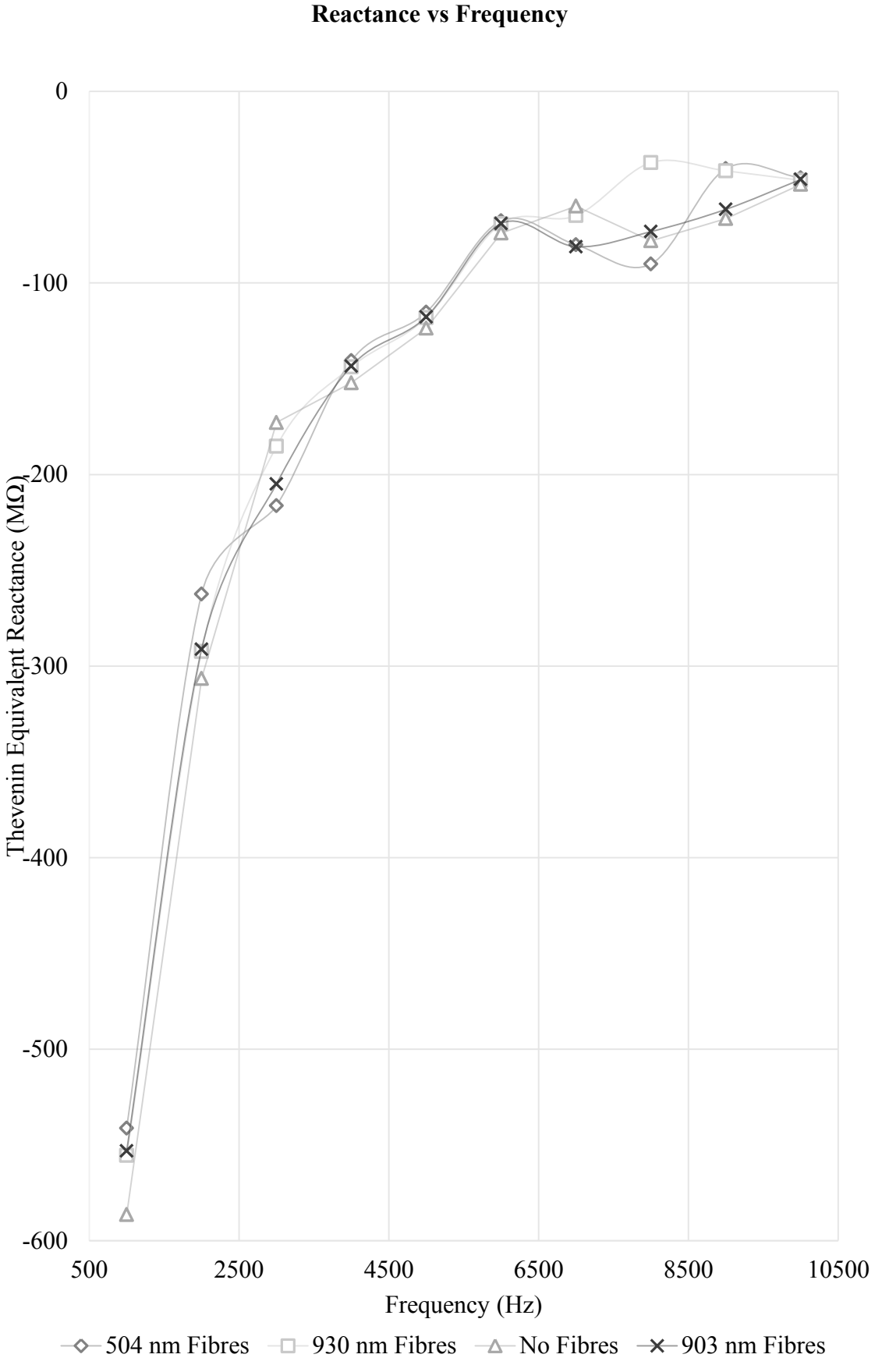

Figure 5.9: Reactance response of air gaps containing different types of nanofibres

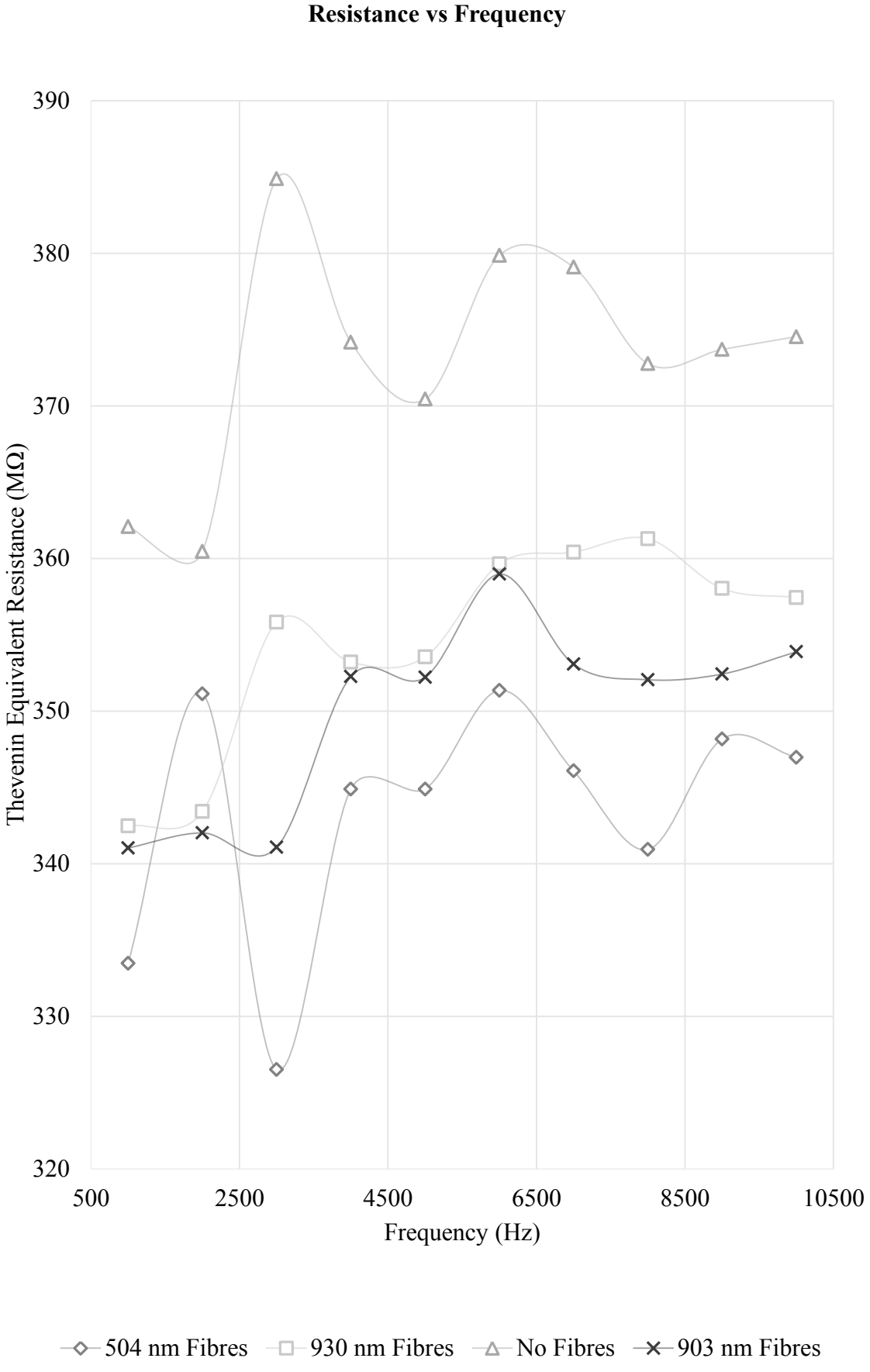

Figure 5.10: Resistance response of air gaps containing different types of nanofibres

5.3. Infra-red spectroscopy

Infra-red spectroscopy was performed on electrospun nanofibres to confirm their composition. Fibres were ground and mixed with potassium bromide powder. The mixture was placed under high pressure to form a clear disc. Infra-red rays were passed through the disc so that the spectrum of the sample could be obtained by a detector. The results are shown in figure 5.11.

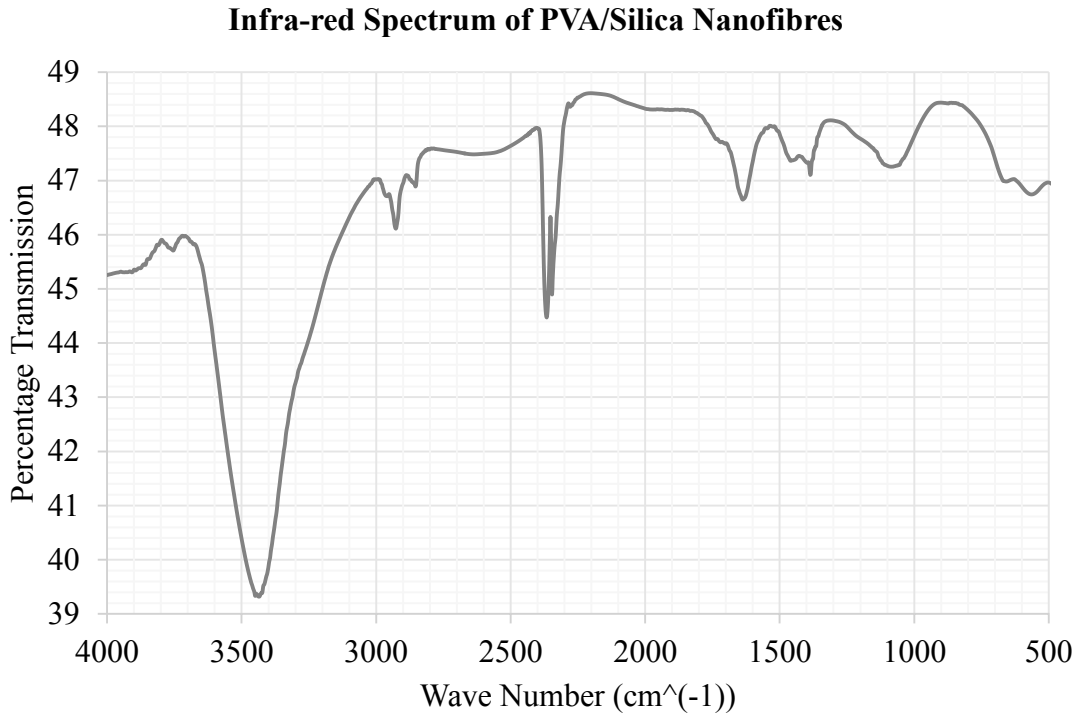

Figure 5.11: FTIR plot for PVA/Silica nanofibres showing wavelengths of infra-red light absorbed by the fibres

The large dip in transmission after wavenumber 3500 cm^{-1}(Oxygen bonds) followed by the spike between wavenumbers 2500 $cm^{-1}$and 2000 cm^{-1}(Carbon-hydrogen bonds) show the presence of PVA [81]. The smaller spikes past wavenumber 2000 cm^{-1}indicate the presence of silica [82], [83]. It was expected that the amount of silica would be lower than PVA since they were mixed in the ratio 2:1. The silica therefore produces lower absorption of the infra-red spectrum than PVA.

6. CONCLUSION

The experimentation presented here aimed to investigate the merit of further investigation. This was done by producing composite PVA/silica nanofibres using electrospinning and then testing the effects of the fibres on the impedance of an air gap.

The apparatus to be used to perform electrospinning was designed, built and optimized successfully based on information gathered in the literature review and experimentation with parameters. It was found that using a copper plate with a hole to hold the spinneret required the critical voltage of electrospinning to be too high. Voltages higher than 25kV induced significant corona on the syringe pump. The plate was therefore removed. Unfortunately this meant the critical voltage of electrospinning could no longer be calculated.

The solution used for electrospinning was initially a replica of the solution used in one of the first experiments to produce pure silica nanofibres. This solution was modified many times to reduce the synthesis time and find a good viscosity. The final solution had a modified ratio of PVA to silica sol and had a mixing agent to allow water and TEOS to mix so that hydrolysis could occur faster. As a result the synthesis was shortened to a few hours and the solution was used to electrospin fibres without spraying.

Once fibres were being produced consistently, parameters of the electrospinning process were varied to see the effect on the morphology of electrospun fibres. A parameter dubbed area of deposition was defined to help characterize the nanofibre deposition. Fibres were electrospun at 19kV applied voltage and 4ml/h flow rate while a 15 gauge stainless steel blunt needle was being used as a spinneret. Changes were made to these parameters. It was found that increasing the applied voltage to 25kV produced more uniformly distributed fibres with smaller diameter while decreasing the applied voltage to 13kV produced less uniform fibres with larger diameters. Changing the flow rate of solution to a larger value of 5ml/h or a smaller value of 3ml/h decreased fibre diameter and increased wastage of solution. For larger flow rates solution was wasted due to overflow of solution while at lower flow rates excessive whipping of the jet caused fibres to deposit on areas other than the collector. Fibres electrospun using a plastic spinneret were found to have one difference from the metal spinneret. This was the area of deposition percentage. The difference is attributed to a combination of differences in

surface tension and electric field strength at the point of release of the solution. The electrospun fibres were tested using infra-red spectroscopy to confirm their composition. The results showed the presence of expected materials, PVA and silica.

Some samples of nanofibres with different average diameters and relatively close areas of deposition were selected for addition to an air gap. The results of testing showed that all samples containing nanofibres decreased the impedance of an air gap. As nanofibre average diameter decreased, so did the sample impedance. Differences in impedance were attributed to changes in resistance since the reactance measurements did not clearly show which samples had higher reactance on average. The phase angle frequency response was found to behave differently in different frequency bands. Further research is required to investigate the reasoning for this behaviour.

REFERENCES

[1] Z. M. Huang, Y. Z. Zhang, M. Kotaki and S. Ramakrishna, "A review on polymer nanofibres by electrospinning and their applications in nanocomposites," *Composites Science and Technology,* vol. 63, no. 1, pp. 2223-2253, 2003.

[2] N. Bhardwaj and S. C. Kundu, "Electrospinning: A fascinating fiber fabrication technique," *Biotechnology Advances,* vol. 28, no. 1, pp. 325-347, 2010.

[3] R. Sahay, P. S. Kumar, R. Sridhar, J. Sundaramurthy, J. Venugopal, S. G. Mhaisalkar and S. Ramakrishna, "Electrospun composite nanofibers and their multifaceted applications," *Journal of Material Chemistry,* vol. 22, no. 1, pp. 12953-12971, 2012.

[4] G. Wang, Z. Tan, X. Liu, S. Chawda, J. S. Koo, V. Samuilov and M. Dudley, "Conducting MWNT/poly(vinyl acetate) composite nanofibres by electrospinning," *Nanotechnology,* vol. 17, no. 1, pp. 5829-5835, 2006.

[5] P. S. Kumar, R. Sahay, V. Aravindan, J. Sundaramurthy, W. C. Ling, V. Thavasi, S. G. Mhaisalkar, S. Madhavi and S. Ramakrishna, "Free-standing electrospun carbon nanofibres-a high performance anode material for lithium ion batteries," *Journal of Physics D: Applied Physics,* vol. 45, pp. 265302-265307, 2012.

[6] H. Wu, L. Hu, M. W. Rowell, D. Kong, J. J. Cha, J. R. McDonough, J. Zhu, M. D. McGehee and Y. Cui, "Electrospun Metal Nanofiber Webs as High-Performance Transparent Electrode," *Nano Letters,* vol. 10, pp. 4242-4248, 2010.

[7] C. Shao, H. Kim, G. Gong and D. Lee, "A novel method for making silica nanofibres by using electrospun fibres of polyvinylalcohol/silica composite as precursor," *Nanotechnology,* vol. 13, pp. 635-637, 2002.

[8] Y. Zhao, H. Wang, X. Lu, X. Li, Y. Yang and C. Wang, "Fabrication of refining mesoporous silica nanofibres via electrospinning," *Materials Letters,* vol. 62, pp. 143-145, 2008.

[9] G. Zang, W. Kataphinan, R. Teye-Mensah, P. Katta, L. Khatri, E. A. Evans, G. G. Chase, R. D. Ramsier and D. H. Reneker, "Electrospun nanofibers for potential space-based applications," *Materials Science and Engineering B,* vol. 116, pp. 353-358, 2005.

[10] M. Wang, N. Jing, C. B. Su, J. Kameoka, C. K. Chou, M. C. Hung and K. A. Chang, "Electrospinning of silica nanochannels for single molecule detection," *Applied Physics Letters,* vol. 88, pp. 033106_1-033106_3, 2006.

[11] L. Chetty, I. Serukenya and N. M. Ijumba, “Vegetable oil based nanocomposite dielectric,” *South African Journal of Science,* vol. 109, 2013.

[12] P. Preetha and M. J. Thomas, “AC Breakdown Characteristics of Epoxy Nanocomposites,” *IEEE Transactions on Dielectrics and Electrical Insulation,* vol. 18, no. 5, pp. 1526-1534, 2011.

[13] R. Liao, J. Hao, G. Chen, Z. Ma and L. Yang, “A Comparative Study of Physiochemical, Dielectric and Thermal Properties of Pressboard Insulation,” *IEEE Transactions on Dielectrics and Electrical Insulation,* vol. 18, no. 5, pp. 1626-1637, 2011.

[14] C. Calebrese, L. Hui, L. S. Schadler and J. K. Nelson, “A Review of Nanocomposite Processing to Enhance Electrical Insulation,” *IEEE Transactions on Dielectrics and Electrical Insulation,* vol. 18, no. 4, pp. 938-945, 2011.

[15] G. Iyer, R. S. Gorur, R. Richer, A. Krivda and L. E. Schmidt, “Dielectric Properties of Epoxy based Nanocomposites for High Voltage Insulation,” *IEEE Transactions on Dielectrics and Electrical Insulation,* vol. 18, no. 5, pp. 659-666, 2011.

[16] S. Li, G. Yin, S. Bai and J. Li, “A New Potential Barrier Modl in Epoxy Resin Nanodielectrics,” *IEEE Transactions on Dielectrics and Electrical Insulation,* vol. 18, no. 5, pp. 1535-1543, 2011.

[17] Z. M. Dang, J. W. Zha, Y. Yu, T. Zhou, H. T. Song and S. T. Li, “Microstructure and Dielectric Characterization of Micro-nanosize Co-filled Composite Films with High Dielectric Permittivity,” *IEEE Transaction on Dielectrics and Electrical Insulation,* vol. 18, no. 5, pp. 1518-1525, 2011.

[18] J. Castellon, H. N. Nguyen, S. Agnel, A. Toureille, M. Frechette, S. Savoie, A. Krivda and L. E. Schmidt, “Electrical Properties Analysis of Micro and Nano Composite Epoxy Resin Materials,” *IEEE Transactions on Dielectrics and Electrical Insulation,* vol. 18, no. 3, pp. 651-658, 2011.

[19] J. C. Fothergill, S. J. Dodd, L. A. Dissado, T. Liu and U. H. Nilsson, “The Measurement of Very Low Conductivity and Dielectric Loss in XLPE Cables: A Possible Method to Detect Degradation Due to Thermal Aging,” *IEEE Transactions on Dielectrics and Electrical Insulation,* vol. 18, no. 5, pp. 1544-1553, 2011.

[20] J. Orbzut, N. Noda and R. Nozaki, “Broadband Characterization of High-Dielectric Constant Films forPower-Ground Decoupling,” *IEEE Transaction on Instrumentaton and Measurement,* vol. 51, no. 4, pp. 829-832, 2002.

[21] N. Bonanos, P. Pissis and J. R. MacDonald, “Impedance Spectroscopy of

Dielectrics and Electronic Conductors," *Characterization of Materials,* pp. 1-14, 2012.

[22] W. E. Teo and S. Ramakrishna, "A review on electrospinning design and nanofibre assemblies," *Nanotechnology,* vol. 17, pp. R89-R106, 2006.

[23] L. S. Carnell, E. J. Siochi, R. A. Wincheski, N. M. Holloway and R. L. Clark, "Electric field effects on fiber alignment using auxilary electrode during electrospining," *Scripta Materialia,* vol. 60, pp. 359-361, 2009.

[24] M. M. L. Arras, C. Grasl, H. Bergmeister and H. Schima, "Electrospinning of aligned fibers with adjustable orientation using auxiliary electrodes," *Science and Technology of Advanced Materials,* vol. 13, pp. 035008-035016, 2012.

[25] J. M. Deitzel, J. D. Kleinmeyer, J. K. Hirvonen and N. C. B. Tan, "Controlled deposition of electrospun poly(ethylene oxide) fibers," *Polymer,* vol. 42, pp. 8163-8170, 2001.

[26] C. J. Angammana and S. H. Jayaram, "Effects of Electric Field on the Multi-jet Eectrospinning Process and Fiber Morphology," *IEEE Transactions on Industry Applications,* vol. 47, no. 2, pp. 1028-1035, 2011.

[27] W. E. Teo, R. Inai and S. Ramakrishna, "Technological advances in electrospinning of nanofibers," *Science and Technology of Advanced Materials,* vol. 12, pp. 013002-013021, 2011.

[28] Y. A. Seo, H. R. Pant, R. Nirmala, J. H. Lee, K. G. Song and H. Y. Kim, "Fabrication of highly porous poly (epsilon-caprolactone) microfibers via electrospinning," *Journal of Porous Materials,* vol. 19, pp. 217-223, 2012.

[29] W. E. Teo and S. Ramakrishna, "Electrospun fibre bundle made of aligned nanofibres over two fixed points," *Nanotechnology,* vol. 16, pp. 1878-1884, 2005.

[30] S. Y. Gu, J. Ren and G. J. Vansco, "Process optimization and empirical modeling for electrospun polycrylonitrile (PAN) nanofiber precursor of carbon nanofibers," *European Polymer Journal,* vol. 41, pp. 2559-2568, 2005.

[31] D. Rodoplu and M. Mutlu, "Effects of Electrospinning Setup and Process Parameters on Nanofiber Morphology Intended for the Modification of Quartz Crystal Microbalance Surfaces," *Journal of Engineered Fibers and Fabrics,* vol. 7, no. 2, pp. 118-123, 2012.

[32] M. Chowdhury and G. Stylios, "Effect of experimental parameters on the morphology of electrospun nylon 6 fibres," *International Journal of Basic and Applied Sciences,* vol. 10, no. 6, pp. 116-131, 2010.

[33] S. Zargham, S. Bazgir, A. Tavakoli, A. S. Rashidi and R. Damerchely, "The Effect of Flow Rate on Morphology and Deposition Area of Nylon 6 Nanofiber," *Journal of Engineered Fibers and Fabrics,* vol. 7, no. 4, pp. 42-49, 2012.

[34] T. Mazoochi, M. Hamadanian, M. Ahmadi and V. Jabbari, "Investigation on the morphological characteristics of nanofiberous membrane as electrospun in the different processing parameters," *International Journal of Industrial Chemistry,* vol. 3, no. 2, 2012.

[35] P. Gupta, C. Elkins, T. E. Long and G. L. Wilkes, "Electrospinning of linear homopolymers of poly (methyl methacrylate): exploring relationships between fiber formation, viscosity, molecular weight and concentration in a good solvent," *Polymer,* vol. 46, pp. 4799-4810, 2005.

[36] J. M. Deitzel, J. D. Kleinmeyer, D. Harris and N. C. B. Tan, "The effect of processing variables on the morphology of electrospun nanofibers and textiles," *Polymer,* vol. 42, pp. 261-272, 2001.

[37] W. K. Son, J. H. Youk, T. S. Lee and W. H. Park, "The effects of solution properties and polyelectrolyte on electrospinning of ultrafine poly (ethylene oxide) fibers," *Polymer,* vol. 45, pp. 2959-2966, 2004.

[38] B. Veleirinho, M. F. Rei and J. A. Lopes-da-Silva, "Solvent and Concentration Effects on the Properties of Electrospun Poly (Ethylene terephthalate) Nanofiber Mats," *Journal of Polymer Science Part B: Polymer Physics,* vol. 46, pp. 460-471, 2008.

[39] C. Mit-uppatham, M. Nithitanakul and P. Supaphol, "Effetcs of Solution Concentration, Emitting Electrode Polarity, Solvent Type and Salt Addition on Electrospun Polyamide-6 Fibers: A Preliminary Report," *Macromolecular Symposium,* vol. 216, pp. 293-299, 2004.

[40] K. H. Lee, H. Y. Kim, M. S. Khil, Y. M. Ra and D. R. Lee, "Characterization of nano-structured poly(epsilon-caprolactone) nonwoven mats via electrospinning," *Polymer,* vol. 44, pp. 1287-1294, 2003.

[41] S. DeVrieze, T. Van Camp, A. Nelvig, Hagstrom, P. Westbroek and K. DeClerck, "The effect of temperature and humididty on electrospinning," *Journal of Materials Science,* vol. 44, pp. 1357-1362, 2009.

[42] C. L. Casper, J. S. Stephens, N. G. Tassi, D. B. Chase and J. F. Rabolt, "Controlling Surface Morphology of Electrospun Polystyrene Fibers: Effect of Humidity and Molecular Weight in the Electrospinning Process," *Macromolecules,* vol. 37, pp. 573-578, 2004.

[43] J. Kameoka, S. S. Verbridge, H. Liu, D. A. Czaplewski and H. G. Craighead, "Fabrication of Suspended Silica Glass Nanofibers from Polymeric Materials Using a Scanned Electrospinning Source," *Nano Leters,* vol. 4, no. 11, pp. 2105-2108, 2004.

[44] M. Krissanasaeranee, T. Vongsetskul, R. Rangkupan, P. Supaphol and S. Wongkasemjit, "Preparation of Ultra-Fine Fibers Using Electrospun Poly(Vinyl Alcohol)/Silatrane Composite Fibers as Precursor," *Journal of the American Ceramic Society,* vol. 91, no. 9, pp. 2830-2835, 2008.

[45] S. S. Choi, S. G. Lee, S. S. Im, S. H. Kim and Y. L. Joo, "Silica nanofibers from electrospinning/sol-gel process," *Journal of Materials Science Letters,* vol. 22, pp. 891-893, 2003.

[46] G. S. Sur, T. J. Lee, J. E. Mark, H. L. Sun and S. G. Lyu, "Composites Prepared by Penetrating Poly (Ethylene Oxide) Chains into Mesoporous Silica," *Colloidal and Polymer Science,* vol. 281, no. 11, pp. 1040-1045, 2003.

[47] C. J. Brinker, "Hydrolysis and Condensation of Silicates: Effects on Structure," *Journal of Non Crystalline Solids,* vol. 100, pp. 31-50, 1988.

[48] A. Bandyopadhyay, M. D. Sarkar and M. K. Bhowmick, "Poly (Vinyl Alcohol)/Silica Nanocomposites by Sol-gel Technique: Synthesis and Properties," *Journal of Materials Science,* vol. 40, pp. 5233-5241, 2005.

[49] Y. Shirosaki, H. Yoshihara, S. Chen, M. Belvins, Y. Nakamura, N. Hanagata, S. Hayakawa, A. Stamboulis and A. Osaka, "Electrospun Poly(Vinyl Alcohol) as a Template of Silica Hollow and Solid Micro-fibrous Mats," *Journal of the Ceramic Society of Japan,* vol. 120, no. 11, pp. 520-524, 2012.

[50] L. L. Hench and J. K. West, "The Sol-Gel Process," *Chemical Reviews,* vol. 90, pp. 33-72, 1990.

[51] B. Karmakar, G. De and D. Ganguli, "Dense Silica Microspheres from Organic and Inorganic Acid Hydrolysis of TEOS," *Journal of Non-crystalline Solids,* vol. 272, pp. 119-126, 2000.

[52] F. Venditti, R. Angelico, G. Palazzo, G. Colafemmina, A. Ceglie and F. Lopez, "Preparation of Nanosize Silica in Reverse Micelles: Ethanol Produced During TEOS Hydrolysis Affects Microemulsion Structure," *Langmuir,* vol. 23, pp. 10063-10068, 2007.

[53] G. Taylor, "Electrically Driven Jets," *Proceedings of the Royal Society of London,* vol. 313, pp. 453-475, 1969.

[54] G. Taylor, "The Force Exerted by an Electric Field on a Long Cylindrical Conductor," *Proceeding of the Royal Society of London,* vol. 291, no. 1425, pp. 145-158, 1966.

[55] E. C. Stauffer, "The Measurement of Surface Tension by the Pendant Drop Technique," *The Journal of Physical Chemistry,* vol. 69, no. 6, pp. 1933-1938, 1965.

[56] A. F. Spivak, Y. A. Dzenis and D. H. Reneker, "A model of Steady State Jet in the Electrospinning Process," *Mechanics Research Communications,* vol. 27, no. 1, pp. 37-42, 2000.

[57] D. H. Reneker, A. L. Yarin, H. Fong and S. Koombhongse, "Bending instability of electrically charged liquid jets of polymer solutions in electrospinning," *Journal of Applied Physics,* vol. 87, no. 9, pp. 4531-4547, 2000.

[58] A. L. Yarin, S. Koombhongse and D. H. Reneker, "Bending instability in electrospinning of nanofibers," *Journal of Applied Physics,* vol. 89, no. 5, pp. 3018-3026, 2001.

[59] M. M. Hohman, M. Shin, G. Rutledge and M. P. Brenner, "Electrospinning and electrically forced jets. I. Stability theory," *Physics of Fluids,* vol. 13, no. 8, pp. 2201-2220, 2001.

[60] M. M. Hohman, M. Shin, G. Rutledge and M. P. Brenner, "Electrospinning and electrically forced jets. II. Applications," *Physics of Fluids,* vol. 13, no. 8, pp. 2221-2236, 2001.

[61] J. J. Feng, "The stretching of an electrified non-Newtonian jet: A model for electrospinning," *Physics of Fluids,* vol. 14, no. 11, pp. 3912-3926, 2002.

[62] C. Hontoria-Lucas, A. J. Lopez-Peinado, J. D. Lopez-Gonzalez, M. L. Rojas-Cervantes and R. M. Martin-Aranda, "Study of Oxygen-Containing Groups in a Series of Graphite Oxides: Physical and Chemical Characterization," *Carbon,* vol. 33, no. 11, pp. 1585-1592, 1995.

[63] W. M. Doyle, "Principles and applications of Fourier transform infrared (FTIR) process analysis," *Process Control and Quality,* vol. 2, no. 50, pp. 11-41, 1992.

[64] V. G. Kohn, "On the Theory of X-Ray Diffraction and X-Ray Standing Waves in the Multilayered Crystal Systems," *Physica Status Solidi (b),* vol. 231, no. 1, pp. 132-148, 2002.

[65] A. L. Ryland, "X-RAY DIFFRACTION," *Journal of chemical education,* vol. 35, no. 2, pp. 80-83, 1958.

[66] P. L. B. Araujo, E. S. Araujo, R. F. S. Santos and A. P. L. Pacheco, "Synthesis and morphological characterization of PMMA/polyaniline nanofiber composites," *Microelectronis Journal,* vol. 36, pp. 1055-1057, 2005.

[67] A. J. Wilkinson and P. B. Hirsch, "Electron Diffraction Based Techniques in Scanning Electron Microscopy of Bulk Materials," *Micron,* vol. 28, no. 4, pp. 279-308, 1997.

[68] E. P. S. Tan and C. T. Lim, "Mechanical characterization of nanofibers- A review," *Composites Science and Technology,* vol. 66, pp. 1102-1111, 2006.

[69] M. A. Haque and M. T. A. Saif, "In-situ Tensile Testing of Nano-scale Specimens in SEM and TEM," *Experimental Mechanics,* vol. 42, no. 1, pp. 123-128, 2002.

[70] E. P. S. Tan, S. Y. Ng and C. T. Lim, "Tensile testing of a single ultrafine polymeric fiber," *Biomaterials,* vol. 26, pp. 1453-1456, 2005.

[71] S. H. Lee, C. Tekemen and W. M. Sigmund, "Three-point bending of electrospun TiO2 nanofibers," *Materials Science and Engineering A,* vol. 398, pp. 77-81, 2005.

[72] X. Chen, Z. H. Xu, X. Li, M. A. Shaibat, Y. Ishii and R. S. Ruoff, "Structural and mechanical characterization of platelet graphite nanofibers," *Carbon,* vol. 45, pp. 416-423, 2007.

[73] Z. M. Myat, T. T. Win, Y. M. Maung and K. K. K. Soe, "Dielectric properties of composite LaMnO3 nanofiber by electrospinning technique," *American Journal of Nanoscience and Nanotechnology,* vol. 1, no. 3, pp. 65-69, 2013.

[74] Pressman, I. Abraham, Billings, Keith, Morey and Taylor, Switching Power Supply Design, 3rd ed., McGraw-Hill, 2009.

[75] M. M. Weiner, "Analysis of Cockroft-Walton Voltage Multipliers with an Arbitrary Number of Stages," *Review of Scientific Instruments,* vol. 40, no. 2, pp. 330-334, 1969.

[76] K. Ma and Y. Lee, "An Integrated Flyback Converter for DC Uninterruptible Power Supply," *IEEE Transactions on Power Electronics,* vol. 11, no. 2, pp. 318-327, 1996.

[77] W. Li, F. Xie, D. Hua, C. Zhang, C. Dai, Z. Yu, M. Qi and S. Yu, "Preparation of P2O5-SiO2 Hollow Microspheres in the Presence of Phosphoric Acid," *Frontiers of Chemical Science and Engineering,* vol. 5, no. 3, pp. 314-317, 2011.

[78] Y. D. Shen, Y. N. Zhao and X. R. Li, "Use of a sol-gel processed polyvinyl alcohol/inorganic silica hybrid material to improve the surface strength of recycled

fibre sheets," *Tappi Journal,* pp. 41-45, 2011.

[79] T. Pirzada, S. A. Arvidson, C. D. Saquing, S. S. Shah and S. A. Khan, "Hybrid PVA-Silica Nanofibres via Sol-Gel Electrospinning," *Langmuir,* vol. 28, pp. 5834-5844, 2012.

[80] M. K. Leach, Z. Feng, S. J. Tuck and J. M. Corey, "Electrospinning Fundamentals: Optimizing Solution and Apparatus Parameters," *Journal of Visualized Experiments,* vol. 2494, no. 47, 2011.

[81] N. Ahad, E. Saion and E. Gharibshahi, "Structural, Thermal and Electrical Properties of PVA-Sodium Salicylate Solid Composite Polymer Electrolyte," *Journal of Nanomaterials,* vol. 2012, 2012.

[82] S. Wu, F. Li, R. Xu, S. Wei and H. Wang, "Preparation of poly (vinyl alcohol)/silica composite nanofibers membrane functionalized with mercapto groups by electrospinning," *Materials Letters,* vol. 64, pp. 1295-1298, 2010.

[83] K. Sasipriya, R. Suriyaprabha, P. Prabu and V. Rajendran, "Synthesis and Characterization of Polymeric Nanofibers Poly (vinyl alcohol) and Poly (vinyl alcohol)/Silica Using Indigenous Electrospinning Set Up," *Materials Research,* vol. 16, no. 4, pp. 824-830, 2013.

[84] Open Source Software, "ImageJ Version 1.49e," Open Source Software, 2014.

APPENDIX

This appendix shall contain all figures, equations and tables relevant to the research undertaken but not presented in the main text.

Appendix A1

The derivation of the equation used to calculate total impedance of the test cell is presented in this section of the appendix. Refer to figure A1.

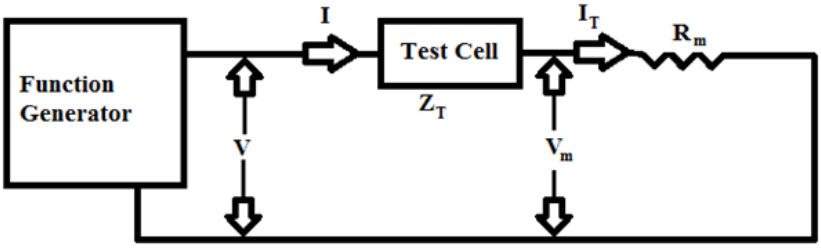

Figure A 1: Electrical diagram of impedance test apparatus showing relevant voltages, currents and impedances

Since the test cell is in series with the measurement resistor:

$$I = I_T$$

$$\frac{V}{Z_T + R_m} = \frac{V_m \angle \theta}{R_m}$$

$$Z_T + R_m = \frac{V . R_m}{V_m \angle \theta}$$

$$Z_T = R_m\left(\frac{V}{V_m \angle \theta} - 1\right)$$

Appendix A2

This section of the appendix contains all SEM images not presented in the main text. They are listed by sample number and the order in which they were taken.

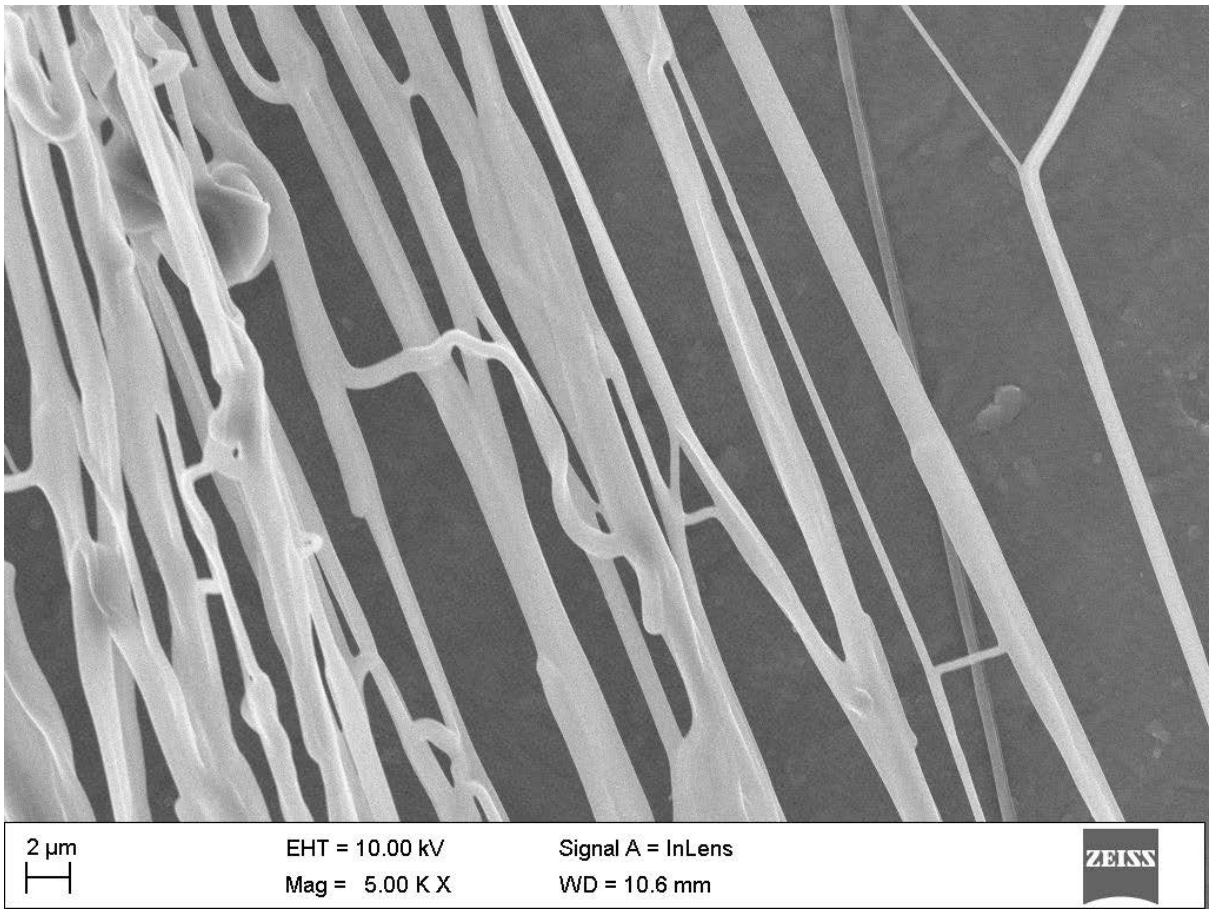

Figure A 2: Sample 1 random area 2electrospun at 19kV, 4ml/h using a 15 gauge needle

The average diameter of fibres in random area 2 of sample 1 approximated to 884 nm. The area not covered by fibres was calculated to be 1086.953 μm^2. The minimum fibre diameter is 236 nm and the maximum fibre diameter is 1733 nm.

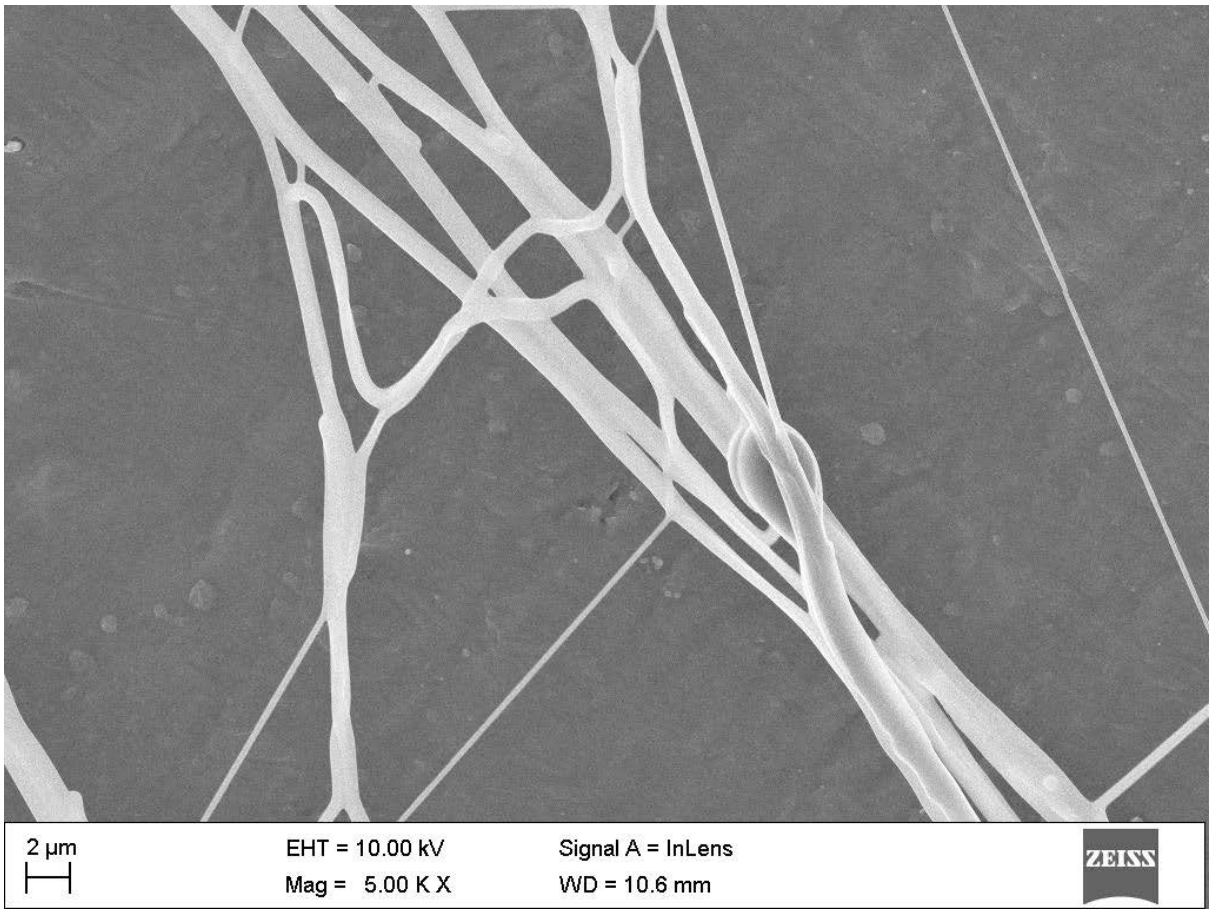

Figure A 3: Sample 1 random area 3electrospun at 19kV, 4ml/h using a 15 gauge needle

The average diameter of fibres in random area 3 of sample 1 approximated to 898 nm. The area not covered by fibres was calculated to be 1635.503 μm^2. The minimum fibre diameter is 259 nm and the maximum fibre diameter is 2036 nm.

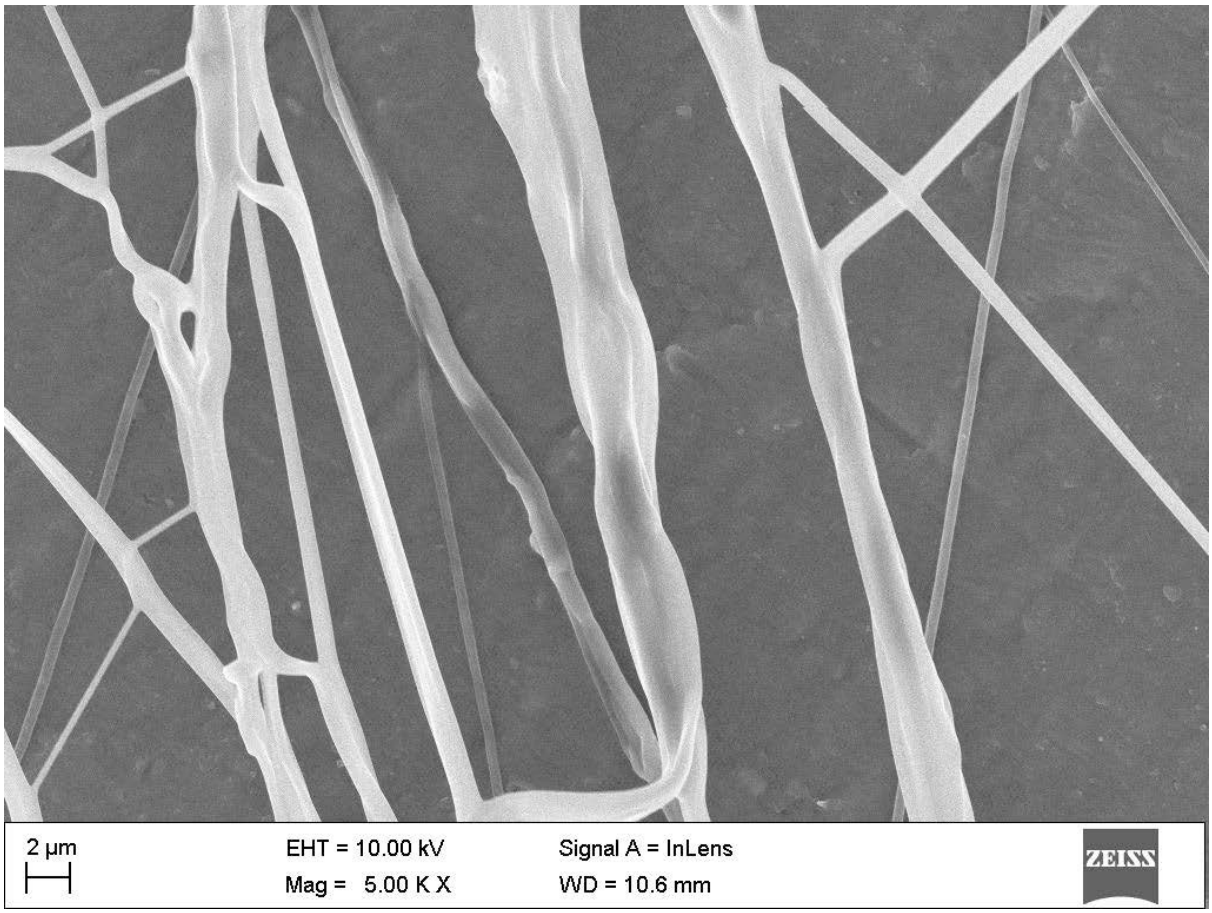

Figure A 4:Sample 1 random area 4electrospun at 19kV, 4ml/h using a 15 gauge needle

The average diameter of fibres in random area 4 of sample 1 approximated to 934 nm. The area not covered by fibres was calculated to be 1507.665 μm^2. The minimum fibre diameter is 320 nm and the maximum fibre diameter is 2700 nm.

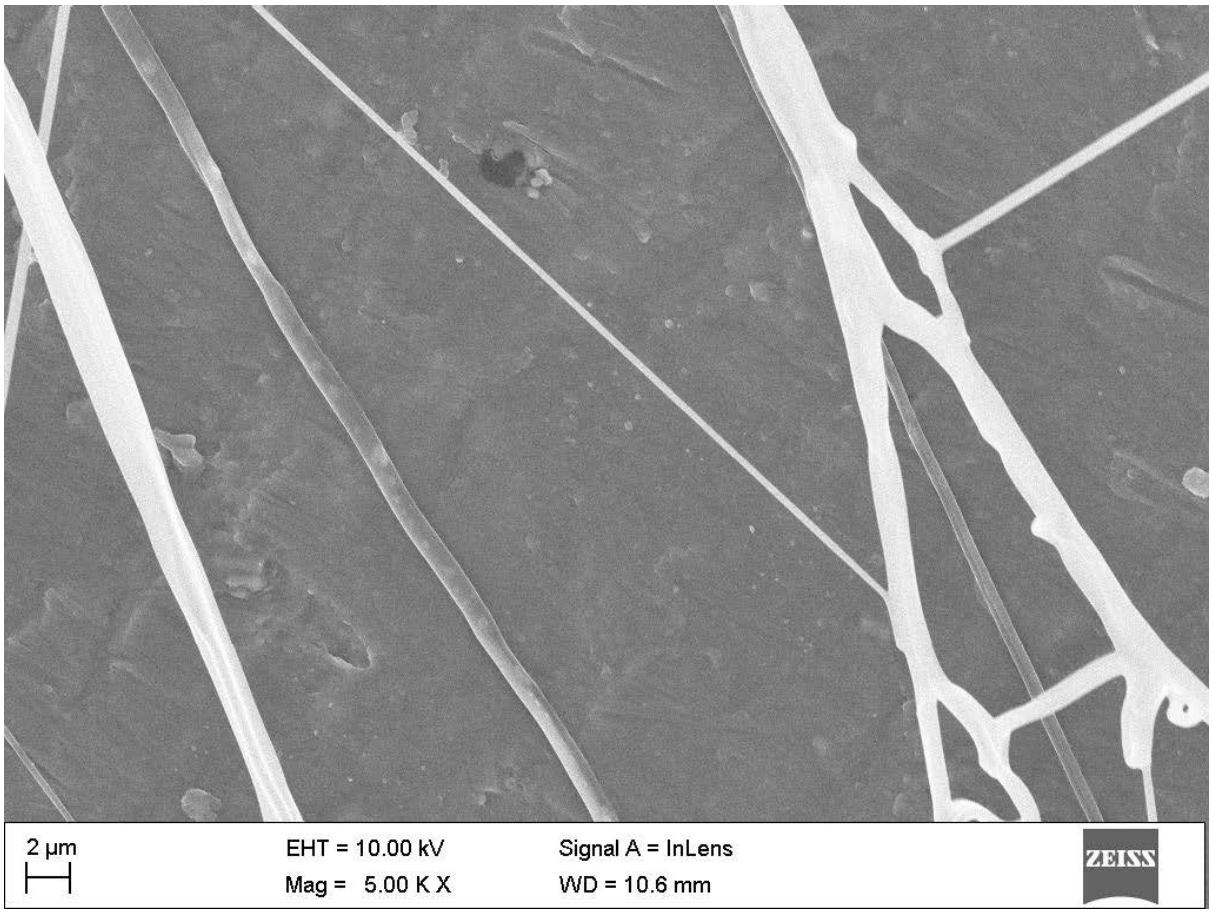

Figure A 5: Sample 1 random area 5electrospun at 19kV, 4ml/h using a 15 gauge needle

The average diameter of fibres in random area 5 of sample 1 approximated to 1030 nm. The area not covered by fibres was calculated to be 1728.504 μm^2. The minimum fibre diameter is 302 nm and the maximum fibre diameter is 2546 nm.

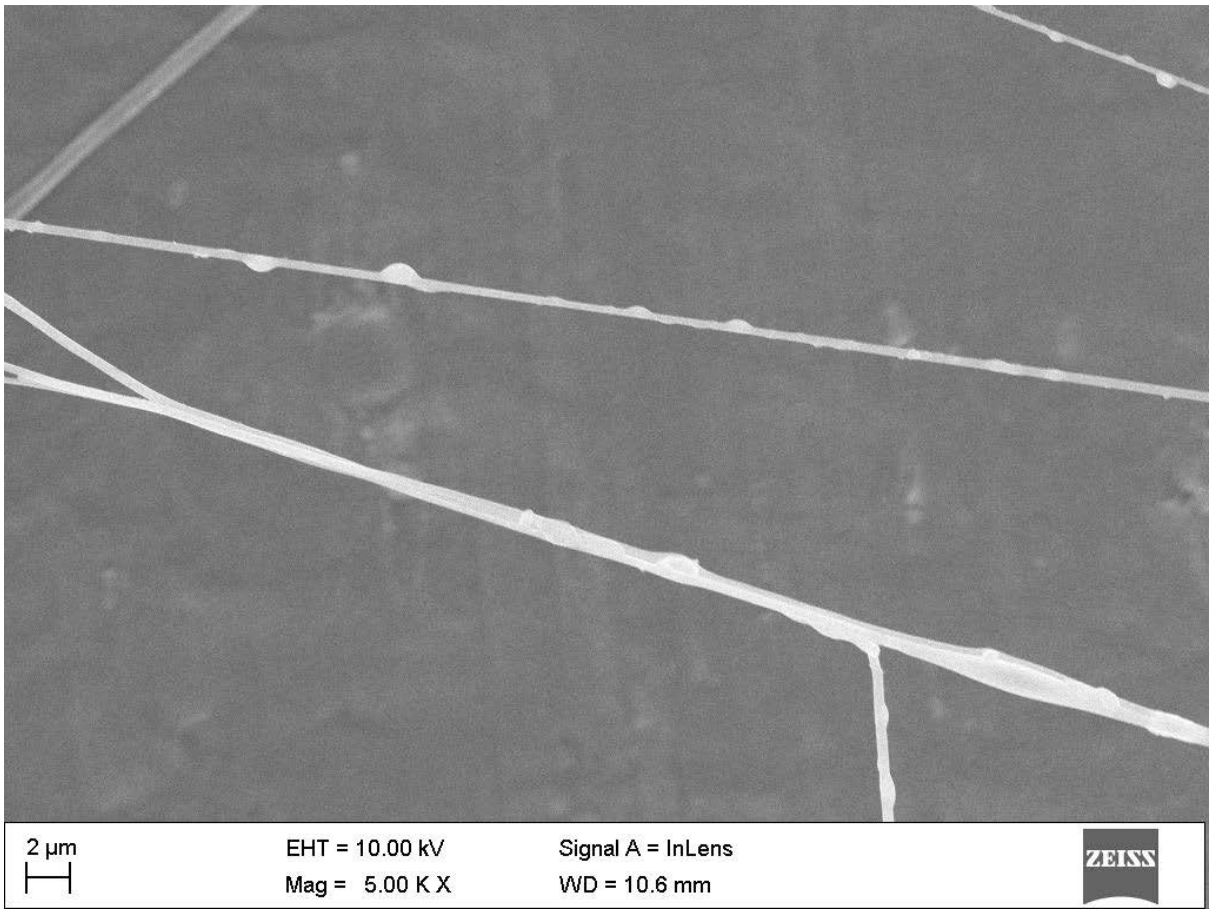

Figure A 6: Sample 2 random area 2electrospun at 13kV, 4ml/h using a 15 gauge needle

The average diameter of fibres in random area 2 of sample 2 approximated to 578 nm. The area not covered by fibres was calculated to be 1833.937 μm^2. The minimum fibre diameter is 259 nm and the maximum fibre diameter is 1018 nm.

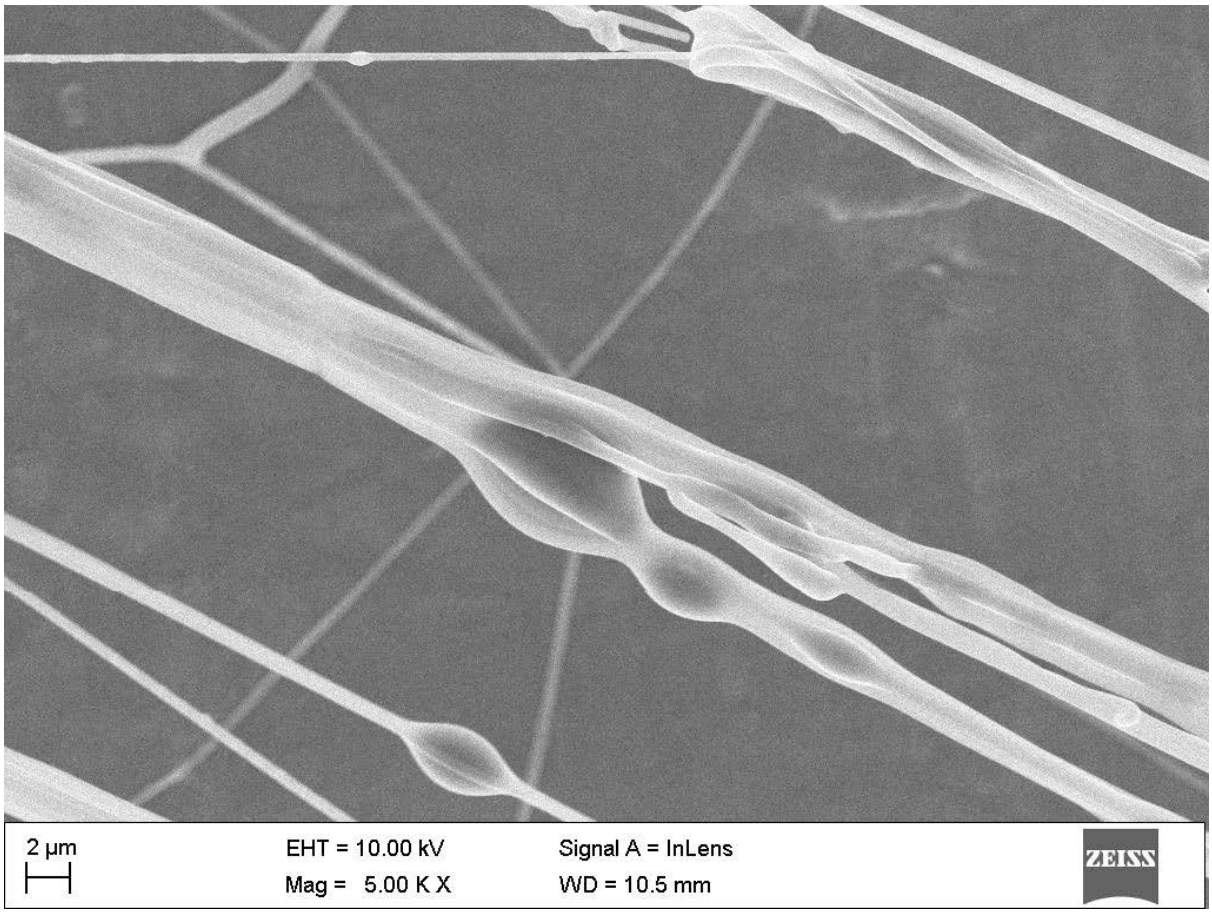

Figure A 7: Sample 2 random area 3electrospun at 13kV, 4ml/h using a 15 gauge needle

The average diameter of fibres in random area 3 of sample 2 approximated to 930 nm. The area not covered by fibres was calculated to be 1504.768 μm^2. The minimum fibre diameter is 382 nm and the maximum fibre diameter is 1508 nm.

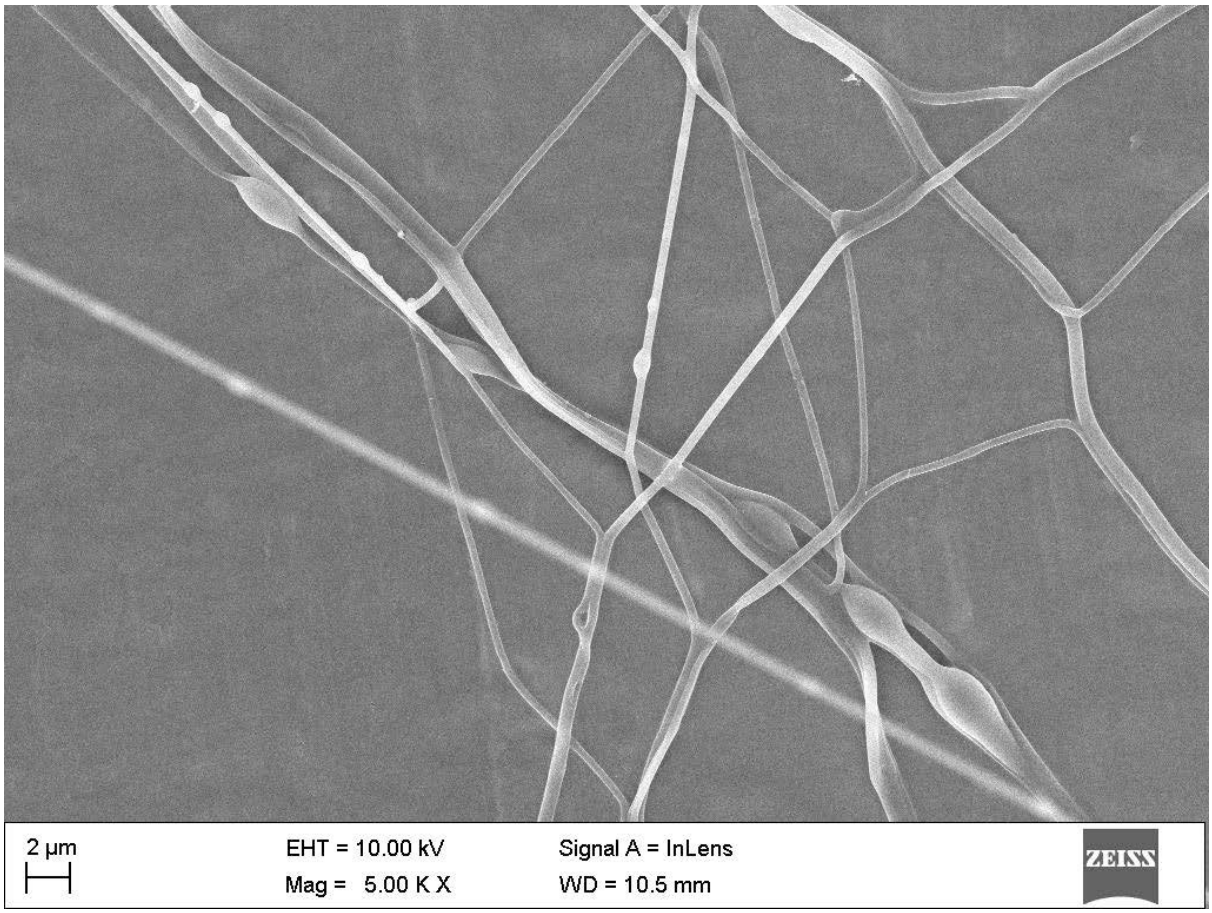

Figure A8: Sample 2 random area 4electrospun at 13kV, 4ml/h using a 15 gauge needle

The average diameter of fibres in random area 4 of sample 2 approximated to 759 nm. The area not covered by fibres was calculated to be 1793.305 μm^2. The minimum fibre diameter is 417 nm and the maximum fibre diameter is 1265 nm.

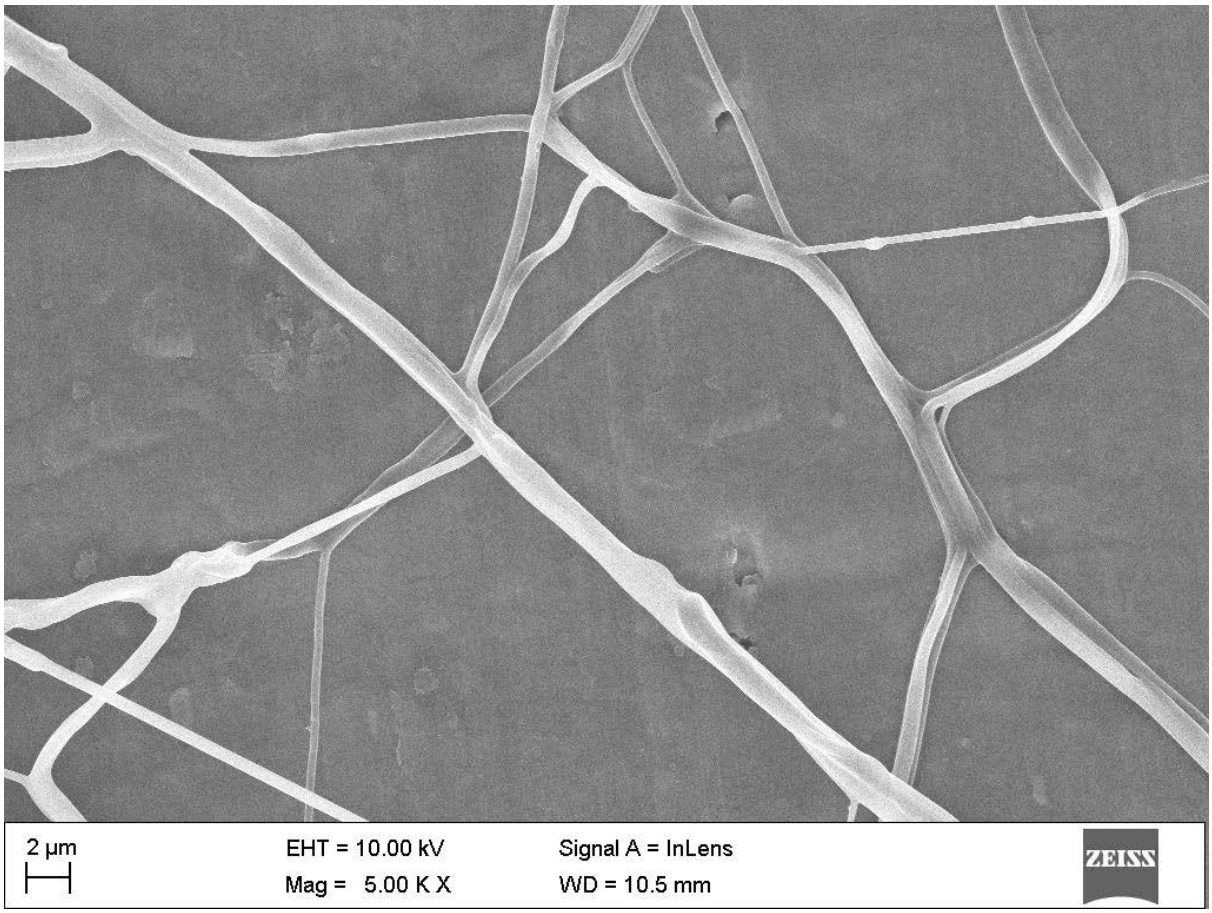

Figure A 9: Sample 2 random area 5electrospun at 13kV, 4ml/h using a 15 gauge needle

The average diameter of fibres in random area 5 of sample 2 approximated to 1110 nm. The area not covered by fibres was calculated to be 871.916 μm^2. The minimum fibre diameter is 356 nm and the maximum fibre diameter is 1365 nm.

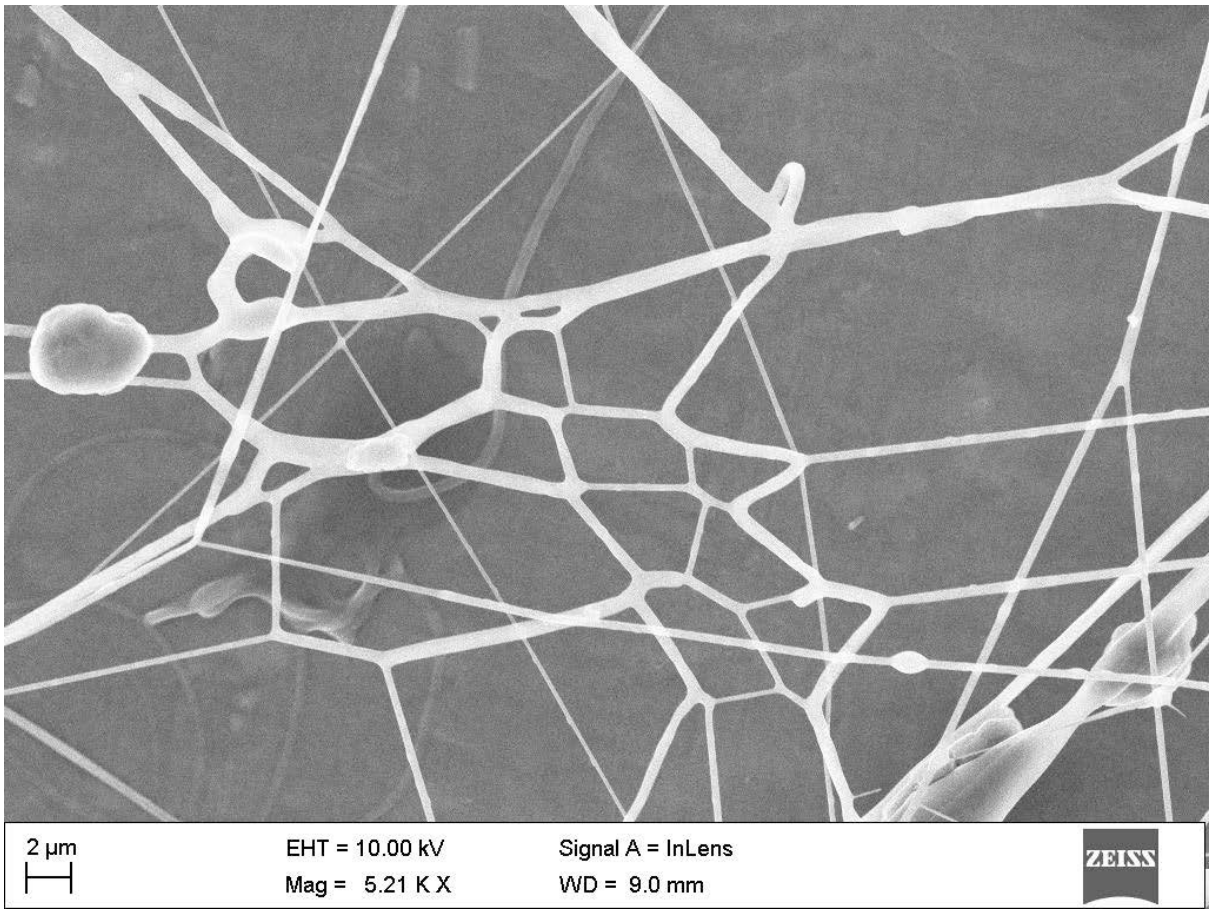

Figure A 10: Sample 3 random area 2electrospun at 25kV, 4ml/h using a 15 gauge needle

The average diameter of fibres in random area 2 of sample 3 approximated to 558 nm. The area not covered by fibres was calculated to be 1628.891 μm^2. The minimum fibre diameter is 150 nm and the maximum fibre diameter is 1020 nm.

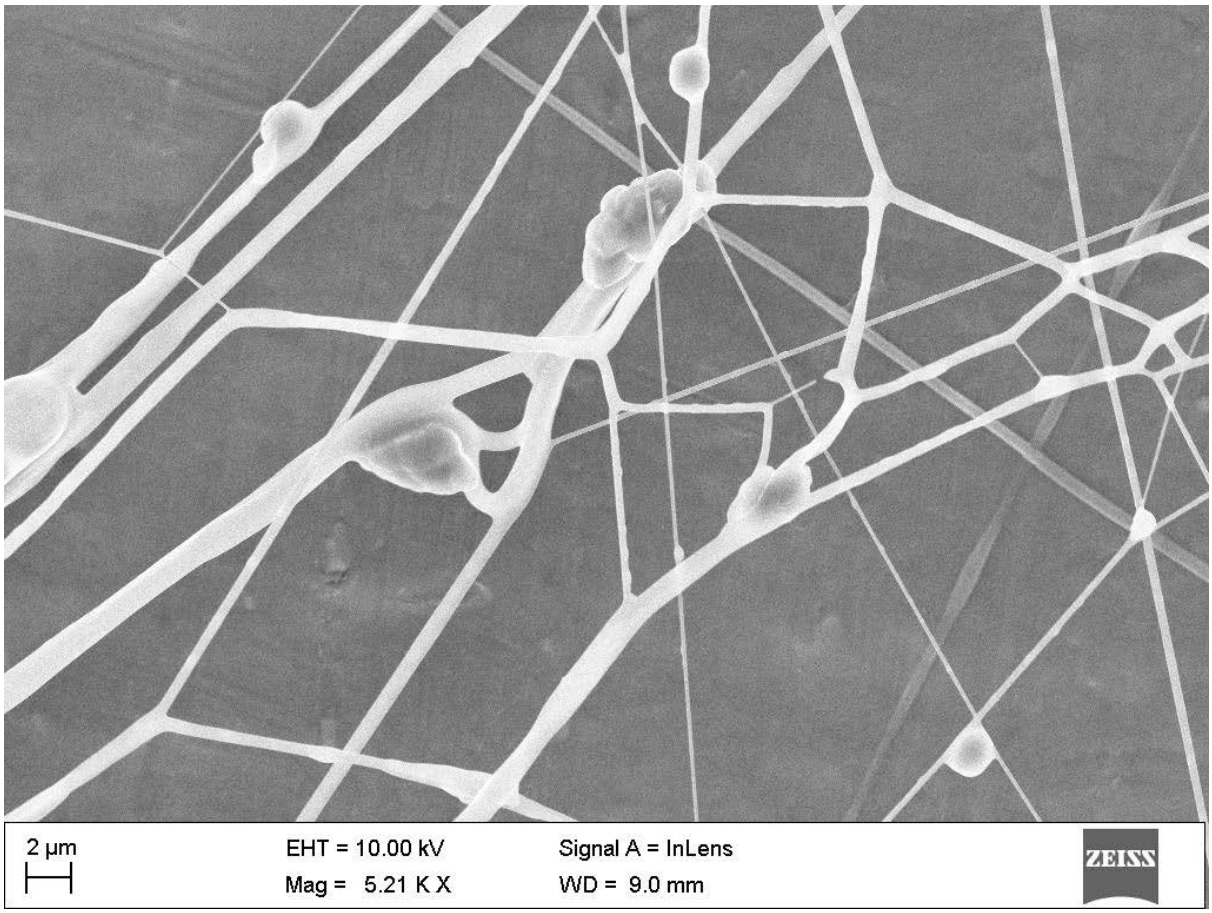

Figure A11: Sample 3 random area 3electrospun at 25kV, 4ml/h using a 15 gauge needle

The average diameter of fibres in random area 3 of sample 3 approximated to 457 nm. The area not covered by fibres was calculated to be 1586.622 μm^2. The minimum fibre diameter is 140 nm and the maximum fibre diameter is 1309 nm.

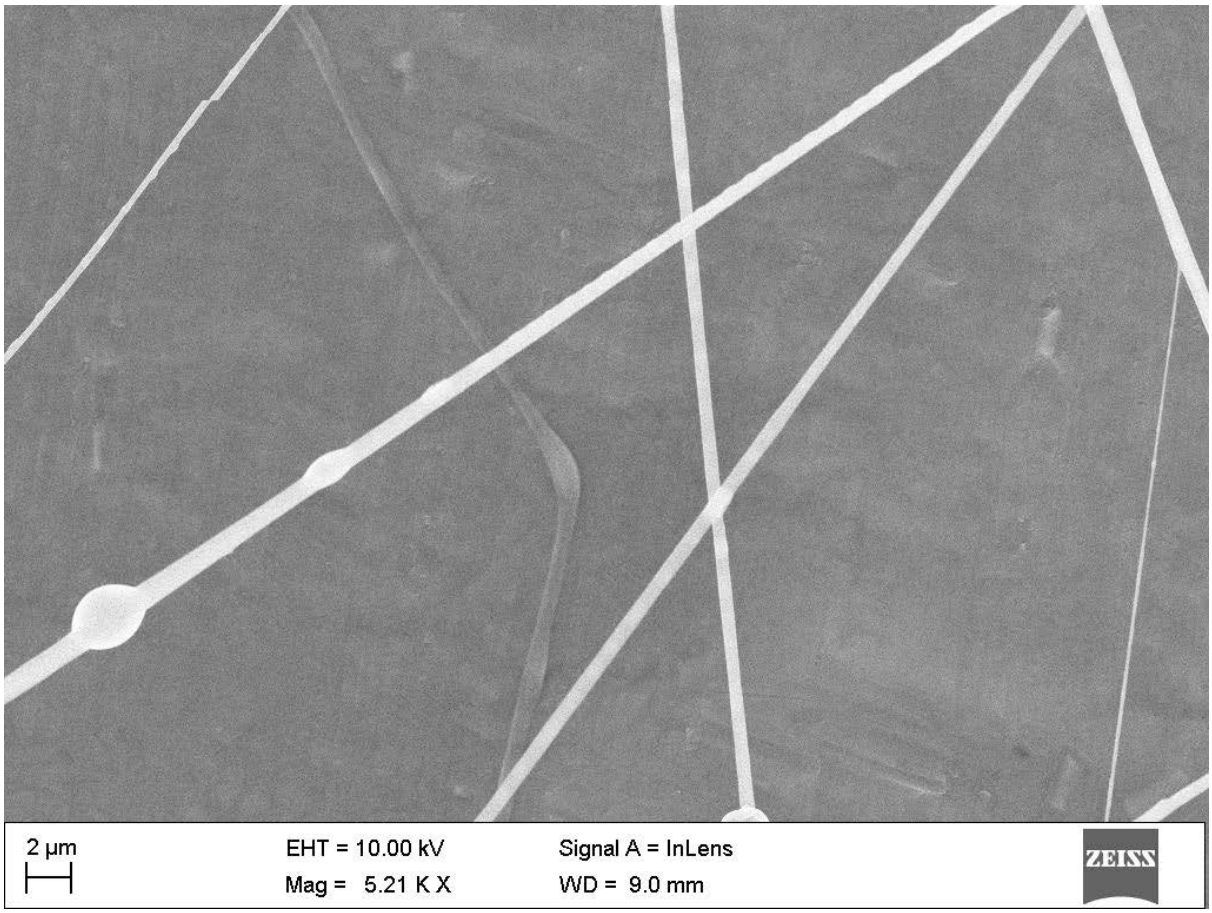

Figure A 12: Sample 3 random area 4electrospun at 25kV, 4ml/h using a 15 gauge needle

The average diameter of fibres in random area 4 of sample 3 approximated to 466 nm. The area not covered by fibres was calculated to be 1844.216 μm^2. The minimum fibre diameter is 175 nm and the maximum fibre diameter is 1206 nm.

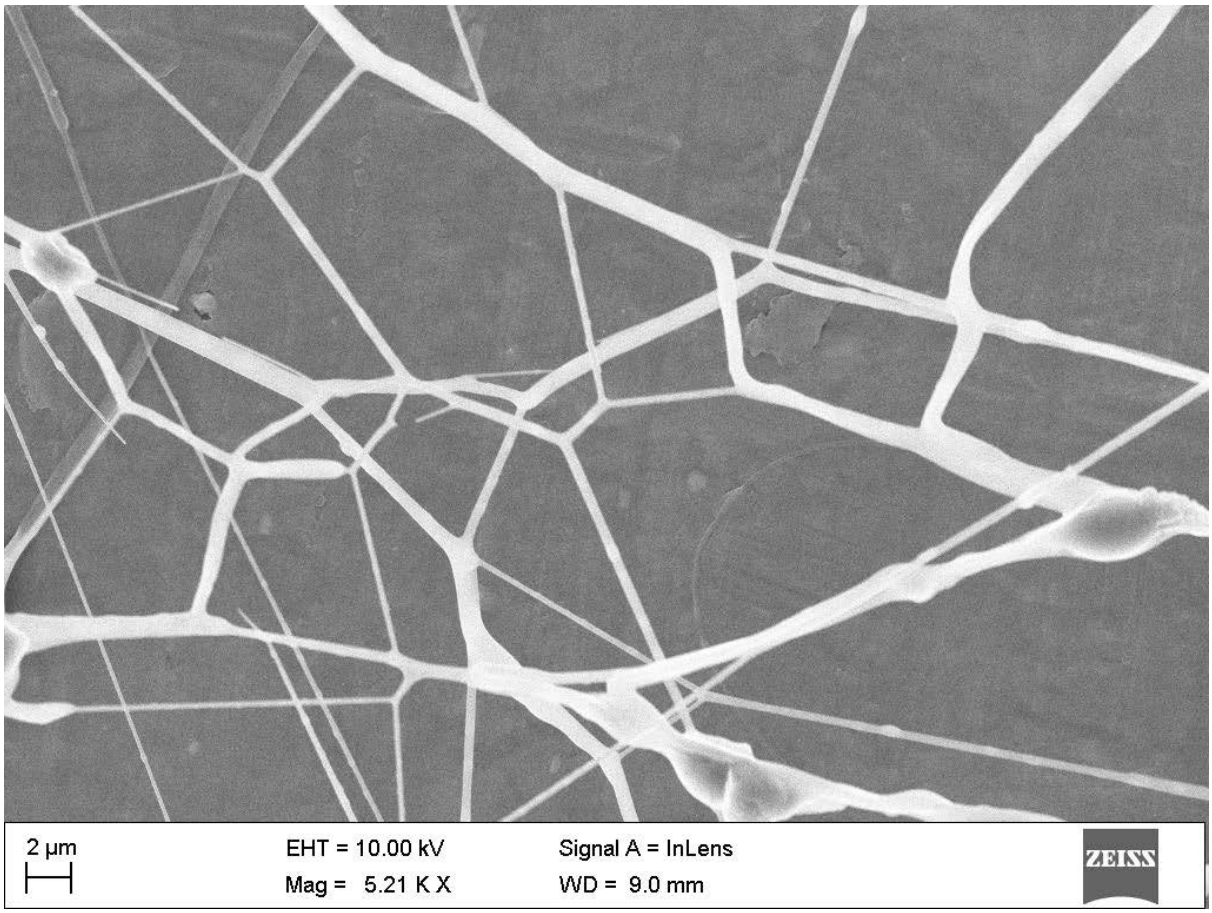

Figure A 13:Sample 3 random area 5electrospun at 25kV, 4ml/h using a 15 gauge needle

The average diameter of fibres in random area 5 of sample 3 approximated to 620 nm. The area not covered by fibres was calculated to be 1631.591 μm^2. The minimum fibre diameter is 200 nm and the maximum fibre diameter is 1583 nm.

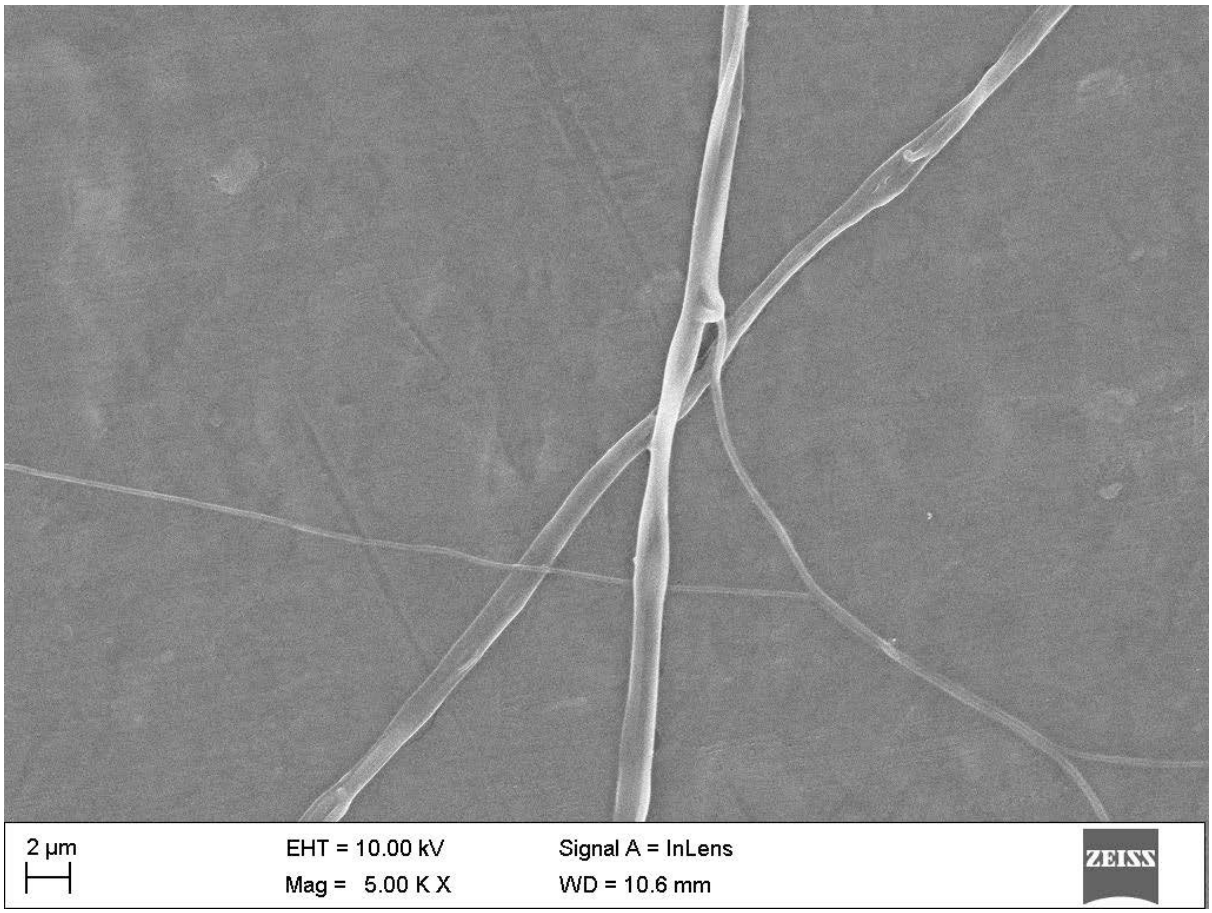

Figure A 14: Sample 4 random area 2electrospun at 19kV, 3ml/h using a 15 gauge needle

The average diameter of fibres in random area 2 of sample 4 approximated to 690 nm. The area not covered by fibres was calculated to be 1842.207 μm^2. The minimum fibre diameter is 351 nm and the maximum fibre diameter is 1350 nm.

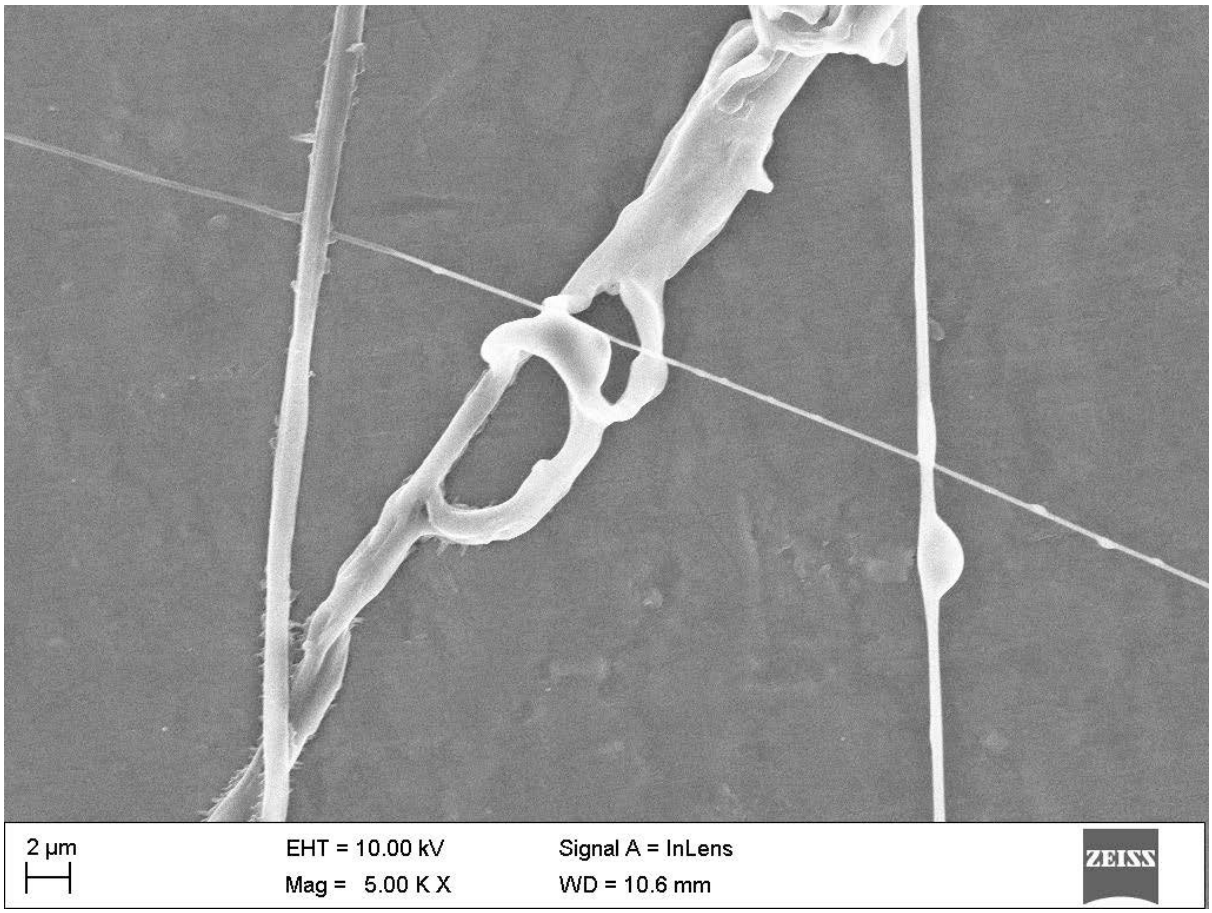

Figure A 15: Sample 4 random area 3 electrospun at 19kV, 3ml/h using a 15 gauge needle

The average diameter of fibres in random area 3 of sample 4 approximated to 880 nm. The area not covered by fibres was calculated to be 1732.542 μm^2. The minimum fibre diameter is 140 nm and the maximum fibre diameter is 1674 nm.

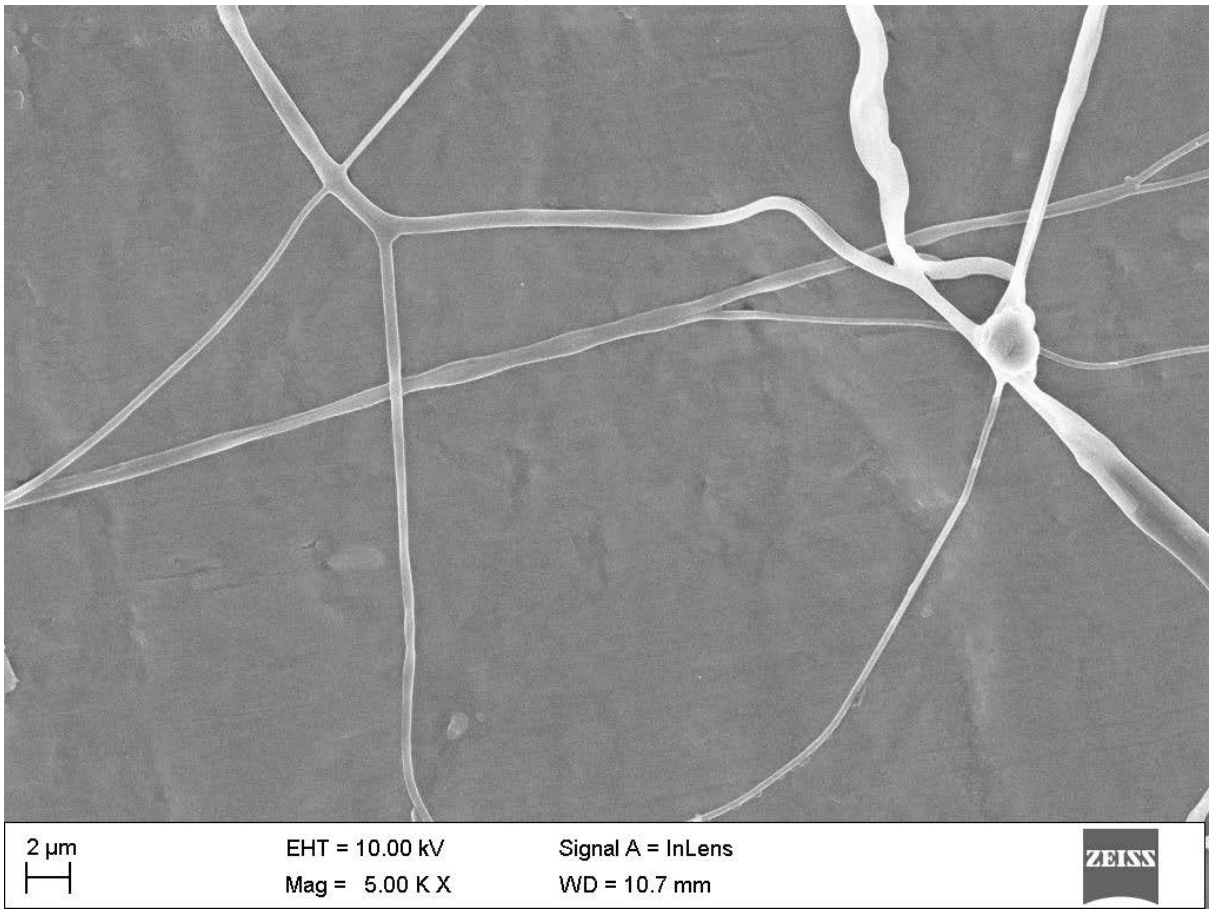

Figure A 16: Sample 4 random area 4 electrospun at 19kV, 3ml/h using a 15 gauge needle

The average diameter of fibres in random area 4 of sample 4 approximated to 497 nm. The area not covered by fibres was calculated to be 1766.137 μm^2. The minimum fibre diameter is 274 nm and the maximum fibre diameter is 837 nm.

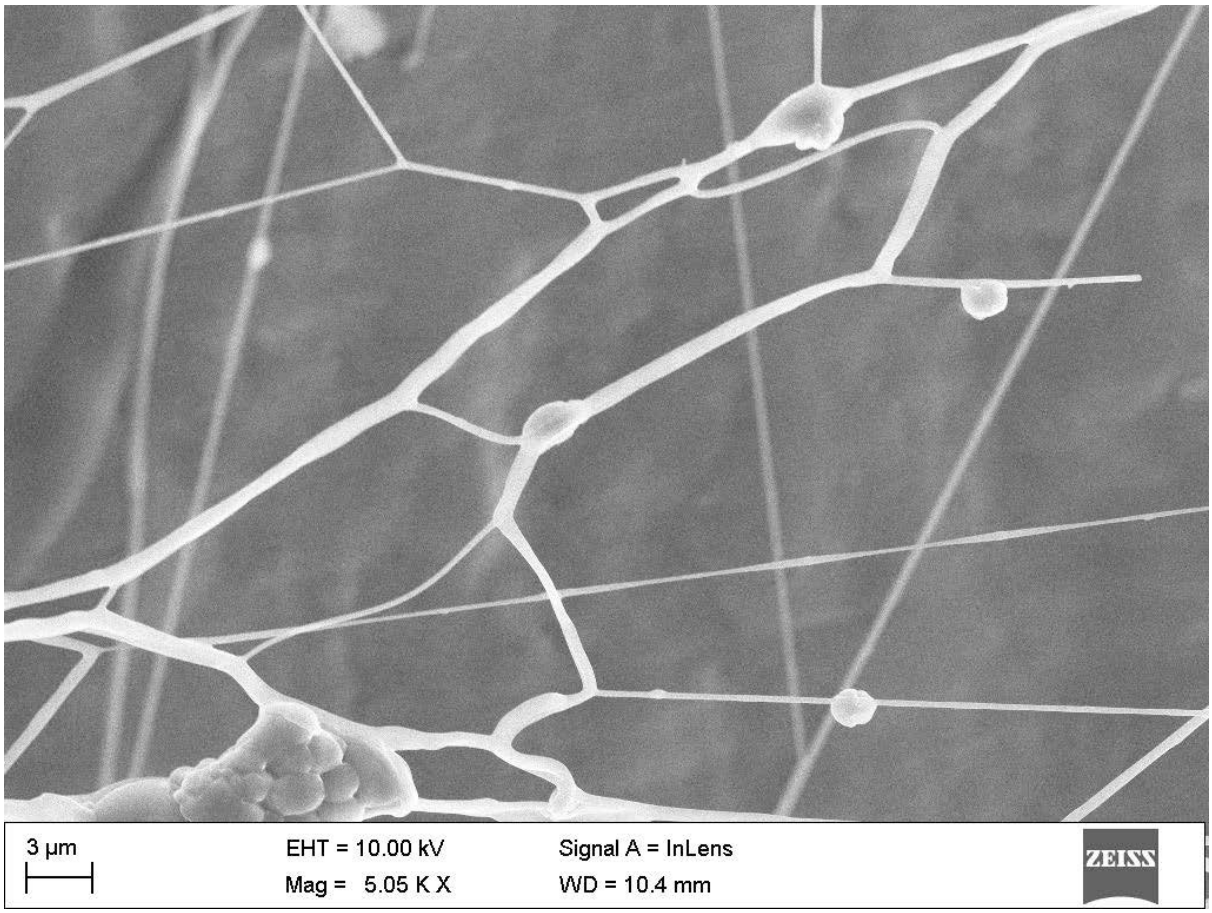

Figure A 17: Sample 4 random area 5 electrospun at 19kV, 3ml/h using a 15 gauge needle

The average diameter of fibres in random area 5 of sample 4 approximated to 563 nm. The area not covered by fibres was calculated to be 1722.720 μm^2. The minimum fibre diameter is 281 nm and the maximum fibre diameter is 900 nm.

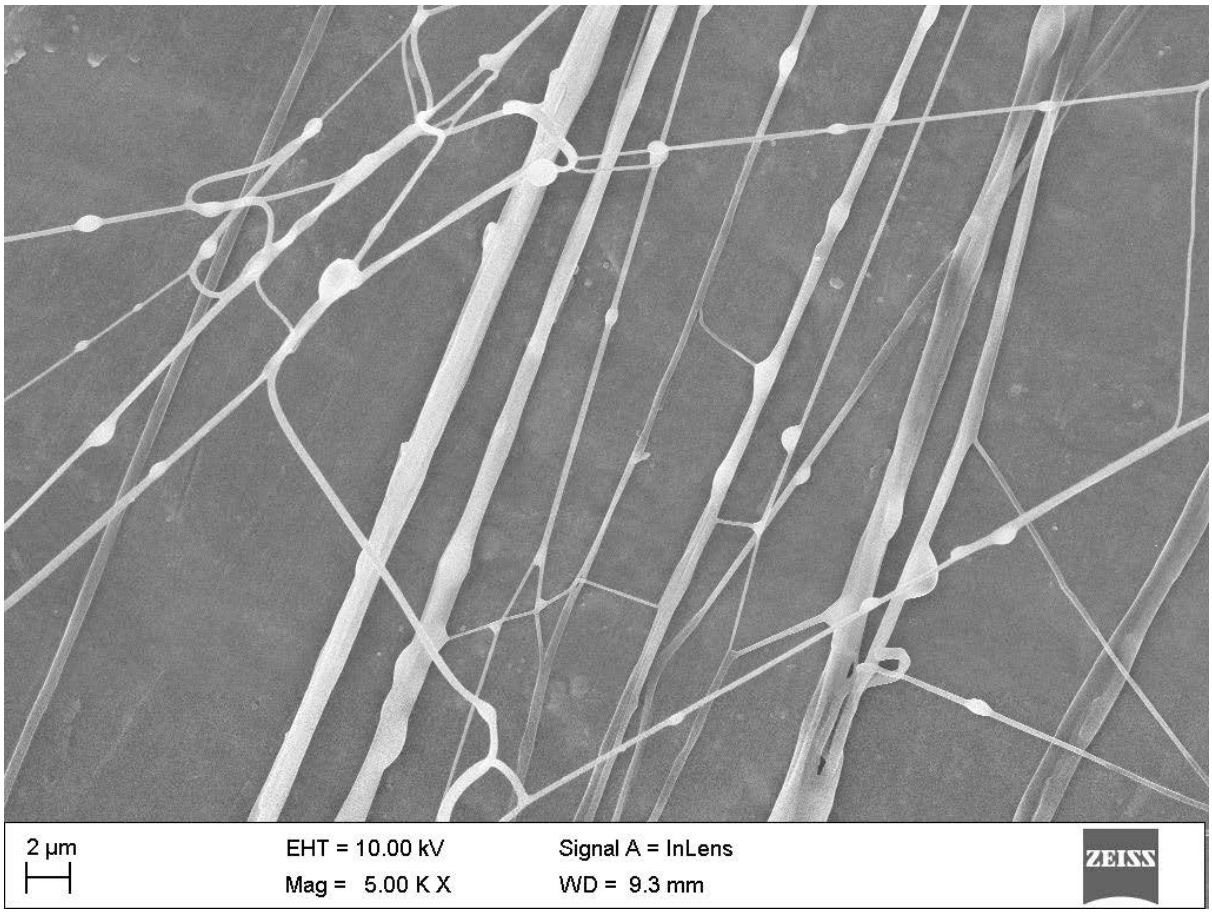

Figure A18: Sample 5 random area 2 electrospun at 19kV, 5ml/h using a 15 gauge needle

The average diameter of fibres in random area 2 of sample 5 approximated to 520 nm. The area not covered by fibres was calculated to be 1645.214 μm^2. The minimum fibre diameter is 169 nm and the maximum fibre diameter is 1437 nm.

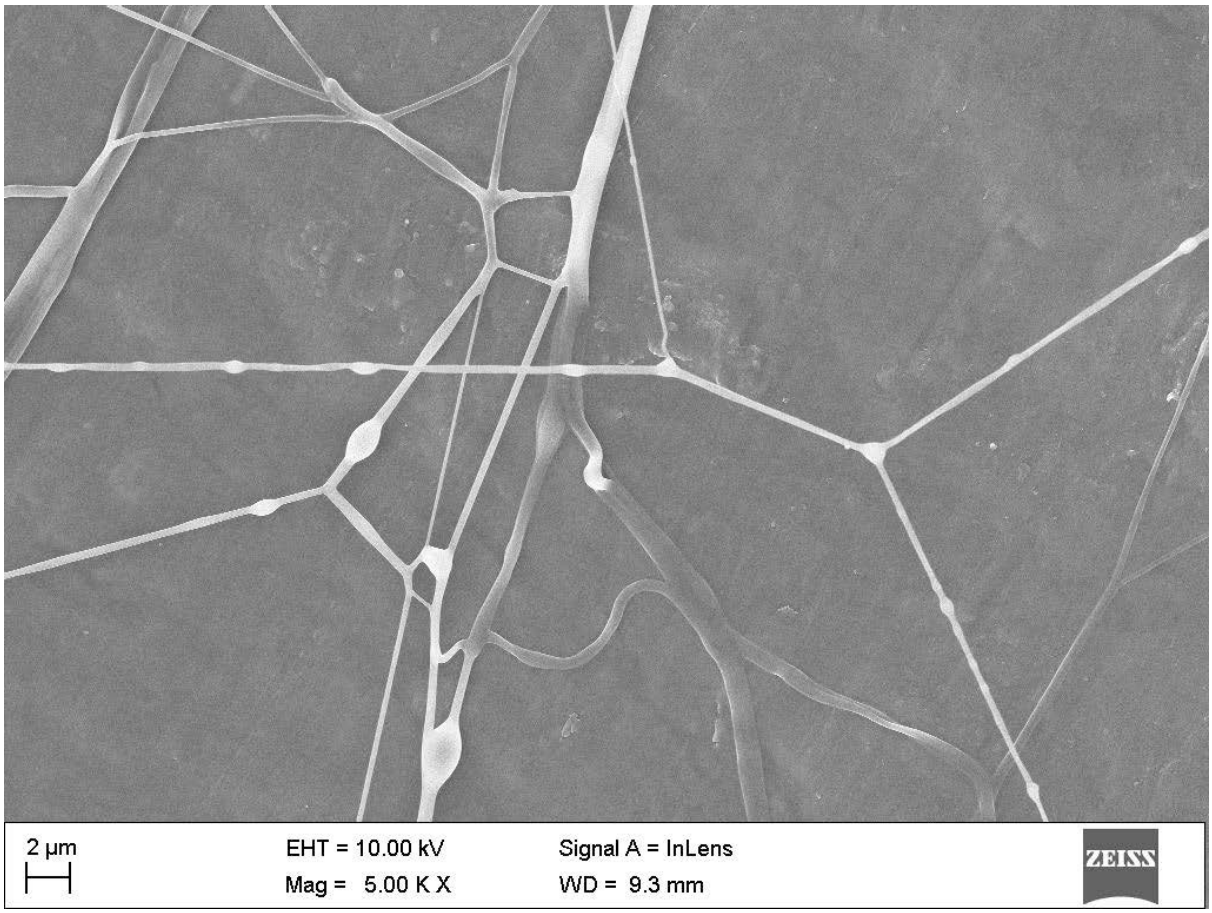

Figure A 19: Sample 5 random area 3 electrospun at 19kV, 5ml/h using a 15 gauge needle

The average diameter of fibres in random area 3 of sample 5 approximated to 471 nm. The area not covered by fibres was calculated to be 1855.240 μm^2. The minimum fibre diameter is 171 nm and the maximum fibre diameter is 1210 nm.

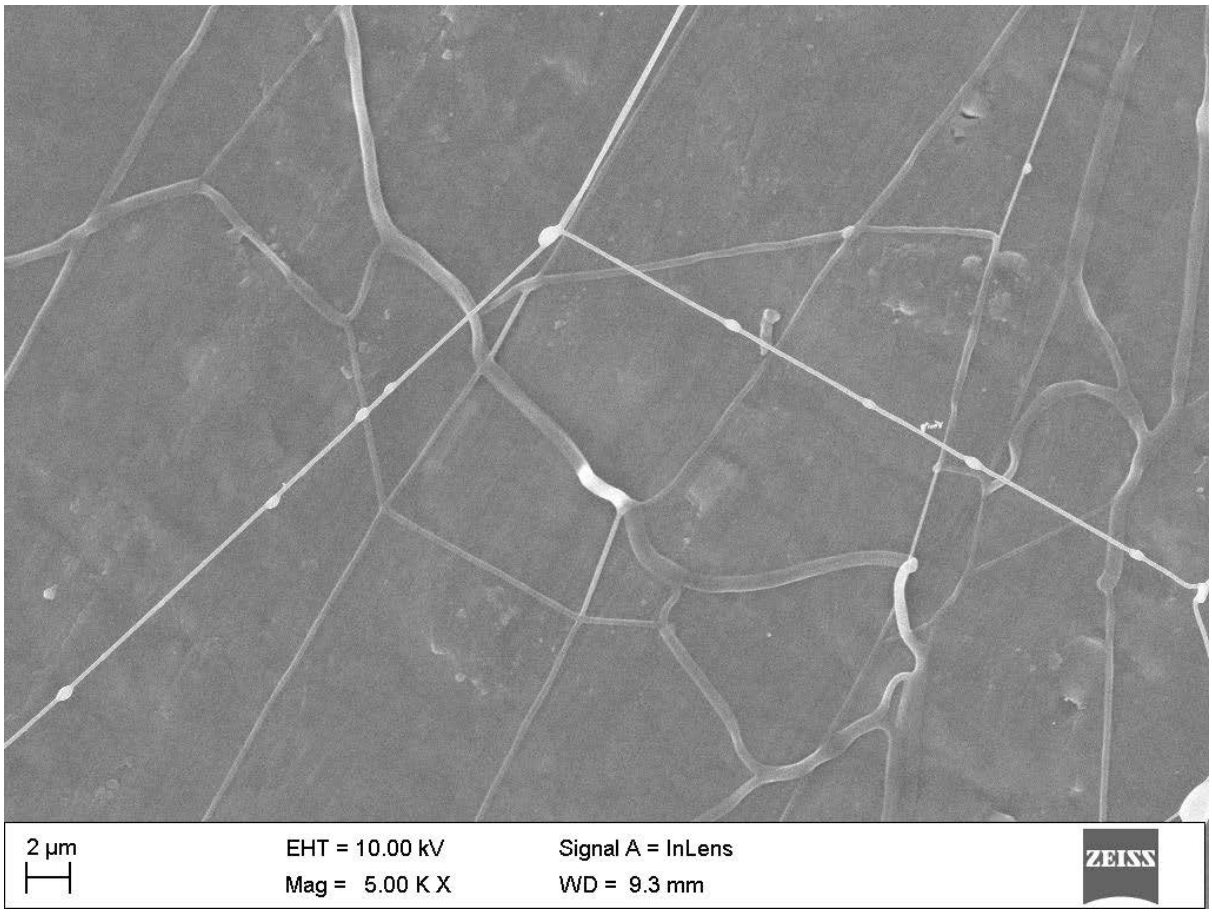

Figure A 20: Sample 5 random area 4 electrospun at 19kV, 5ml/h using a 15 gauge needle

The average diameter of fibres in random area 4 of sample 5 approximated to 427 nm. The area not covered by fibres was calculated to be 1810.118 μm^2. The minimum fibre diameter is 224 nm and the maximum fibre diameter is 751 nm.

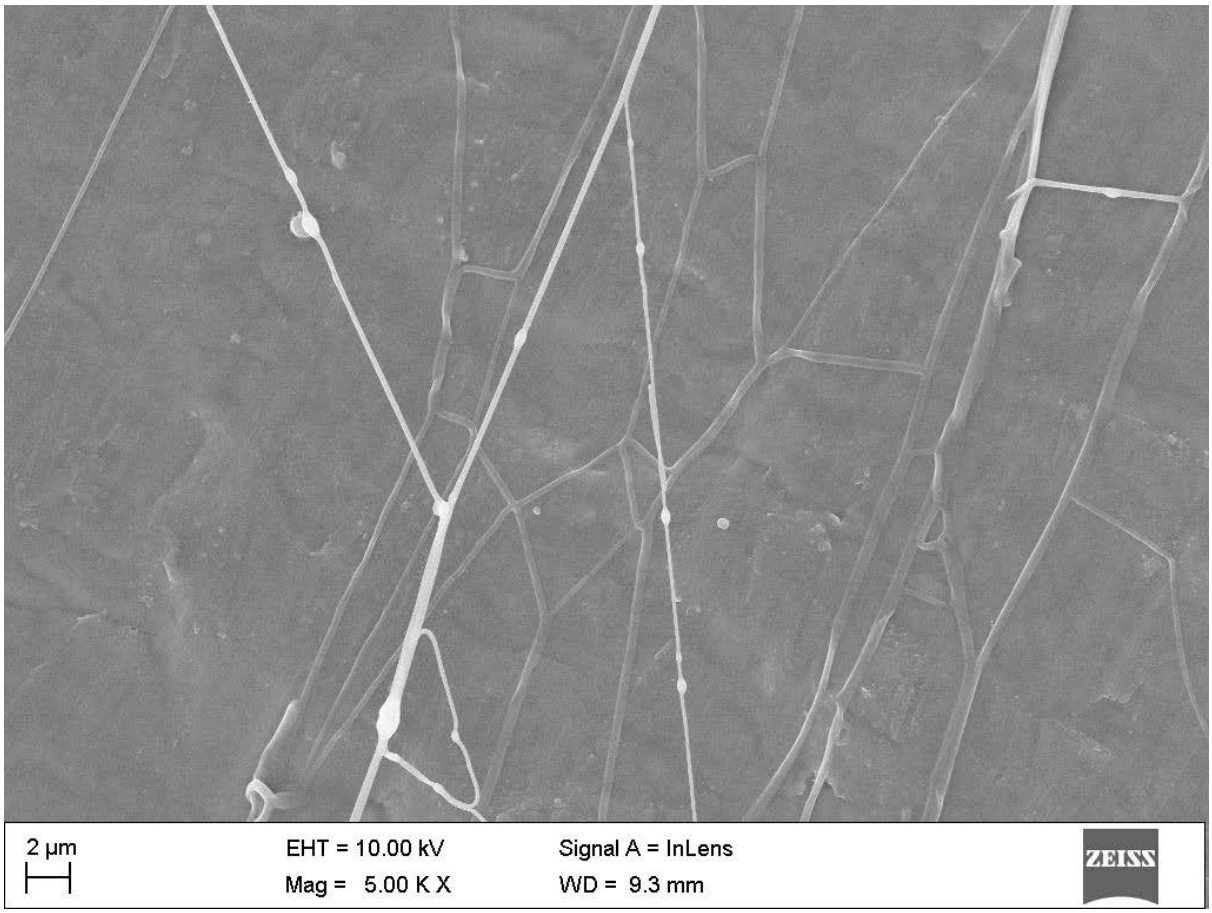

Figure A 21: Sample 5 random area 5 electrospun at 19kV, 5ml/h using a 15 gauge needle

The average diameter of fibres in random area 5 of sample 5 approximated to 290 nm. The area not covered by fibres was calculated to be 1796.465 μm^2. The minimum fibre diameter is 208 nm and the maximum fibre diameter is 932 nm.

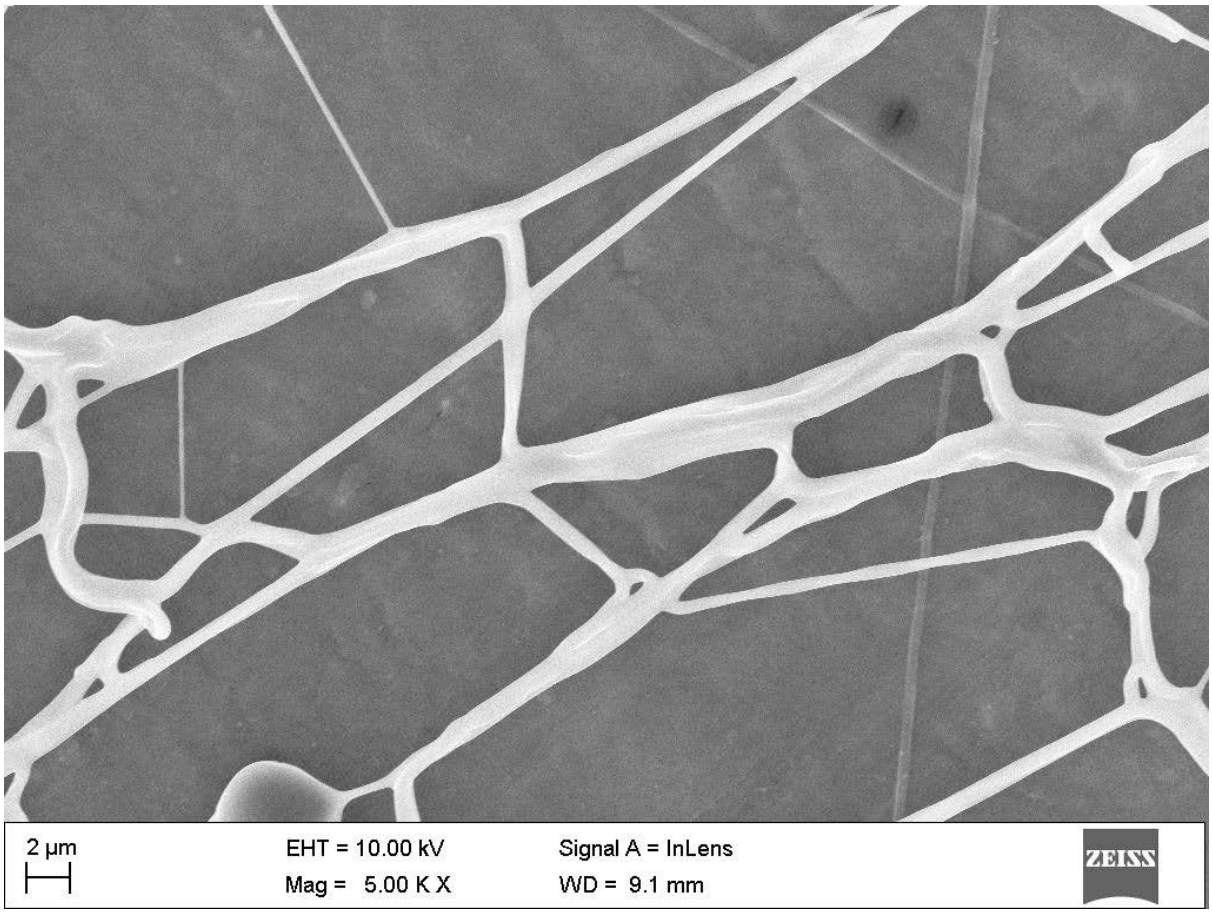

Figure A 22: Sample 6 random area 2 electrospun at 19kV, 4ml/h using a plastic pipette

The average diameter of fibres in random area 2 of sample 6 approximated to 658 nm. The area not covered by fibres was calculated to be 1591.360 μm^2. The minimum fibre diameter is 361 nm and the maximum fibre diameter is 1000 nm.

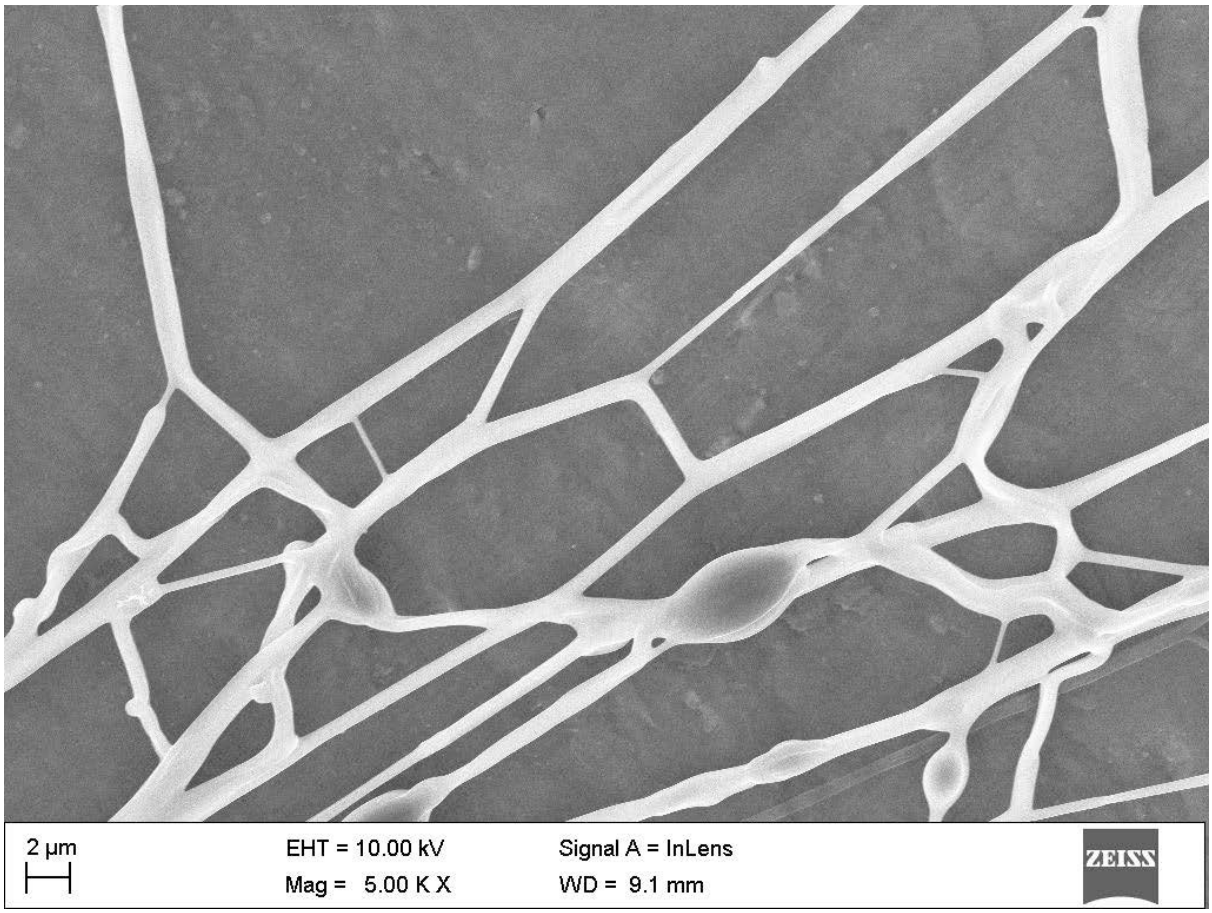

Figure A 23: Sample 6 random area 3 electrospun at 19kV, 4ml/h using a plastic pipette

The average diameter of fibres in random area 3 of sample 6 approximated to 846 nm. The area not covered by fibres was calculated to be 1542.471 μm^2. The minimum fibre diameter is 595 nm and the maximum fibre diameter is 1005 nm.

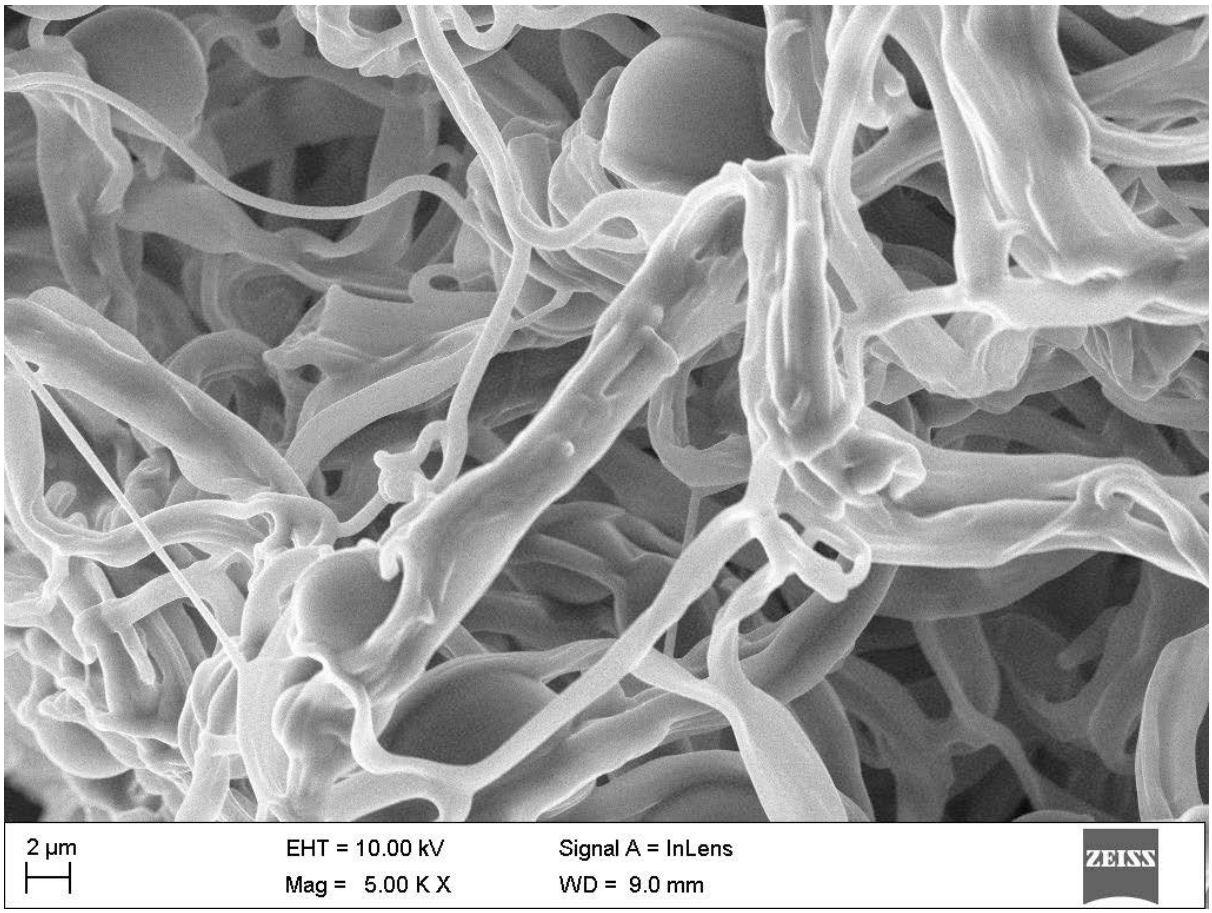

Figure A 24: Sample 6 random area 4 electrospun at 19kV, 4ml/h using a plastic pipette

The average diameter of fibres in random area 4 of sample 6 approximated to 1247 nm. The area not covered by fibres was calculated to be 217.518 μm^2. The minimum fibre diameter is 253 nm and the maximum fibre diameter is 3387 nm.

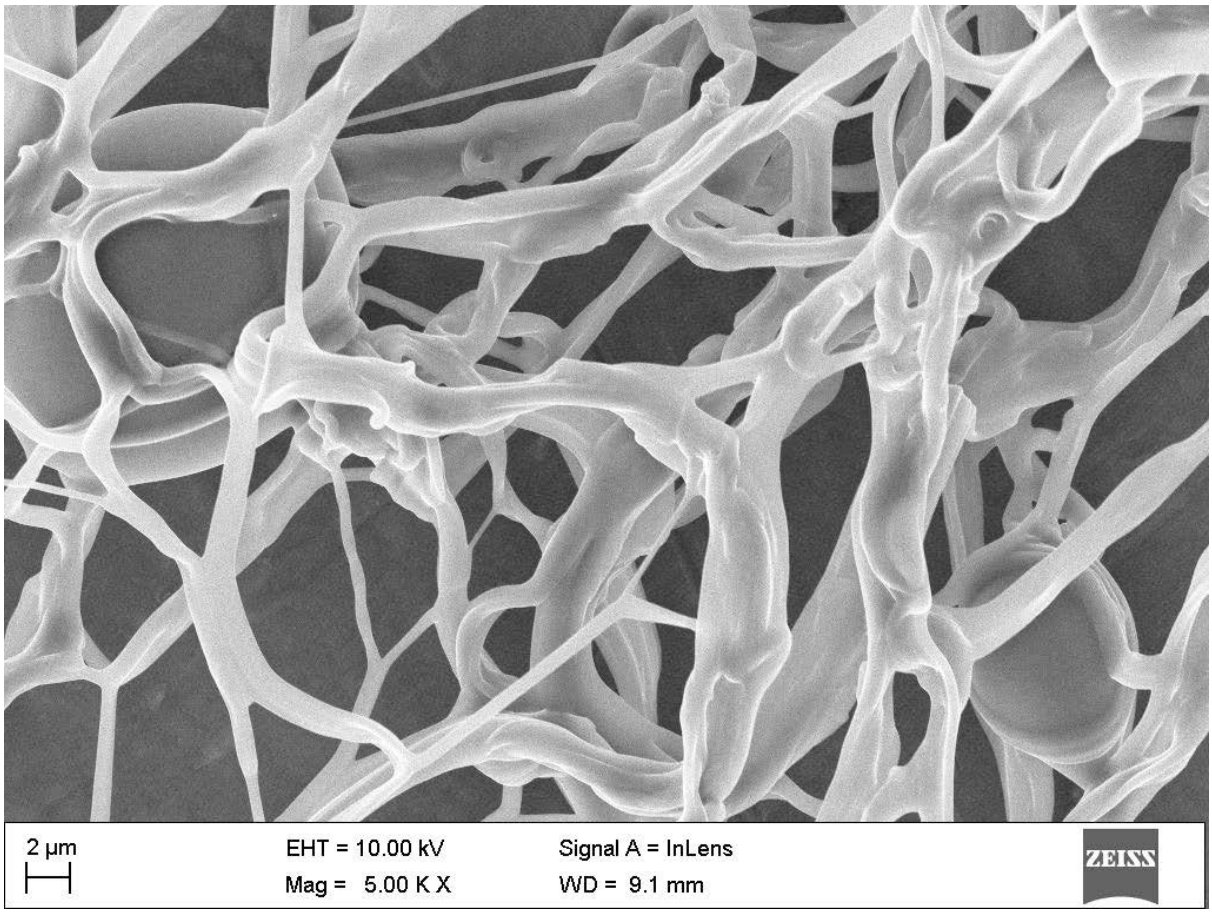

Figure A 25: Sample 6 random area 5 electrospun at 19kV, 4ml/h using a plastic pipette

The average diameter of fibres in random area 5 of sample 6 approximated to 1091 nm. The area not covered by fibres was calculated to be 925.631 μm^2. The minimum fibre diameter is 211 nm and the maximum fibre diameter is 2829 nm.

Appendix A3

Appendix A3 contains the raw measurement data obtained from the oscilloscope during the impedance spectroscopy. The raw measurement data included: (a.) Peak to peak voltage measured across the 10MΩresistor, (b.) The times at which one oscillation of the input voltage sin wave started and ended and (c.) The time at which the output sin wave (across the 10 MΩ resistor) oscillation closest to the measured input oscillation start time started. The phase angle was calculated by finding the difference in the start times of the two sin waves as a fraction of the period of the input sin wave (Difference between input sin wave end time and input sin wave start time) then multiplying by 360^0.

Table 10: Raw impedance spectroscopy data for 504 nm fibres case

Frequency (Hz)	Peak-peak Voltage (mV)	Input sin wave start time (µs)	Input sin wave end time (µs)	Output sin wave start time (µs)
1000	325	-260	740	-420
2000	466.7	-130	370	-180
3000	520.8	-80	250	-110
4000	545.8	-65	185	-80
5000	558.3	-50	150	-60
6000	566.7	-45	125	-50
7000	570.8	-40	102	-45
8000	575	-30	95	-35
9000	578	-30	82	-32
10000	579	-26	74	-28

Table 11: Raw impedance spectroscopy data for 930 nm fibres case

Frequency	Peak-peak Voltage	Input sin wave start time	Input sin wave end time	Output sin wave start time
1000	316.7	-260	740	-420
2000	454.2	-130	370	-185
3000	508	-85	250	-110
4000	533.3	-65	185	-80
5000	545	-55	145	-65
6000	554	-45	125	-50
7000	554	-40	105	-44
8000	558.3	-34	92	-36
9000	562.5	-30	82	-32
10000	562.5	-26	74	-28

Table 12: Raw impedance spectroscopy data for no fibres case

Frequency	Peak-peak Voltage	Input sin wave start time	Input sin wave end time	Output sin wave start time
1000	300	-260	740	-420
2000	433.3	-130	370	-185
3000	483.3	-90	245	-112
4000	504.2	-65	185	-80
5000	520.8	-50	150	-60
6000	525	-45	122.5	-50
7000	529.2	-39	105	-42.5
8000	533.3	-33	92	-37
9000	535	-29	81	-32
10000	537.5	-27	73	-29

Table 13: Raw impedance spectroscopy data for 903 nm fibres case

Frequency	Peak-peak Voltage	Input sin wave start time	Input sin wave end time	Output sin wave start time
1000	318	-260	740	-420
2000	456	-130	370	-185
3000	512.5	-87	246	-115
4000	534.7	-65	185	-80
5000	547	-55	145	-65
6000	555	-45	125	-50
7000	560	-38	105	-43
8000	564	-34	92	-38
9000	566.7	-30	82	-33
10000	568	-27	73	-29